1-1-1971

Investigation of the systems calcium fluoride:dysprosium and calcium fluoride:holmium by optical methods.

C. Timothy Kwan
University of Windsor

INVESTIGATION OF THE SYSTEMS $CaF_2:Dy^{3+}$ and $CaF_2:Ho^{3+}$ BY OPTICAL METHODS

by

C. Timothy Kwan

Submitted to the Faculty of Graduate Studies through the Department of Physics in Partial Fulfillment of the Requirements for the Degree of Doctor of Philosophy at the University of Windsor

Windsor, Ontario

1971

APPROVED BY:

Dr. M. Schlesinger (Chairman)

Dr. F. Holuj

Dr. N. E. Hedgecock

343559

ABSTRACT

The ruby laser was employed to enhance the phosphorescence decay of the system ($RE^{2+} \rightarrow RE^{3+}$) in CaF_2. A simple model is proposed whose mechanism is very similar to that of thermoluminescence. The process involved was shown to be one involving a single photon. Spectral distributions were obtained using point by point plotting. The general features agree very well with the fluorescence or thermoluminescence spectra. As the laser was operated in a Q-switched mode, the pulse duration was much shorter than the decay time so that individual decay curves could be photographed on an oscilloscope and the decay constant measured.

The system $CaF_2:Dy^{3+}$ was investigated by this method. Emission from the level $^4F_{9/2}$ only was observed, the terminating levels of the transitions are $^6H_{13/2}$ and $^6H_{15/2}$. Two different decay constants were obtained from two components of the same transition, indicating co-existence of luminescence centres at sites of two different symmetries. This in turn implies that reduction of RE^{3+} into RE^{2+} by x-rays is possible for ions at sites with point symmetries other than cubic.

For the system $CaF_2:Ho^{3+}$ emission corresponding to transitions between four upper levels and the ground state was observed. Four decay constants were measured.

By heating the crystal samples in open air, sites of tetragonal and trigonal symmetry were introduced. This was manifested in the change in the spectral distributions of the enhanced phosphorescence as well as in the decay times. For $CaF_2:Dy^{3+}$ the decay times were

shortened to half, while the reduction was some twenty folds for $CaF_2:Ho^{3+}$.

Thermoluminescence spectra of $CaF_2:Dy^{3+}$ were taken. Emission in the 'yellow' (corresponding to $^4F_{9/2}$ to $^6H_{13/2}$ transition) was also observed. This has not been reported in the literature before. The total emission was well divided among the three glow peaks. The spectra from the isolated peaks were found to be identical, contrary to the case of $CaF_2:Ho^{3+}$. After heat treatment, two more glow peaks appeared on the high temperature end. Almost all the light emitted came from the last glow peak. Other than this the heating affected the spectra to only a limited degree.

Excitation spectra of $CaF_2:Dy^{3+}$ were also taken. But the emission was so weak that limited accuracy was achieved. Only tentative identification of the levels was made because of the complexity of the spectra and the lack of adequate theoretical calculations.

Re-excitation experiments were also performed with a view to elucidating the nature of the carriers responsible for thermoluminescence in CaF_2. While in $CaF_2:Gd^{3+}$ it was possible to re-excite all the glow peaks and the efficiency of re-excitation peaked at 3800 Å, no similar conclusion could be drawn for the system $CaF_2:Ce^{3+}$.

ACKNOWLEDGEMENTS

It was entirely through the continual guidance of Professor M. Schlesinger that this research project could be accomplished. I am indebted to my supervisor for suggesting the problem and his unfailing interest throughout the project.

I would like to thank Professor F. Holuj for the use of his equipment for heating and polishing crystal samples.

The cooperation from the technical staff of the Physics Department is much appreciated.

The award of a fellowship from the Provincial Government of Ontario is gratefully acknowledged.

Finally, I want to express my very sincere gratitude to Shirley for her constant encouragement and prayer support back home throughout these years.

TABLE OF CONTENTS

LIST OF FIGURES

Page

Page

Page

LIST OF TABLES

CHAPTER 0. INTRODUCTION

The rare-earth series is formed by the successive filling of the 4f shell* in addition to a xenon configuration ($1s^2 2s^2 2p^6 3s^2 3p^6 3d^{10} 4s^2 4p^6 4d^{10} 5s^2 5p^6$) together with two ($5d6s$ or $6s^2$) or three ($5d6s^2$) outer electrons. The 4f orbitals are drawn towards the nucleus as one proceeds from the beginning of the series with cerium; the wave-function of the third member, neodymium, has already had its maximum inside the $5s^2 5p^6$ subshells. This lanthanide contraction comes from the ineffectiveness of the 4f electrons in screening the nuclear charge for one another.(1) Most of the rare-earth ions exist in the trivalent state, after the removal from the neutral atoms of the outermost electrons, and also a 4f electron in certain cases. When embedded in a crystal lattice they present a very good system for studying the free ions themselves because of the shielding furnished by the outer closed ($5s^2 5p^6$) subshells. On the other hand, a knowledge of the free ion properties enables one to explore the effect of the crystal lattice on the ion. In most cases, the crystal field has a relatively small effect on the 4f electrons compared with the spin-orbit interaction as contrast to the iron group in which the crystal field dominates over the spin-orbit interaction. As the charge distribution of the ion is affected by the crystal field, the energy levels are mildly perturbed from the free ion values.

---

* The term rare-earth used throughout this dissertation refers to the lanthanides only, although some authors include the actinides as well.

Whereas intra-configuration electric dipole transitions, in which there is no change of parity, are Laporte forbidden[2] for the free ions, many such transitions are observed when the ions are incorporated in a crystal lattice. This is made possible through mixing of states with opposite parity by the crystal field and by phonon interaction.

The presence of the crystal lattice provides another channel for energy dissipation when the ion is in an excited state. The fluorescence lifetimes will be influenced by the ion-lattice interaction; in some cases the fluorescence is even quenched through radiationless transitions.

CaF_2 is a convenient crystal matrix to incorporate the rare-earth ions because of the cubic symmetry and a wide range of optical transparency (from 12μ to .13μ)[3]. Similarity in ionic radii between Ca^{2+} (~ 1Å) and the rare-earth ions (~ 0.9Å)[4] enables the latter to enter the matrix easily by substituting for a divalent calcium ion. For electrical neutrality a RE^{3+} ion replacing a Ca^{2+} ion requires charge compensation. This can be achieved, for example, by an interstitial F^- or OH^-, or an O^{2-} occupying a lattice fluorine site. Consequently a local distortion of the cubic symmetry is created. If this distortion is near enough to be felt by the rare-earth ion, the spectra as well as the lifetime of the latter can give information of the nature of the distortion.

Technically the method of thermoluminescence is a very 'clean' method of obtaining emission spectra since the sample is the sole emitter of radiation. However, due to ion-lattice interaction, thermoluminescence does not give all the information obtainable from other techniques, such as luminescence excitation.

There has been much interest in the thermoluminescence of rare-earth ions in alkaline earth fluorides ever since it was found that most of the triply ionized rare-earth ions can be reduced to the divalent state by ionizing radiation.[5] While the spectra of the RE^{3+} ions consist of sharp but weak lines, those of the divalent ions have strong and broad bands. A reduction-oxidation mechanism was proposed by Kiss and Staebler,[6] in the case of Dy^{3+}. Their work and those of a number of others[7-10] seemed to have indicated that reduction by ionizing radiation was possible only for those rare-earth ions occupying cubic sites in the crystal lattice. Schlesinger et al. are among another school who have shown that, at least in the case of Gd^{3+}, rare-earth ions in sites of other symmetries than cubic can also be reduced.[11-13] This diversity in opinion can perhaps be resolved considering the fact that optical spectra obtained by various workers depend on the conditions under which the crystals were grown, impurities, etc., as pointed out earlier by Stepanov and Feofilov.[14]

In their work, Stepanov and Feofilov classified as type I spectra those originating from centres involving oxygen, and type II for those from crystals grown under reductive conditions. These two types of spectra are similar in the number and approximate positions of groups of lines, but are different in structure within each group.

A great amount of experimental work has been done by the Johns Hopkins group both on the rare-earth free ions and rare-earth salts or rare-earth doped crystals. The work of Dieke et al.[15] on free ions provides a very helpful guideline for the crystal spectra since the centre of gravity of free ion energy levels are not much modified when

the ions are embedded in a crystal. The Russian scientists have also contributed a considerable amount in this field. The book by El'yashevich[16] embodied quite a thorough survey of earlier works.

Many of the energy levels do not give rise to fluorescence, and these have to be probed by absorption measurements. Even for the fluorescent levels absorption measurements are valuable complementary information. However, conventional absorption technique is not adequate for 'opaque' samples. Selective excitation is another means of probing levels lying above the fluorescent ones. High resolution selective excitation as a means of studying higher energy levels was first reported from this laboratory in $CaF_2:Ho^{3+}$,[17] and was found to be suitable for other rare-earths. The fact that not all energy levels give rise to fluorescence indicates that some role is played by ion-lattice interaction. In LaF_3 matrix, it was found[18] that radiative transitions usually do not arise from an energy level if there are lower ones within 1600 cm^{-1}. The excitation energy received by the ion is dissipated through the crystal lattice. When the dopant concentration exceeds 1%, the ion-ion interaction becomes important.[19-21] (In the work presented in this dissertation, samples of low dopant concentration were used to avoid such complication.)

The amount of ion-lattice interaction is best studied by lifetime measurements. Many different techniques have been employed by different workers.[22-25] Dieke and Hall[26] worked on rare-earth salts and found little temperature dependence of the lifetimes. On the other hand, the lifetimes decrease with increasing temperature when the rare-earth ions are incorporated in LaF_3.[27] Similar work on CaF_2 is scattered among a few rare-earth ions.[18,28-35]

Among many other applications, the laser finds its use as a new tool in the field of spectroscopy. Because of its high intensity, at its particular wavelength, the laser makes possible the observation of multiphoton processes.[36-46] Atomic population at excited states is low or short-lived under normal conditions. A high intensity photon flux from a laser, when absorbed, can leave many atoms in an excited state from which a probe beam can lift them higher, thus extending the ceiling of probing energy levels. Some work of excited state spectroscopy has been done on the alkali halides,[47-52] but little was done on CaF_2.

The work embodied in this dissertation centered on the systems $CaF_2:Dy^{3+}$ and $CaF_2:Ho^{3+}$. Conventional fluorescence, thermoluminescence and selective excitation techniques were employed in addition to an unconventional use of the ruby laser--enhancement of phosphorescence decay.

CHAPTER I. RESUME OF SPECTROSCOPY OF RARE-EARTH IONS

A. Electrostatic Interaction

The electronic structure of isolated rare-earth atoms (or free ions) is largely determined by electrostatic interactions. In the first approximation, the Hamiltonian for an N-electron atom is

$$H_1 = H_o + H_c . \tag{1.1}$$

This is a sum of one-particle operators

$$H_o = \sum_i h_i = \sum_i \left(\frac{p_i^2}{2m} - \frac{Ze^2}{r_i} \right) , \tag{1.2}$$

together with a sum of two-particle operators

$$H_c = \sum_{i<j} \frac{e^2}{r_{ij}} \tag{1.3}$$

where e and m are electronic charge and mass respectively;

r_i and p_i are radial coordinate and momentum of the i^{th} electron respectively;

r_{ij} is the distance between the i^{th} and j^{th} electron;

Z is the effective charge[1] of the nucleus; and the summation is over all electrons.

The term H_c prevents the separation of variables in the Hamiltonian H_1; besides, it is so large that it cannot be treated as a perturbation. One then assumes a central field potential $U(r_i)$ as the starting point of the perturbation theory, i.e.,

$$H' = \sum_i \left[\frac{1}{2m} p_i^2 + U(r_i) \right]$$

The perturbing potential takes the difference

$$H_1 - H' = - \sum_i \left[\frac{Ze^2}{r_i} + U(r_i) \right] + \sum_{i<j} \frac{e^2}{r_{ij}} \qquad (1.4)$$

The operator H' has a product function of the form

$$\Phi(ab \ldots k|12 \ldots N) \equiv \phi(b|2) \ldots \phi(k|N)$$

as eigenfunction, where a represents a set of four quantum numbers (n, l, m, μ) associated with electron number one, b with electron number two and so on. The first summation in (1.4) produces a uniform shift for all the levels and is dropped from the subsequent discussion.

One approximates an N-electron wavefunction by some suitable linear combinations of product functions of the form

$$\tilde{\Phi} = (N!)^{-\frac{1}{2}} \begin{vmatrix} \phi(a|1) & \phi(b|1) & \ldots \\ & \phi(a|2) & \end{vmatrix} \qquad (1.5)$$

Here Pauli's principle has been included. The energy is given by the expectation value of H_1.

$$\langle \tilde{\Phi}(ab \ldots k) | H_1 | \tilde{\Phi}(a'b' \ldots k') \rangle = \sum_i \langle \tilde{\Phi}(ab \ldots k) | h_i | \tilde{\Phi}(a'b' \ldots k') \rangle + e^2 \sum_{i<j} \langle \tilde{\Phi}(ab..) \left| \frac{1}{r_{ij}} \right| \tilde{\Phi}(a'b'..k \qquad (1.6)$$

The first sum gives $\langle a|h|a\rangle + \langle b|h|b\rangle + \ldots + \langle k|h|k\rangle$.

These integrals are of the type

$$I(a) \equiv \frac{1}{a_o} \int dr\, P_a(r) \left[-\frac{d^2}{dr^2} + \frac{\ell(\ell+1)}{r^2} - \frac{2\,U(r)}{a_o} \right] P_a(r) \qquad (1.7)$$

where a_o is the Bohr radius and

P_a is the radial function depending on n and ℓ.

The second sum in (1.6) gives

$$\langle ab|\frac{1}{r_{12}}|ab\rangle - \langle ab|\frac{1}{r_{12}}|ba\rangle + \langle ac|\frac{1}{r_{12}}|ac\rangle - \langle ac|\frac{1}{r_{12}}|ca\rangle + \cdots \qquad (1.8)$$

Expanding in normalized spherical harmonics,[2]

$$\frac{1}{r_{12}} = \sum_{k=1}^{\infty} \frac{r_<^k}{r_>^{k+1}} \sum_{q=-k}^{k} (-)^q\, C_q^{(k)}(1)\, C_{-q}^{(k)}(2)$$

where $r_<$, $r_>$ are respectively the smaller and larger of the radial distances of the two electrons;

$$C_q^{(k)} = \left(\frac{4\pi}{2k+1}\right)^{1/2} Y_{kq}$$

Each pair of integrals of (18) has the form:

$$\sum_k \left[f_k(a,b) F^k(a,b) - g(a,b) G^k(a,b) \right]$$

where

$$f_k(a,b) = C^k(a,a)\ C^k(b,b)$$

$$= \langle \phi(a|1)|C_q^{(k)}(1)|\phi(a|1)\rangle\langle\phi(b|2)|C_{-q}^{(k)}(2)|\phi(b|2)\rangle \qquad (1.9)$$

$$g_k(a,b) = C^k(a,b)\ C^k(a,b)$$

$$= \langle \phi(a|1)|C_q^{(k)}(1)|\phi(b|1)\rangle\langle\phi(a|2)|C_{-q}^{(k)}(2)|\phi(b|2)\rangle$$

$$F^k(a,b) = \int dr_1 \int dr_2\ P_a(1)\ P_b(2)\ \frac{r_<^k}{r_>^{k+1}}\ P_a(1)\ P_b(2) \qquad (1.10)$$

$$G^k(a,b) = \int dr_1 \int dr_2\ P_a(1)\ P_b(2)\ \frac{r_<^k}{r_>^{k+1}}\ P_b(1)\ P_a(2)$$

Thus

$$\langle \tilde{\Phi}|H_1|\tilde{\Phi}\rangle = I(a) + I(b) + \ldots + \sum_k (f_k F^k - g_k G^k) + \ldots \qquad (1.11)$$

The quantities f_k and g_k may be found from a table of values[3] for $c^k(\ell m, \ell' m')$; they are fixed by the properties of angular momentum functions. The integrals $I(a)$, $I(b)$, ... and the Slater integrals F^k and exchange integrals G^k depend on the choice of radial functions; these must be prescribed or used as parameters to fit experimental data.

B. Spin-Orbit Interaction

The next term to be considered in the Hamiltonian of a rare-earth ion is that due to spin-orbit interaction.

Let

$$H_2 = H_1 + H_{so} \tag{1.12}$$

where

$$H_{so} = \sum_i \xi(r_i)\, \underline{\ell}_i \cdot \underline{s}_i \ ,$$

$$\xi(r_i) = -\frac{\hbar^2}{2m^2c^2}\ \frac{1}{r_i}\ \frac{\partial\varphi(r_i)}{\partial r_i} \ ,$$

$\varphi(r_i)$ = average potential seen by the i^{th} electron.

One seeks suitable linear combinations of (antisymmetric) product functions to diagonalize H_2. Thus

$$\tilde{\Psi}(\gamma|12\ldots N) = \sum C(\gamma|12\ldots N)\Phi(ab\ldots k|12\ldots N) \tag{1.13}$$

where γ represents a set of collective quantum numbers required to label $\tilde{\Psi}$. Noting that H_2 is invariant under spatial inversion, eigenfunctions of H_2 have well-defined parity $\pi = (-)^{\sum \ell_i}$. The mixture (1.13) consists of either odd parity function or even parity functions.

H_2 is invariant under rotation. Hence eigenfunctions of H_2 are eigenfunctions of the total angular momentum; i.e., one can obtain eigenfunctions of H_2 that are labelled by good quantum numbers J and M.

In the first approximation, the Russell-Saunders coupling scheme can be adopted for the rare-earth ions.

$$\Psi(\alpha LSJM|12\ldots N) = \Psi(n_a \ell_a m_a \mu_a,\ n_b \ell_b m_b \mu_b,\ \ldots\ ;\ LSJM|12\ \ldots\ N)$$

$$= \Sigma(\ell_a m_a,\ \ell_b m_b|L'M'_L)(L'M'_L,\ \ell_c m_c|L''M''_L)\ldots(12\ldots|LM_L)$$

$$\times\ (\tfrac{1}{2}\mu_a,\ \tfrac{1}{2}\mu_b|S'M'_s)(S'M'_s,\ \tfrac{1}{2}\mu_c|S''M''_s)\ldots(12\ldots|SM_s)$$

$$\times\ (LM_L,\ SM_s|JM)\ \Phi\ (ab\ldots k|12\ldots N) \qquad (1.14)$$

where the summation is taken over all m_a, m_b, $\ldots$, μ_a, μ_b, $\ldots$ L', M'_L, $\ldots$ S', and M'_s, and α is any other quantum number required to specify Ψ. The expansion coefficients are Clebsch Gordan coefficients. Here the electrons are coupled together one after another.

Treating H_{so} as perturbation to H_1, the matrix element

$$\langle \alpha LSJM|\ H_{so}\ |\ \alpha'\ L'\ S'\ J'\ M'\rangle$$

is required. For simplicity, the case of two electrons is considered below. Noting that $\underline{L}$ and $\underline{S}$ are tensor operators of rank one,

$$\langle n_a \ell_a n_b \ell_b LSJM|\sum_i \xi(r_i)\underline{L}(i)\cdot\underline{S}(i)|n_a'\ell_a'\ell_b'L'S'J'M'\rangle = \delta_{JJ'}\delta_{MM'}(-)^{J+L+S}\begin{Bmatrix} J & L & S \\ 1 & S' & L' \end{Bmatrix}$$

$$\times \sum_i [\zeta_i \langle \ell_a \ell_b L\|\underline{L}(i)\|\ell_a'\ell_b'L'\rangle\langle \tfrac{1}{2}\ \tfrac{1}{2}\ S\|\underline{S}(i)\|\ \tfrac{1}{2}\ \tfrac{1}{2}\ S'\rangle \qquad (1.15)$$

where $\zeta_i = \int dr\ P_i(r)\ \xi\ (r)\ P_i(r)$ contains the radial dependence.

Values of the 6-j symbol $\{\ \}$ can be found from tables,[4] so that the diagonal part of (1.5) can be written explicitly as

$$\langle n_a \ell_a n_b \ell_b LSJM | H_{so} | n_a \ell_a n_b \ell_b\ LSJM \rangle = \frac{1}{2}\left[J(J+1) - L(L+1) - S(S+1)\right] \zeta(abSL) \quad (1.16)$$

The spin-orbit interaction removes part of the degeneracy of the energy levels. It separates the levels (labelled by J) of a given term (labelled by L and S). The diagonal matrix elements of H_{so} are

$$E(abSLJ) = I(a) + I(b) + \sum_k f_k(\ell_a \ell_b SL)F^k + (-)^s g_k(\ell_a \ell_b SL)G^k$$

$$+ \frac{1}{2}\left[J(J+1) - L(L+1) - S(S+1)\right] \zeta(abSL) \quad (1.17)$$

The splitting between adjacent levels is

$$\Delta = E(abSLJ) - E(abSLJ-1) = J\ \zeta\ (abSL) \quad (1.18)$$

This is the Lande interval rule: the level splitting is proportional to J.

The spin-orbit interaction is diagonal in J, but it connects functions of different S and L. Since $\underline{L}$ and $\underline{S}$ are tensors of order one, there are matrix elements between S and $S' = S \pm 1$ and between L and $L' = L \pm 1$. Thus the interaction mixes singlets and triplets only.

The preceding formulae apply to electrons belonging to different orbitals. Equivalent electrons require a different treatment.

As shown by Condon and Shortley and Racah, the F^k and G^k are positive quantities and decreasing functions of k.[5,2] In the semi-empirical approach, one leaves the integrals I, F^k, and G^k as unknown parameters, to be determined from the experiments. This makes definite predictions about the ordering of energy levels and their relative spacing. Deviations from these predictions can indicate the influence of configuration mixing or spin-orbit interaction. If the observed energy levels of an atom fit the pattern predicted by (1.17), then one can expect the LSJ functions to provide reasonable approximations for other atomic properties.

In the construction of coupled function (1.14) from product functions, Ψ carries the 2N labels $\{n_i \ell_i\}$ of the N electrons, four collective labels LSJM and 2N-4 intermediate labels $\{L_i S_i\}$. The last set of labels is called the 'parentage' of the term.* One particular term may result from different 'parents' through coupling of the same electrons in a particular coupling scheme.

In many cases, one can deduce atomic properties of a system without a detailed knowledge of the actual wavefunctions. So instead of following the tedious determinantal wavefunction calculation one may define a coupled function by displaying certain operator for which it is an eigenfunction, and then apply tensor operator technique and recoupling procedure.

C. Equivalent Electrons

When some of the electrons are equivalent (same n and ℓ), not every possible state function built up by the usual vector coupling

*This represents the sequence of coupling to give the LSJ term and is different from the coefficient of fractional parentage.

scheme is allowed by the exclusion principle. Racah[6] proposed to make use of the powerful matrix method developed by Condon and Shortley[7] to calculate the eigenfunction of the configuration ℓ^n as a linear combination of the eigenfunction obtained by the addition of a further electron to the configuration ℓ^{n-1}. In the vector coupling of three equivalent electrons, one can form

$$\psi\,(\ell^2(S'L')\ell;\ S\ L) \quad \text{or} \quad \psi\,(\ell,\ell\ell(S''L'');\ S\ L)$$

They are related by the unitary transformation matrix

$$(s_1\ell_1 s_2\ell_2(S'L')\ s_3\ell_3;S\ L|s_1\ell_1,s_2\ell_2\ s_3\ell_3\ (S''L'');\ S\ L)\ .$$

Not all values S'', L'' are allowed by the exclusion principle. Only such a linear combination

$$\overline{\Psi}(\ell^3\alpha\ SL) = \sum_{S'L'\alpha'} (\ell^2(\alpha'S'L')\ell SL\}\ell^3\alpha SL)\psi(\ell^2(\alpha'S'L')\ell SL)$$

may be eigenfunction of ℓ^3 for which the coefficient of fractional parentage (CFP)

$$(\ell^2(\alpha'S'L')\ell SL\}\ell^3\alpha SL)$$

satisfies the equation system

$$\sum_{S''L''} (\ell,\ell\ell(S''L''), SL|\ell^2(S'L')\ell SL)(\ell^2(S'L')\ell SL\}\ell^3\alpha SL) = 0\,, \quad (S''+L''=\text{odd})$$

More generally, if one knows the fractional parentage of ℓ^{n-1}, one can construct eigenfunction of ℓ^n. Thus

$$\bar{\Psi}(\ell^n\alpha SL) = \sum_{\alpha'S'L'} (\ell^{n-1}(\alpha'S'L')\ell SL\}\ell^n\alpha SL)\psi(\ell^{n-1}(\alpha'S'L')\ell SL)$$

$$= \sum_{\substack{\alpha'S'L' \\ \alpha''S''L''}} (\ell^{n-1}(\alpha'S'L')\ell SL\}\ell^n\alpha SL)(\ell^{n-2}(\alpha''S''L'')\ell'S'L'\}\ell^{n-1}\alpha'S'L')$$

$$\times\ \psi(\ell^{n-2}(\alpha''S''L'')\ell'(S'L')\ell SL)$$

and the CFP must satisfy the euqation system

$$\sum_{\alpha'S'L'} (S''L'',\ell\ell(S'''L'''), SL|S''L''\ell(S'L')\ell SL) \times (\ell^{n-2}(\alpha''S''L')\ell'S'L'\}\ell^{n-1}\alpha'S'L')$$

$$\times\ (\ell^{n-1}(\alpha'S'L')\ell SL\}\ell^n\alpha SL) = 0, \qquad (S''' + L''' = \text{odd}).$$

The process of adding equivalent orbitals must terminate on reaching the closed shell function that has $N = 2(2\ell + 1)$ orbitals. The nature of the closed shell function is easily seen by noting that m_ℓ and m_s can take the values

$$m_\ell = \pm\ell, \pm(\ell-1), \ldots \pm 1, 0;$$
$$m_s = \pm 1/2$$

so that $S = L = 0$, and $J = M = 0$. Since equivalent d or f orbitals have several terms of the same type, one must have some way to distinguish between them. One way is to specify the principal parent (S'L'), principal grandparent (S''L''), etc. This genealogical scheme is not widely used. Racah developed the seniority scheme[6] based on pairs of orbitals coupled to a ^1S state. Essentially the same spectroscopic term is obtained for ℓ^v as one couples to it the 2-electron function $\Psi(\ell^2 0)$. Thus the term ^3F is contained in the chain

$$f^2(^3F);\ f^2(^3F) + f^2(^1S) = f^4(^3F);\ f^4(^3F) + f^2(^1S) = f^6(^3F);\ \text{etc.}$$

One can define a seniority number of a term in the following way: from the chain of terms, delete all pairs of ^1S electrons leaving ℓ^v. Then v is the seniority number. In other words, ℓ^v is the configuration in which the term SL occurs for the first time.

CHAPTER II. GROUP THEORETICAL CONSIDERATION

A. Free Ions

As mentioned before, eigenfunctions of angular momentum are used because of the rotational invariance of the Hamiltonian of a free ion. This spherical symmetry is destroyed once the ion is incorporated into a crystal lattice. Hence eigenfunctions must be constructed from those operators compatible with the new symmetry.

When a Hamiltonian is invariant under a group G of symmetry transformations, the eigenfunctions belonging to one energy level form a basis for a representation of G. This can be taken as a fundamental theorem, the importance of which lies in the fact that one can label and describe an energy level and its eigenfunction simply by naming the representation associated with it.

The Hamiltonian (1.1)

$$H_1 = H_o + H_c = \sum_i \frac{p_i^2}{2m} - \frac{Ze^2}{r_i} + \sum_{i>j} \frac{e^2}{r_{ij}} \qquad (2.1)$$

does not operate on the spin. The term eigenfunction (including spin) therefore is $(2L + 1)(2S + 1)$-fold degenerate. This degeneracy corresponds to the fact that H_1 is invariant under a rotation of all spatial coordinates

or of all spin coordinates simultaneously. The Hamiltonian

$$H_2 = H_1 + H_{so}$$

$$= H_1 + \sum_i \xi(r_i)\, \underline{l}_i \cdot \underline{s}_i \qquad (2.2)$$

contains products of vectors, and is therefore no longer invariant under orbital and spin rotations separately. It follows that L, M_L, S, M_S are no longer good quantum numbers for characterizing a state. The wavefunction

$$\Psi(LSJM) = \sum_{M_L, M_S} (LM_L SM_S | JM)\psi(LM_L SM_S) \qquad (2.3)$$

is not an exact eigenfunction, which would contain additional contributions from other terms with different L and S but the same J and M. However, $\underline{l}_i \cdot \underline{s}_i$ is invariant under a simultaneous rotation in both orbital and spin space. Hence the term function transforms according to

$$D^{(L)} \times D^{(S)} = \sum_J D^{(J)} \qquad (2.4)$$

under simultaneous orbital and spin rotations, where

$$J = L + S,\ L + S - 1,\ \ldots |L-S|$$

It was noted before that H_1 is invariant under inversion operation π. Since π commutes with every rotation operator R, the matrix equation

$$D(\pi)D(R) = D(R)D(\pi), \quad \forall\ R \in G, \tag{2.5}$$

holds. By Schur's lemma,[1]

$$D(\pi) = P\ I$$

where I is the unit matrix and P a scalar. Since π^2 is the identity transformation

$$P = \pm 1$$

$$\text{therefore} \qquad \pi \Psi = \pm \Psi \tag{2.6}$$

The wavefunction is said to have even (with + sign) or odd (with - sign) parity. Now the spin function space (u_+, u_-) is invariant under π. It transforms according the $D^{(1/2)}$ (double-valued) representation under rotation. The identity transformation is represented by the two matrices I and -I, so that

$$\pi\, u_+ = P\, u_+, \quad \pi\, u_- = P\, u_- \tag{2.7}$$

where P takes values $\pm 1, \pm i$.

Since physically observable quantities contain products like $\psi_i^+ \psi_j$, so $\pi \psi_i^+ \psi_j$ contains the factor $(P^*P)^n = 1$, where n is the number

of electrons. Hence one can choose the spin function to have even parity for simplicity. Also, $\underline{l}_i$ and $\underline{s}_i$ are invariant under π. The Hamiltonian H_2 is therefore invariant under π. Its eigenfunction $\overline{\Psi}$ (L,S,J,M) can be assigned a definite parity $P = (-)^{\Sigma \ell_i}$.

Furthermore, physically measurable quantities appear as, or can be expressed in terms of, matrix elements of the type

$$M_{ij} = \langle \psi_i^{(\lambda)} | Q_k^{(\mu)} | \psi_j^{(\nu)} \rangle \qquad (2.8)$$

If $\psi_i^{(\lambda)}$, $Q_k^{(\mu)}$, $\psi_j^{(\nu)}$ transform according to $D^{(\lambda)}$, $D^{(\mu)}$ and $D^{(\nu)}$ respectively, M_{ij} is non-vanishing only when $D^{(\mu)} \times D^{(\nu)}$ contains $D^{(\lambda)}$. This can be taken as another fundamental theorem.

The spontaneous and induced electric dipole transition probabilities are proportional to

$$|\langle \psi_2 | r_\alpha | \psi_1 \rangle|^2$$

If ψ_1, ψ_2 belong to sets with $J = J_1$, J_2 respectively, then $r_\alpha \psi_1$ transforms according to $D^{(1)} \times D^{(J_1)} = D^{(1+J_1)} + D^{(J)} + D^{(J-1)}$ for $J_1 > 1$. Using the fundamental theorem above, the matrix elements vanish unless $\Delta J = J_2 - J_1 = 0$ or ± 1, but not $J_1 = 0$ to $J_2 = 0$. For the same reason, the electric dipole operator $e\underline{r}$, being an odd operator, does not connect states of the same parity. On the other hand, the magnetic dipole operator $\underline{r} \times \underline{p}$ is even, so that magnetic dipole transitions between the same configuration is allowed by parity. In the case of optical transitions

between crystal field split levels, parity is not entirely a good quantum number because vibrations of the ions in a lattice with centre of inversion destroy the perfect symmetry. Since electric dipole transitions are normally of the order $\frac{1}{\alpha^2} \sim (137)^2$ times as strong as magnetic dipole transitions, even a small breakdown in the parity selection rule allows the electric dipole transitions to dominate.

B. Crystal Field

The crystal matrix of CaF_2 belongs to the fluorite (cubic) systems as shown below:(2)

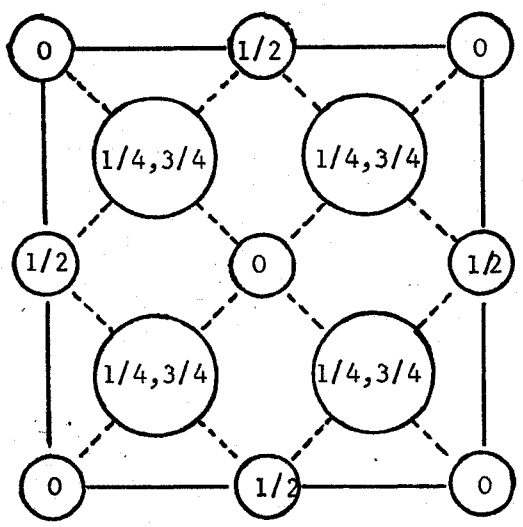

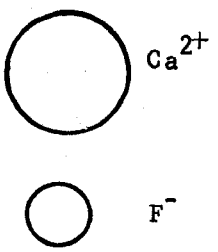

Unit cell of CaF_2 projected on a cube face

But for the present purpose, one may picture that a calcium ion sits at the body centre of every other cube formed by fluorine ions at the lattice sites. Doping can be done, for instance, by adding the rare-earth trifluoride to the melt. The RE^{3+} enters the crystal matrix by substituting a Ca^{2+}. For electrical neutrality charge compensation is required. A commong scheme is compensation by an extra fluorine ion at an interstitial

site. When this charge compensator is remote from the rare-earth ion, the latter finds itself in an essentially cubic field. On the other hand, if the charge compensator is in close proximity of the ion, the symmetry is axial (C_{4v}). Another possible compensation scheme is by the introduction of OH^- or O^{2-}. The rare-earth ion will see a trigonal symmetry (C_{3v}) if one of its neighbouring fluorine ion at a lattice site is replaced by a compensator.(3) The type of charge compensators present as well as their relative abundance depends on the growth condition of the sample and/or subsequent thermal treatment.(4)

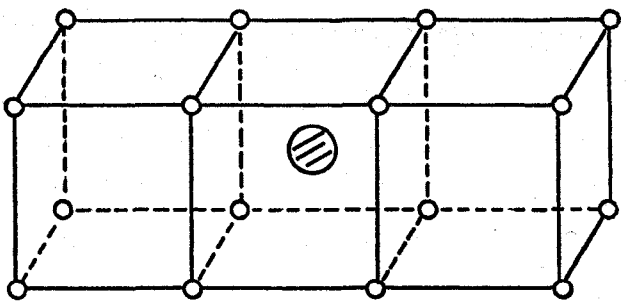

RE^{3+} in cubic site

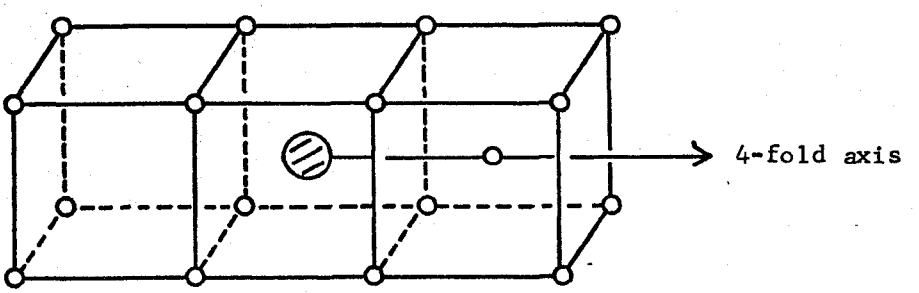

RE^{3+} in C_{4v} site

o Cl^- ⊜ RE^{3+}

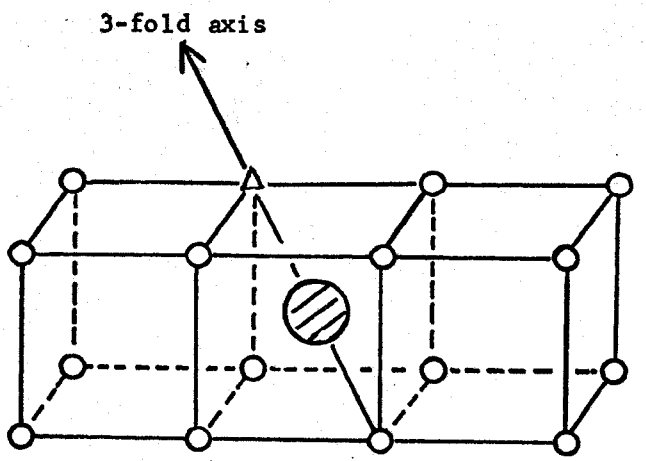

The eigenfunction of a free ion is invariant under rotation and inversion. It transforms as the spherical harmonic $Y_{\ell m}$, which are basis functions of an irreducible representation of dimension $2\ell + 1$. When being placed into a crystal, the ion has its spherical symmetry reduced to that of the site it resides in the crystal. In order to see the extent to which the original degeneracy is lifted, one has only to reduce the representation of the original symmetry group (the full rotation group) belonging to a definite term (specified by J) of the free ion to the representation of the symmetry point group at the ion site. It is immaterial whether the perturbation is small or large, and in particular which form it takes, and whether one calculates the perturbation energy only to the first order or to a higher order.

The introduction of the free ion into the crystal results in the splitting of the representation D_J into components, each of which is an irreducible representation of the group of symmetry operations which leave the crystal potential, V_c, unchanged. Thus

$$D_J = \sum_i c_i \Gamma_i$$

where the c_i's are constants.

A state of the system is represented by a representation Γ_i and its degeneracy is given by the dimension of Γ_i. For example, the levels J = 9/2, 13/2 and 15/2 are split by the crystal field (of different symmetries) in the following manner:[5]

J	O_h	C_{4v}	C_{3v}
9/2	$\Gamma_6+2\Gamma_8$	$3\Gamma_6+2\Gamma_7$	$\Gamma_7+2\Gamma_8+2\Gamma_9$
13/2	$\Gamma_6+2\Gamma_7+2\Gamma_8$	$3\Gamma_6+4\Gamma_7$	$3\Gamma_7+2\Gamma_8+2\Gamma_9$
15/2	$\Gamma_6+\Gamma_7+3\Gamma_8$	$4\Gamma_6+4\Gamma_7$	$3\Gamma_7+2\Gamma_8+3\Gamma_9$

Often it is helpful to know just the number of levels a state of a given J will be split into for a given crystallographic point group. Runciman[6] considered the general problem and showed that for half integral J, the following splitting occurs:

J	1/2	3/2	5/2	7/2	9/2	11/2	13/2	15/2
cubic	1	1	2	3	3	4	5	5
lower symmetries	1	2	3	4	5	6	7	8

Inasmuch as group theory furnishes an exact solution to the number of components into which a state is split, it does not tell the amount of splitting or the relative positions of the levels. In the calculation of crystal field splitting the favorite model involves a static point charge electric field. The charge distribution of the other ions does not penetrate into the rare-earth site. So the crystal field satisfies Laplace's equation

$$\nabla^2 V_c = 0$$

One can then expand V_c as a series in spherical harmonics[5]

$$V_c = \sum_{i,\ell,m} A_{\ell m} r_i^{\ell} Y_{\ell}^{m} (\theta_i, \phi_i)$$

or, in Racah's tensor notation,

$$V_c = \sum_{i,k,q} B_k^q C_q^{(k)}(i) \qquad (2.10)$$

where $A_{\ell m}$, B_k^q remain undetermined coefficients, usually adjusted to fit experimental results, and the summation i is over the f electrons of the ion.

Now all matrix elements of V_c involve integrals of the type

$$\langle \psi^{(j)} \mid V_c \mid \psi^{(i)} \rangle \qquad (2.11)$$

where $\psi^{(i)}$, $\psi^{(j)}$ transform under rotation according to $D^{(3)}$ for f electrons. Using the fundamental theorem above, the matrix element vanishes unless $D^{(3)}$ is contained in $D^{(k)} \times D^{(3)}$; i.e., the set $\{k+3, k+2, \ldots | k-3|\}$ has to contain 3. Therefore $k \leq 6$. By similar reasoning, matrix elements involving odd terms of the spherical harmonics vanish. Thus the series (2.10) terminates. Since $C^{(0)}$ is constant, the first term in the series can be ignored as far as crystal splitting is concerned, leaving

$$V_c = \sum_{i,q} [B_2^q C_q^{(2)}(i) + B_4^q C_q^{(4)}(i) + B_6^q C_q^{(6)}(i)] \quad (2.12)$$

The value of q will be further limited by the point symmetry of the rare-earth ion site, since the Hamiltonian must be invariant under the operation of the point symmetry group. In general, when there is an m-fold axis, V_c will contain $C_m^{(k)}$. For some high symmetry cases there exist relations between the coefficients B_k^q.[7] For instance, in the case of tetragonal symmetry, (C_{4v}), m = 4, one has

$$V_c = \sum_i \{B_2^o C_o^{(2)}(i) + B_4^o C_o^{(4)}(i) + B_4^4 [C_4^{(4)}(i) + C_{-4}^{(4)}(i)] + B_6^o C_o^{(6)}(i) + B_6^6 [C_4^{(6)}(i) + C_{-4}^{(6)}(i)]\}$$

In the SLJ scheme, (2.11) takes the form

$$\sum_{i,k,q} B_k^q \langle f^n \alpha SLJM_J | C_q^{(k)}(i) | f^n \alpha' SL'J'M_J' \rangle$$

$$= \sum_{i,k,q} B_k^q \langle f^n \alpha SLJM_J | U_q^{(k)} C^{(k)}(i) | f^n \alpha' SL'J'M_J' \rangle \quad (2.13)$$

where $U_q^{(k)}$ is Racah's unit tensor operator such that

$$\langle \alpha \ell \mid U_q^{(k)} \mid \alpha' \ell' \rangle = \delta_{\alpha\alpha'} \delta_{\ell\ell'}.$$

Using Wigner Eckart theorem, the matrix element in (2.13) can be written as

$$\langle f^n \alpha SLJM_J \mid U_q^{(k)} \mid f^n \alpha' SL'J'M_J' \rangle \; (f \| C^{(k)} \| f)$$

$$= (-)^{J-M_J} \begin{pmatrix} J & k & J' \\ -M_J & q & M_J' \end{pmatrix} (f^n \alpha SLJ \| U^{(k)} \| f^n \alpha' SL'J')(f \| C^{(k)} \| f)$$

From the 3-j symbol, one obtains the selection rule

$$M_J - M_J' = q \tag{2.14}$$

so that one can introduce a set of crystal quantum numbers , μ, satisfying the relation

$$M_J = \mu \pmod q \tag{2.15}$$

The values of q are restricted to 0, ± 1, ± 2, ± 3, ± 4 and ± 6 depending on the point symmetry of the crystal field. Thus the free ion states may be divided into different classes characterized by the crystal quantum numbers once the ion is incorporated into a crystal field of given symmetry. All states belonging to the same class may interact one with another, but not with any state outside its class.

CHAPTER III. FLUORESCENCE OF IONS IN CRYSTALS

The approximation of treating the ion in an electrostatic crystal field does not account for a number of observations, such as:

1. occurance of Laporte forbidden electric dipole transitions for centres with inversion symmetry,
2. temperature dependence of positions and widths of spectral lines,
3. radiationless processes.

The ion may be considered coupled to the crystal lattice through the crystal field, which is being modulated by the thermal vibrations of the lattice. An excited atom can relax to the ground state either by emission of radiation, or, through this coupling with the lattice, dissipate energy as heat.

Energy transfer through radiationless transitions is an extremely fast process--within 10^{-10} to 10^{-11} sec.--and is normally rather beyond the control of the experimenter. The calculations of the transition probabilities of radiationless (multi-phonon) process is beyond the scope of this dissertation, suffice it to mention that these processes are the less probable the larger is the energy gap between the two levels involved in the transition. When competing with the radiative decay process the radiationless process is a serious loss for a fluorescent system. On the other hand it may be useful in the case where the exciting light brings a

large number of ions to one or more upper excited states from which they quickly decay to a long lived metastable state which becomes the initial state of the fluorescence.

Trivalent rare-earth ions in crystal have sharp absorption lines. Many of these lines also fluoresce. They originate from long-lived (metastable) states whose lifetimes are of the order of 10^{-2} to 10^{-3} sec.; the absorption bands, instead, correspond to short-lived states from which the excited ions quickly decay to the metastable levels.

The following development is comparatively more detailed than before since the main part of the experimental work was done in this direction.

A. Continuous Excitation

Consider a three-level system with one fluorescent level as shown in the diagram below:

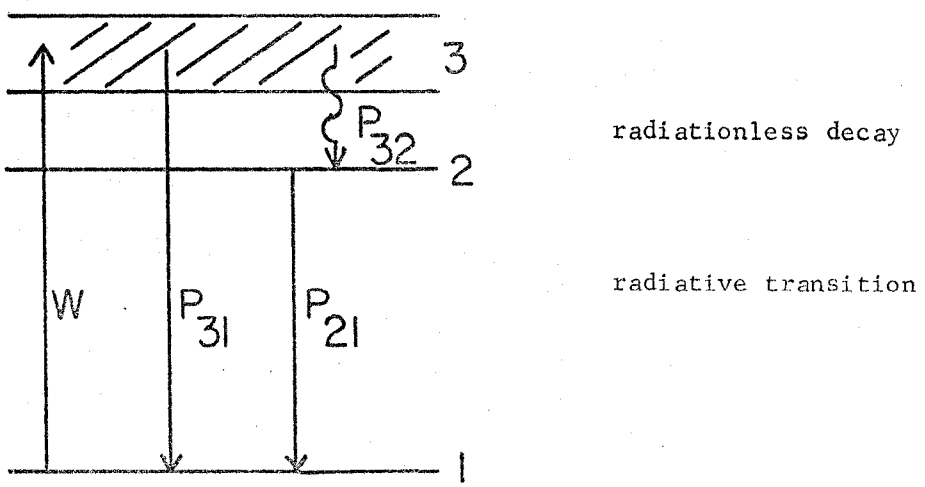

Let w be the probability per unit time for the ion to undergo transition $1 \rightarrow 3$ as a result of absorption of radiation,

p_{31}, p_{32} and p_{21} be the downward transition probabilities per unit time between levels 3,1; 3,2 and 2,1 respectively.

Assume for simplicity that $p_{31} \gg p_{32}, p_{21}$.

Let N_i be the number of atoms occupying the i^{th} level, with a total of N_o atoms in the system.

$$N_o = N_1 + N_2 + N_3.$$

The rate equations are

$$\frac{d}{dt}\begin{bmatrix} N_1 \\ N_2 \\ N_3 \end{bmatrix} = \begin{bmatrix} 0 & -\frac{d}{dt} & -\frac{d}{dt} \\ 0 & -p_{21} & -p_{32} \\ w & 0 & -w-p_{32} \end{bmatrix}\begin{bmatrix} N_1 \\ N_2 \\ N_3 \end{bmatrix} \qquad (3.1)$$

Under continuous excitation, a steady state of thermodynamical equilibrium will be established. For $w \ll p_{21}, p_{32}$

$$N_2 \approx wN_oT$$

where $T = p_{21}^{-1}$ is the natural lifetime of level 2. It includes all the decay processes that originate from level 2 and end on level 1.

One can express w as the product σI_a, where σ is the absorption cross-section and I_a the intensity of incident radiation of

frequency range $d\nu_a$ around ν_a:

$$dN_2(\nu_a) = N_o \sigma I_a T \, d\nu_a \tag{3.2}$$

The intensity of fluorescence emission, I_f, in the frequency range $d\nu_f$ around ν_f, is proportional to the population of the fluorescent level and the probability for radiative transition, w_{21}, to the ground state.

$$I_f d\nu_f = N_o \sigma I_a T w_{21} d\nu_a d\nu_f \ . \tag{3.3}$$

On summing over ν_a while emission at ν_f is monitored, an excitation spectrum is obtained. Such a treatment may disclose absorption bands responsible for the energy storage and subsequent re-emission.

B. Pulsed Excitation

For simplicity, assume a step function time dependence of the exciting light of duration τ,

$$\omega(t) = \omega \left[\Pi(t) - \Pi(t - \tau) \right]$$

where $\Pi(t) = 1$ for $0 \leq t$

$= 0$ otherwise

The rate equations for the three-level system considered before are

$$\begin{aligned} N_o &= N_1 + N_2 + N_3 \\ \frac{dN_2}{dt} &= p_{32} N_3 - p_{21} N_2 \\ \frac{dN_3}{dt} &= -(p_{31} + p_{32}) N_3 + \omega(t)(N_1 - N_3). \end{aligned} \tag{3.4}$$

The solutions for $t \leq \tau$ are

$$N_3(t) = A + B\, e^{s_1 t} + C\, e^{s_2 t}$$

$$N_2(t) = D + E\, e^{s_1 t} + F\, e^{s_2 t}$$

where

$$A = \frac{\omega N_o p_{21}}{p_3 p_{21} + 2\omega p_{21} + \omega p_{32}}$$

$$= \frac{\omega N_o p_{21}}{s_1 s_2} ,$$

$$B = \frac{\omega N_o (s_1 + p_{21})}{s_1 (s_1 - s_2)} ,$$

$$C = \frac{\omega N_o (s_2 + p_{21})}{s_2 (s_2 - s_1)} ,$$

$$D = \frac{\omega N_o p_{32}}{s_1 s_2}$$

$$E = \frac{\omega N_o p_{32}}{s_1 (s_1 - s_2)}$$

$$F = \frac{\omega N_o p_{32}}{s_2 (s_2 - s_1)}$$

$$p_3 = p_{31} + p_{32}$$

$$s_{1,2} = \frac{1}{2} \{ -(p_3 + 2\omega + p_{21}) \pm [(p_3 + 2\omega + p_{21})^2 - 4\omega p_{32}]^{1/2} \}$$

For $t > \tau$,

$$N_3(t) = N_3(\tau)e^{-p_3(t-\tau)}$$

$$N_2(t) = \left[N_2(\tau) + \frac{p_{32}}{p_3-p_{12}} N_3(\tau)\right] e^{-p_{21}(t-\tau)} - \frac{p_{32}N_3(\tau)}{p_3-p_{21}} e^{-p_3(t-\tau)} \qquad (3.6)$$

where $N_2(\tau)$, $N_3(\tau)$ are given by (3.5) for $t = \tau$.

After the end of the exciting pulse, the fluorescence decay follows the same curve as $N_2(t)$ in (3.6).

Case 1 $\quad p_{32} \gg p_{21}$

The fluorescence decay is almost pure exponential with decay time p_{21}^{-1}.

Case 2 $\quad p_{32}N_3(\tau) \geq p_{21}N_2(\tau)$

The fluorescence reaches a maximum after the cessation of excitation and then decays exponentially.

C. Multilevel System

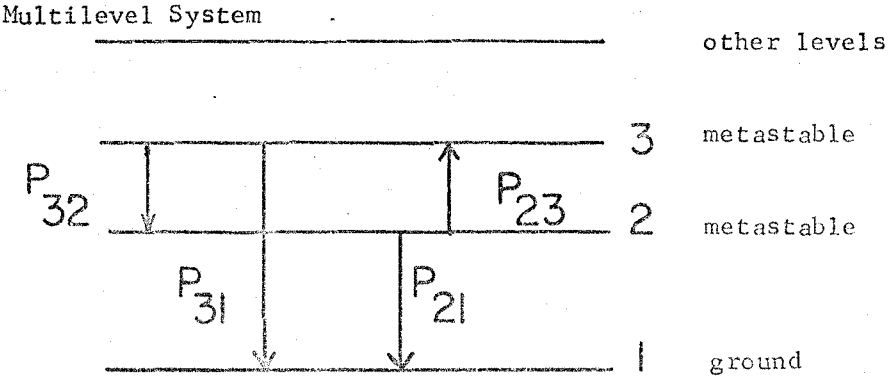

Consider a multilevel system shown schematically above with the usual notation. The transition probabilities include both radiative and non-radiative processes. Starting with an initial population N_3^o and N_2^o, the relaxation process is described by the following rate equations:

$$\frac{dN_3}{dt} = -\beta N_3 + p_{23} N_2$$

$$\frac{dN_2}{dt} = p_{32} N_3 - \alpha N_2 \qquad (3.7)$$

where $\alpha = p_{23} + p_{21}$

$\beta = p_{32} + p_{31}$

The solutions are

$$N_3(t) = \frac{N_3^o(s_1+\alpha)+N_2^o p_{23}}{s_1 - s_2} e^{s_1 t} + \frac{N_3^o(s_2+\alpha)+ N_2^o p_{23}}{s_2 - s_1} e^{s_2 t}$$

$$N_2(t) = \frac{N_2^o(s_2+\beta)+ N_3^o p_{32}}{s_1 - s_2} e^{s_1 t} + \frac{N_2^o(s_2+\beta)+ N_3^o p_{32}}{s_2 - s_1} e^{s_2 t} \qquad (3.8)$$

where $s_{1,2} = \frac{1}{2}\{-(\alpha+\beta) \pm [(\alpha+\beta)^2 - 4(\alpha\beta - p_{32}p_{23})]^{1/2}\}$

Particular case 1: Levels 2 and 3 strongly coupled by radiationless process.

$$P_{32},\ P_{23} \gg P_{21},\ P_{31}$$

$$N_3(t) = \frac{P_{23}(N_3^{\circ} + N_2^{\circ})}{P_{23} + P_{32}} e^{-pt} - \frac{P_{23}N_2^{\circ} - P_{32}N_3^{\circ}}{P_{23} + P_{32}} e^{-(P_{23}+P_{32})t}$$

$$N_2(t) = \frac{P_{32}(N_2^{\circ} + N_3^{\circ})}{P_{23} + P_{32}} e^{-pt} - \frac{P_{32}N_3^{\circ} - P_{23}N_2^{\circ}}{P_{23} + P_{32}} e^{-(P_{23}+P_{32})t} \qquad (3.9)$$

where $$p = \frac{P_{21}P_{32} + P_{31}P_{23}}{P_{32} + P_{23}} .$$

Since radiationless processes are extremely rapid, thermodynamical equilibrium is established very fast, resulting in a Boltzmann distribution of population in levels 2 and 3:

$$\frac{N_3^{\circ}}{N_2^{\circ}} \approx \frac{P_{23}}{P_{32}} = e^{-\frac{\Delta E_{32}}{kT}}$$

Hence (3.9) become

$$N_3(t) = N_3^{\circ}\, e^{-pt}$$

$$N_2(t) = N_2^{\circ}\, e^{-pt} \qquad (3.10)$$

It follows that fluorescence arising from these two levels have a common decay constant. In other words, fluorescence lines with the same decay constant need not come from the same level.

Case 2

$$P_{23} \approx 0.$$

$$N_3(t) = N_3^{\,o}\, e^{-(P_{32} + P_{31})t}$$

$$N_2(t) = \left(N_2^{\,o} + \frac{P_{32}\, N_3^{\,o}}{P_{32}+P_{31}-P_{21}}\right)e^{-P_{21}t} - \frac{P_{32}N_3^{\,o}\, e^{-(P_{32}+P_{31})t}}{P_{32} + P_{31} - P_{21}} \qquad (3.11)$$

A fluorescence line from level 3 has a pure exponential decay, while a line from level 2 decays with a time dependence consisting of the superposition of two exponentials.

Case 3

$$P_{23} \approx P_{32} \approx 0.$$

$$N_3(t) = N_3^{\,o}\, e^{-P_{31}t}$$

$$N_2(t) = N_2^{\,o}\, e^{-P_{21}t} \qquad (3.12)$$

It is obvious that when the two metastable levels are completely disconnected, each line decays with the characteristic time constant of the level from which it originates.

CHAPTER IV. THERMOLUMINESCENCE

From a thermodynamical point of view, a perfect crystal has a very low probability of existence at a finite temperature. A certain amount of defects has to be in equilibrium with the otherwise perfect crystal in order that the free energy of the whole system be a minimum.[1] Two common types of crystal defects are vacancies and interstitials. In the vicinity of the defect, say, a vacancy, the absence of an ion creates a potential well which would trap mobile electrons (or holes) that come close. These trapped electrons (or holes) are released by a supply of adequate thermal or photon energy. The mobile electrons and holes are created in pairs in the interaction of ionizing radiation with a crystal. To be specific, the case of x-irradiation of rare-earth doped CaF_2 will be considered.

When the crystal is x-irradiated at low temperature, an electron from a fluorine ion can be 'knocked' off leaving a hole behind. If the fluorine ion is a lattice ion, it can be represented in the band picture as lifting an electron from the valence band. If the fluorine ion is an interstitial one, it can be represented as removing the electron from a localized level slightly above the valence band, since it requires a little less energy to strip the electron from an interstitial fluorine ion than from one at a lattice site. The electron and hole pair can either recombine immediately or wander apart. In the latter case, the

electron may either find another hole for recombination, or be trapped (in which case the energy is stored in the crystal). The hole behaves in an analogous way.

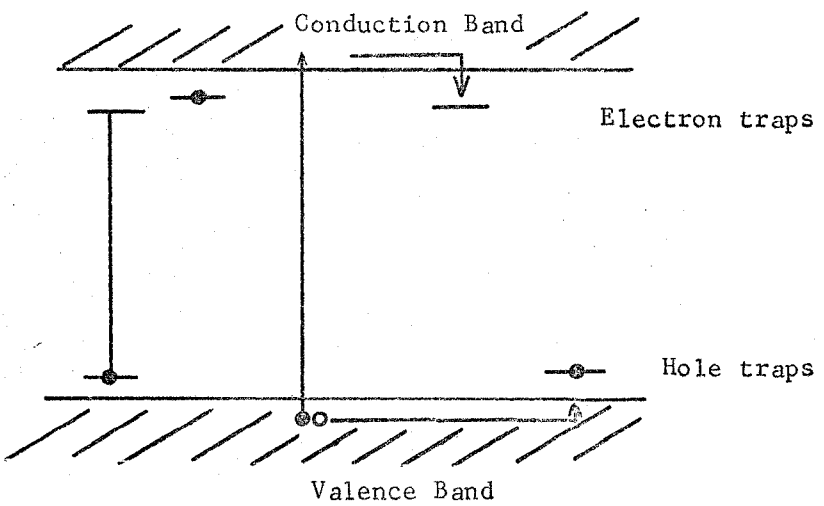

Since the trivalent rare-earth incorporated in CaF_2 is capable of being reduced to the divalent state, it behaves as an electron trap. Thus

$$\left.\begin{aligned} F^- &\xrightarrow{\text{x-ray}} F + e^- , \\ RE^{3+} + e^- &\rightarrow RE^{2+} , \\ F^- + F &\rightarrow \text{hole centre } (F_2^-) . \end{aligned}\right\} \quad (4.1)$$

Upon warming up the crystal, the hole centre is released and is able to meet a RE^{2+} ion from which it captures an electron. The hole centre then is annealed while the rare-earth is oxidized back to an excited trivalent state. Upon relaxation the characteristic radiation of the

RE^{3+} is emitted. Thus

$$\left.\begin{aligned} \text{hole centre} + RE^{2+} &\rightarrow F^- + F^- + RE^{3+}\ (\text{excited}) \\ RE^{3+}\ (\text{excited}) &\rightarrow RE^{3+} + h\nu \end{aligned}\right\} \quad (4\cdot2)$$

The intensity of this emission depends naturally on the rate at which the hole centres are released. The existence of more than one glow peak in thermoluminescence leads to the conclusion that more than one type of hole centres, with different activation energies are present. The nature of these different types of hole centres in CaF_2 is still not well understood. Only one type, viz., the V_k centre, is positively identified[2,3]. It is formed of two atoms of fluorine sharing one electron, like a F_2^- molecule. The axis of the 'molecule' lies along the edge of the cube of the fluorine sub-lattice.

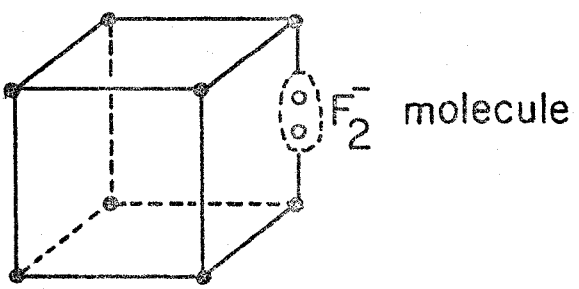

At low temperature, the 'hopping' motion of the V_k centre is limited to one dimension along its axis. At about $130^oK.$, the centre has apparently enough energy to diffuse in all directions and may combine with an electron trap.

The splitting pattern of the emission represented by (4.2) depends on the symmetry the RE^{3+} (excited) has during the annihilation of the hole centre. For instance, if the centre ends up as an interstitial ion adjacent to the rare-earth, the latter has a surrounding with tetragonal symmetry. If, on the other hand, the centre gains back its electron and ends up as a charge compensator far away from the rare-earth, then the latter remains in an essentially cubic environment. Of course, there is every possibility that different rare-earth ions in the sample have different symmetries at the same time, which, unfortunately, complicates the interpretation, if not making it impossible.

As a complementary study to elucidate the nature of these luminescence centres, the method of 're-excitation' can be applied[4]. Basically, the crystal is first x-irradiated at a higher temperature, say, room temperature, and then cooled down to liquid nitrogen temperature, say. If, at this stage, the sample is warmed up, the 'normal' thermoluminescence glow peaks will not appear until the temperature is above that at which the sample is irradiated. This is attributed to the fact that irradiation at high temperature results in the filling of relatively 'deep' traps, which are released only at still higher temperatures. If the sample is exposed to a short burst of ultraviolet light before being warmed up, most of the normal glow peaks can be regained. The ultraviolet light serves to release some of the deeply trapped holes (or electrons) and redistribute them into some of the shallower traps, before the warming. The efficiency of 'exciting' the low temperature peaks seems to depend on the frequency of the ultraviolet light employed. It may serve as an

indicator of the trap depths and/or the amount of retrapping, as well as the nature of the trapped species, i.e. electrons or holes.

CHAPTER V. EXPERIMENTAL

A. Crystal Samples

The crystals used throughout this investigation were obtained from Harshaw Chemical Co. The dopant concentration was about 0.1%. The samples were cleaved or cut and polished into thin slabs of about 1x5x5 mm. and mounted on the cold finger of a vacuum cryostat (custom made by the Andonian Associates Inc.). For heat treatment, the sample was put in an open porcelain crucible and heated in an oven. The temperature of the oven was raised to 900°C. or 1000°C. in three to four hours and maintained thereabout for one hour. Some five to six hours were allowed for the sample to cool to room temperature after heating.

B. Fluorescence and Excitation Spectra of $CaF_2:Dy^{3+}$

The experimental set up was as shown schemetically in Fig. 5.1. The detector used was an RCA 1P28* photomultiplier. The spectrograph was set to pass yellow (corresponding to $^4F_{9/2} - {}^6H_{15/2}$ transition) emission. For recording the two emission spectra, the detector was replaced by a camera. Kodak Tri-X and Kodak Spectroscopic film type 130a-0 respectively were used for the yellow and blue regions. For recording the excitation spectra, the monochromator was driven by a motor for scanning** while the yellow (or blue) emission was monitored. The

---

*Spectral response characteristic S5.

**The motor speed was 1 r.p.m. and was slow enough for the recording system which has a response time of 0.2 sec. Backlash of the monochromator was negligible.

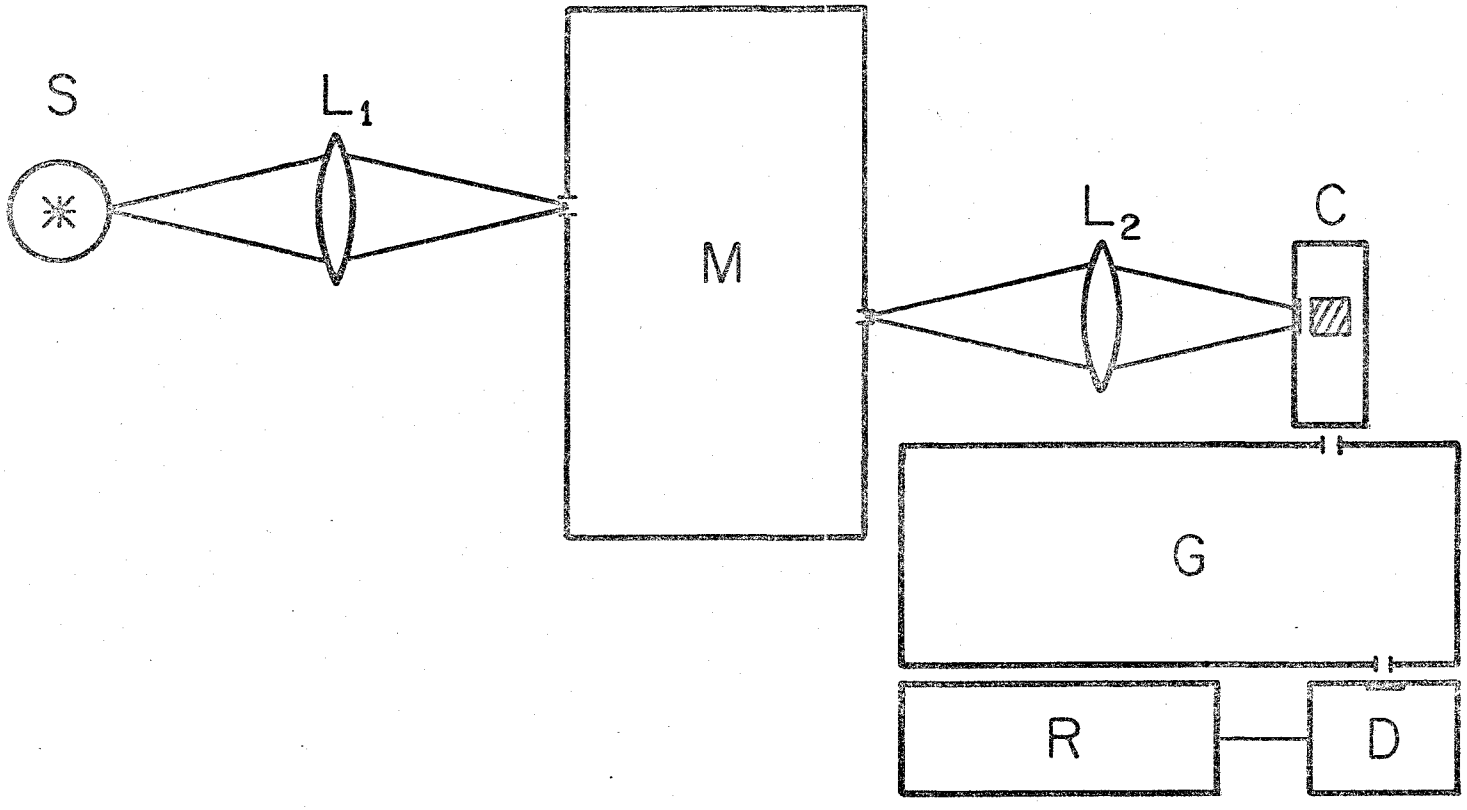

Fig. 5.1. Experimental set up for fluorescence and excitation measurements.

S= 1 kW xenon arc lamp, $L_{1,2}$ = quartz lenses, M = double monochromator

C = crystal in cryostat, G = spectrograph, D = detector, R = recorder.

output of the photomultiplier was fed to a Keithley 610 electrometer and then to a Philips 8100 strip chart recorder.

Fig. 5.2. shows the excitation spectrum in which the yellow emission was monitored. After heat treating the crystal to 900°C., the spectrum was modified to that shown in Fig. 5.3. As the intensity of emission after heat treatment increased about five folds, a narrower slit width could be used resulting in better resolution. Essentially the same spectrum was obtained by monitoring in the blue emission instead of the yellow[1].

Fig. 5.4. to 5.7. are luminescence spectra obtained by illuminating into one of the strong excitation peaks of the excitation spectra.

C. Decay Time Measurements in the $CaF_2:Dy^{3+}$ and $CaF_2:Ho^{3+}$ Systems

The experimental set up is shown schemetically in Fig. 5.8. The power of the Q-switched ruby laser was about half megawatt (pulse duration about $5x10^{-7}$ sec.). The firing rate was once every 90 sec. A small portion of the laser beam was monitored through a beam splitter by an RCA 925 phototube whose output was fed to one of the two beams of a Tektronix 555 oscilloscope. The small He-Ne gas laser shown in the figure was used for alignment purposes. The detector was an RCA 1P28 photomultiplier cooled by liquid air. The dark current has been reduced by almost two orders of magnitude by the cooling.

The crystal was first x-irradiated at liquid nitrogen temperature for 90 minutes, using a copper target x-ray tube operating at

50 KV and 14 mA. After being removed from the x-ray source, the sample decayed spontaneously emitting a very weak phosphorescence, which was just detectable by the system using maximum amplification.

Figs. 5.9a and b show microdensitometer traces of the spontaneous decay spectra at constant (liquid nitrogen) temperature by putting the cryostat directly in front of the spectrograph and exposing for two hours.

The laser light was focused slightly in front of the freshly x-irradiated sample to avoid any damage by concentrated heating. As the laser light hit the crystal, the phosphorescence was much enhanced. The signal from the photomultiplier was fed directly to the other beam of the oscilloscope. The two beams were synchronized and triggered by the laser monitor. The traces were photographed and the decay time measured.* About twenty photographs were taken for the strongest peak in each group and the decay time averaged.

By scanning the monochromator, a spectral distribution of the signal amplitudes was obtained. Figs. 5.10. - 5.13. are such spectral distributions and Figs. 5.14. - 5.15. are typical oscillograms of the enhanced phosphorescence decay for $CaF_2:Dy^{3+}$. Figs. 5.16. - 5.26. are similar results for $CaF_2:Ho^{3+}$.

An effort has been made to determine the decay time at different temperatures. Since it was not practicable to x-irradiate the crystal using liquid helium as cryogen, the x-irradiation was still done at liquid nitrogen temperature, and the sample subsequently cooled down further by liquid helium. At the end of a run, the sample was allowed

---

*By setting the monochromator to pass some scattered laser light the detecting system was found to be useful up to the 10^{-7} sec. range.

to warm up slowly to room temperature and the decay curves taken. Table 5.1 and 5.2 are summary of the decay times measured under different conditions. At present, there is no thermometer available in this laboratory to measure temperatures below 77°K. A rough estimate of the sample temperature was made as the line width narrowed.

TABLE 5.1. DECAY TIMES OF $CaF_2:Dy^{3+}$

Transition	Wavenumber (10^3 cm^{-1})	Temperature	Decay Time*(10^{-3} sec.)	
			Before Heat Treatment	After Heat Treatment
$^4F_{9/2} \rightarrow {}^6H_{15/2}$	20.8	77°K	3.5	
		20°K**	4.5	
	20.1	77°K	2.5	1.6
$^4F_{9/2} \rightarrow {}^6H_{13/2}$	17.2	77°K	2.5	1.6
		20°K		1.4

* Error = ± 10%

** Rough estimate based on narrowing of line width, see Fig. 5.27.

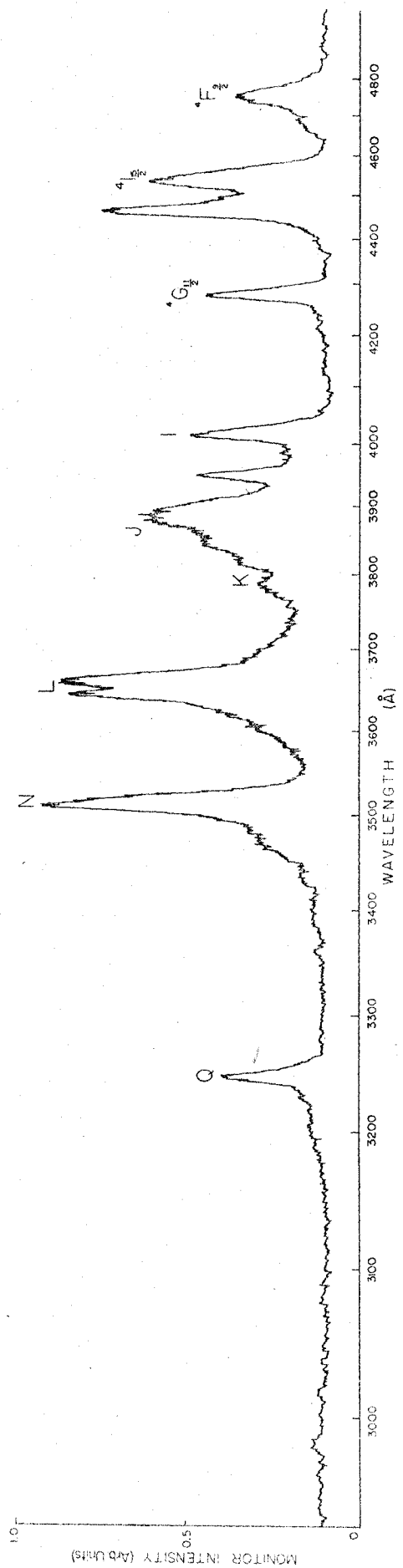

Fig. 5.2 Excitation spectrum of $CaF_2:Dy^{3+}$ at $77^{o}K$ before heat treatment.

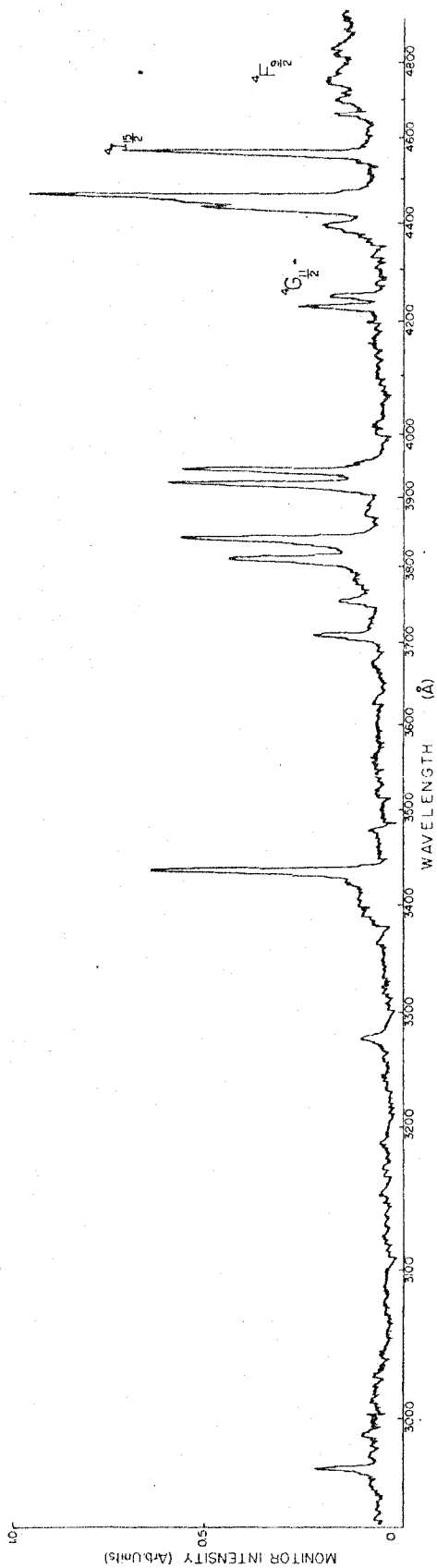

Fig. 5.3 Excitation spectrum of $CaF_2:Dy^{3+}$ at $77^{\circ}K$ after heat treatment.

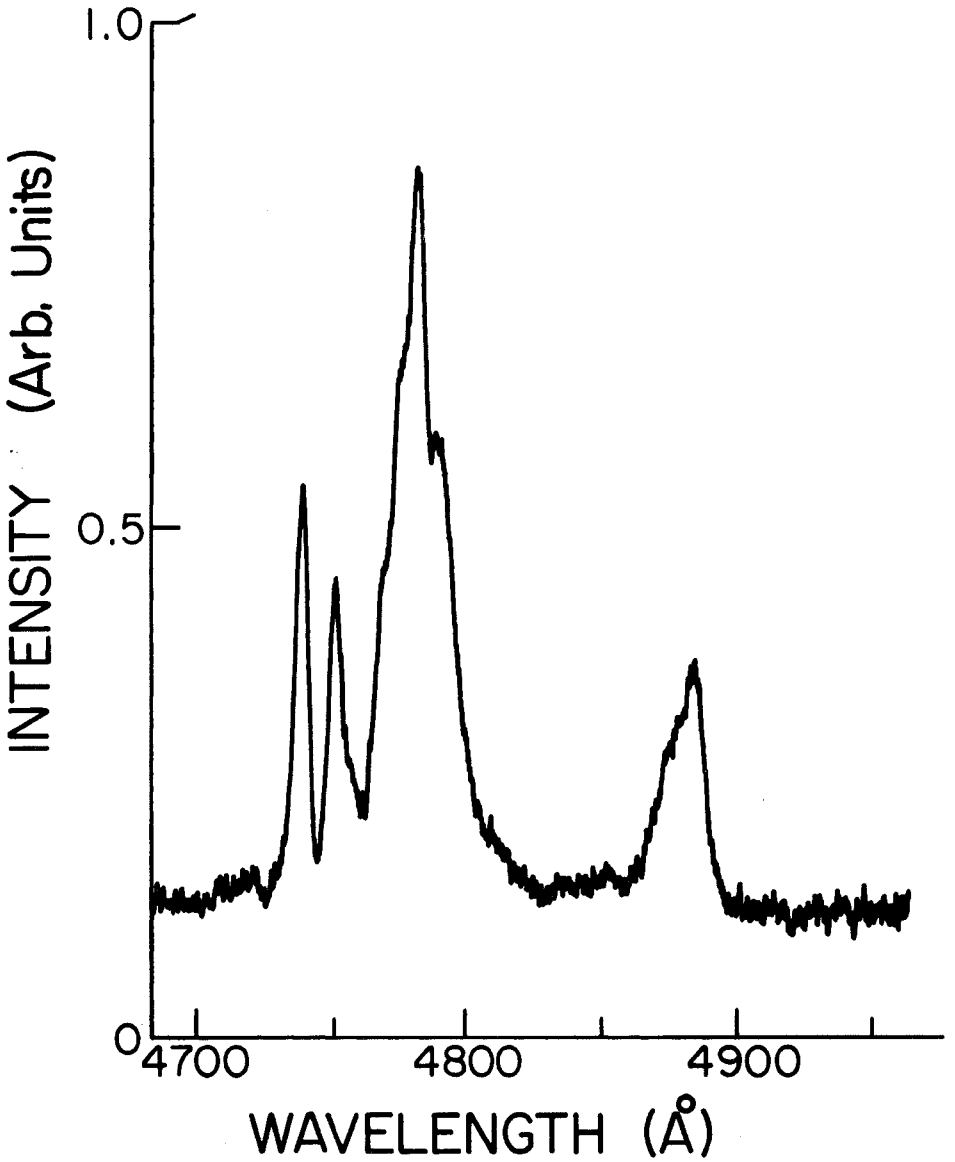

Fig. 5.4. Luminescence spectrum of $CaF_2:Dy^{3+}$ at 77°K before heat treatment.

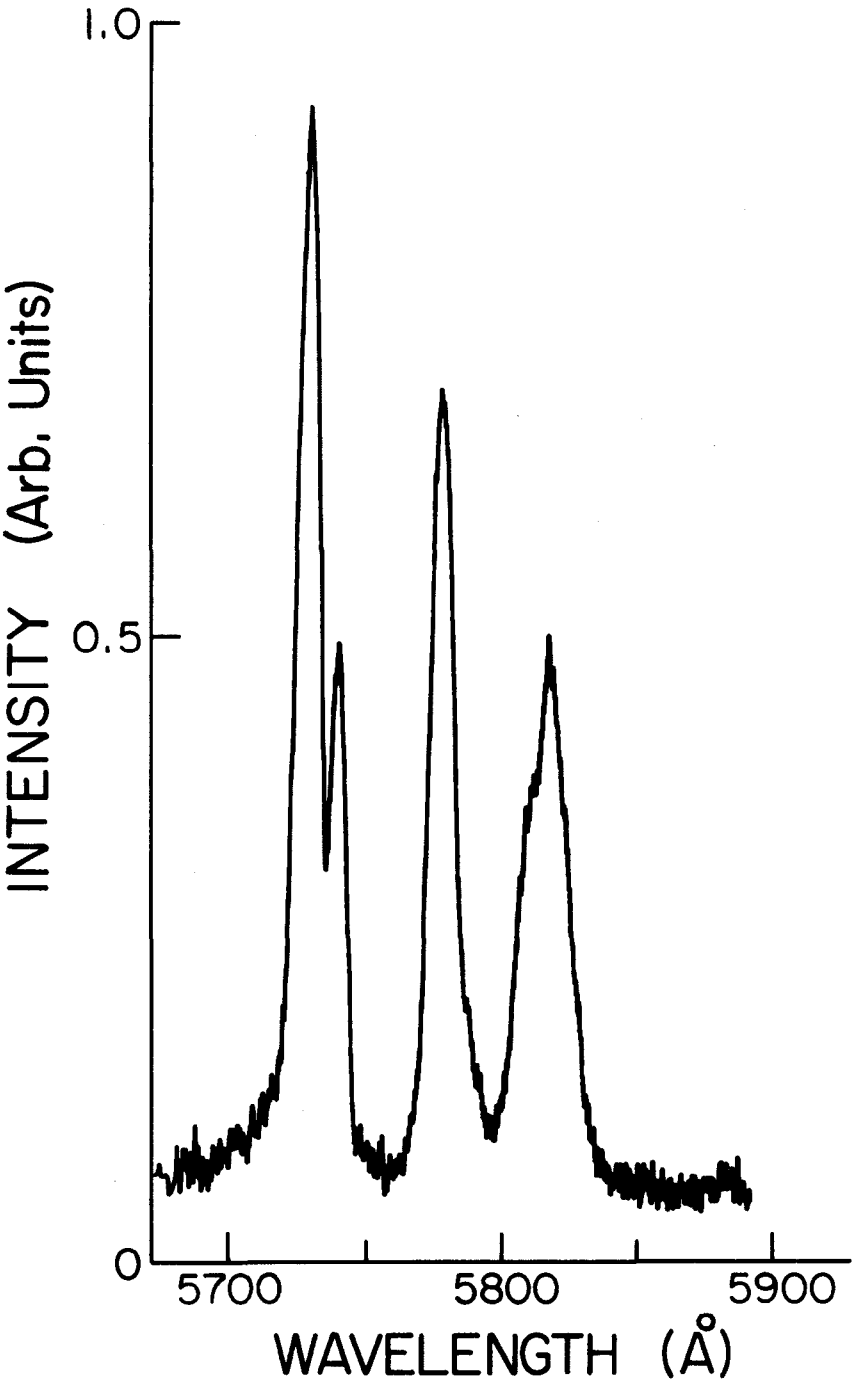

Fig. 5.5 Luminescence spectrum of $CaF_2:Dy^{3+}$ at 77°K before heat treatment.

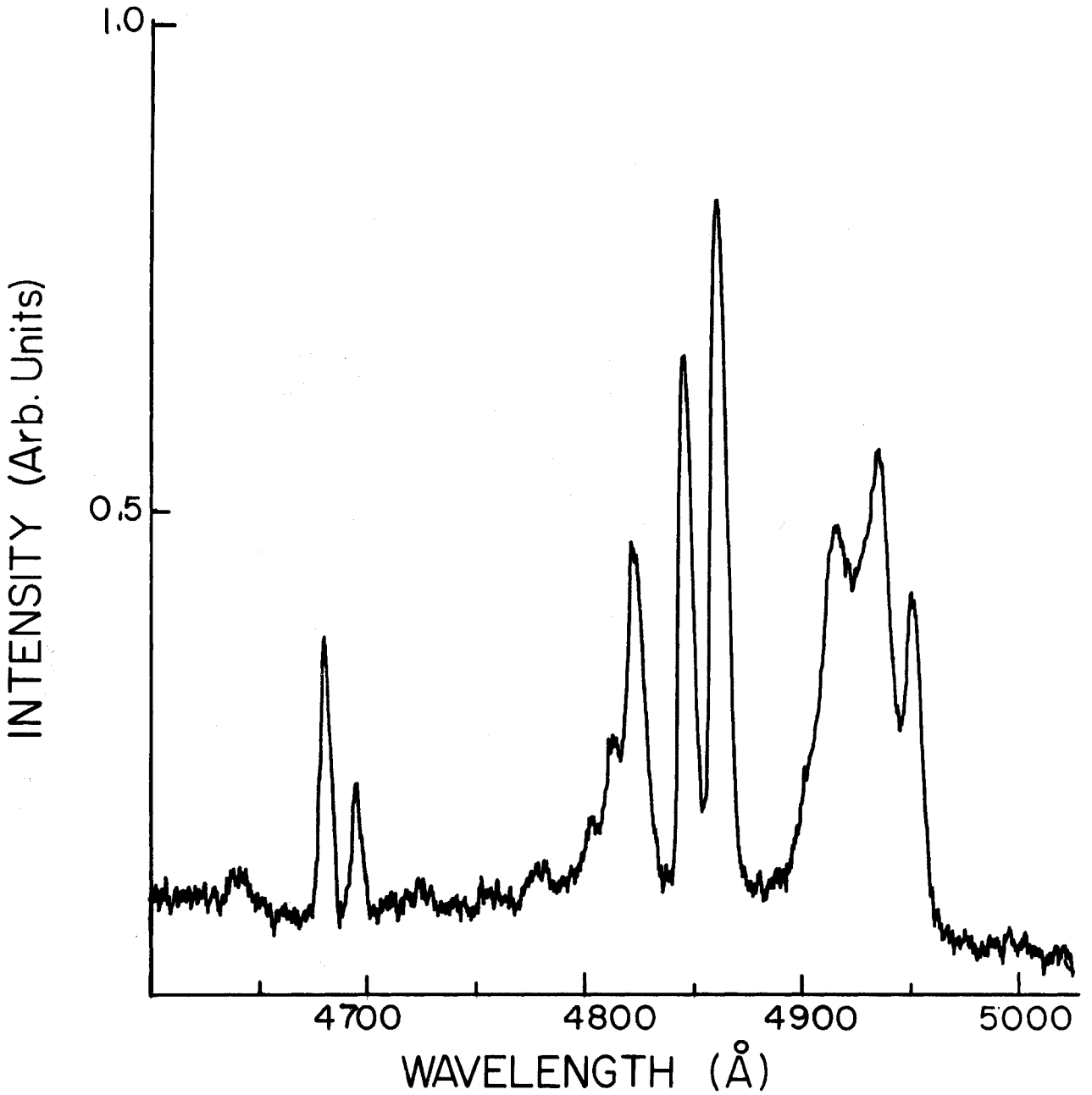

Fig. 5.6 Luminescence spectrum of $CaF_2:Dy^{3+}$ at 77°K after heat treatment.

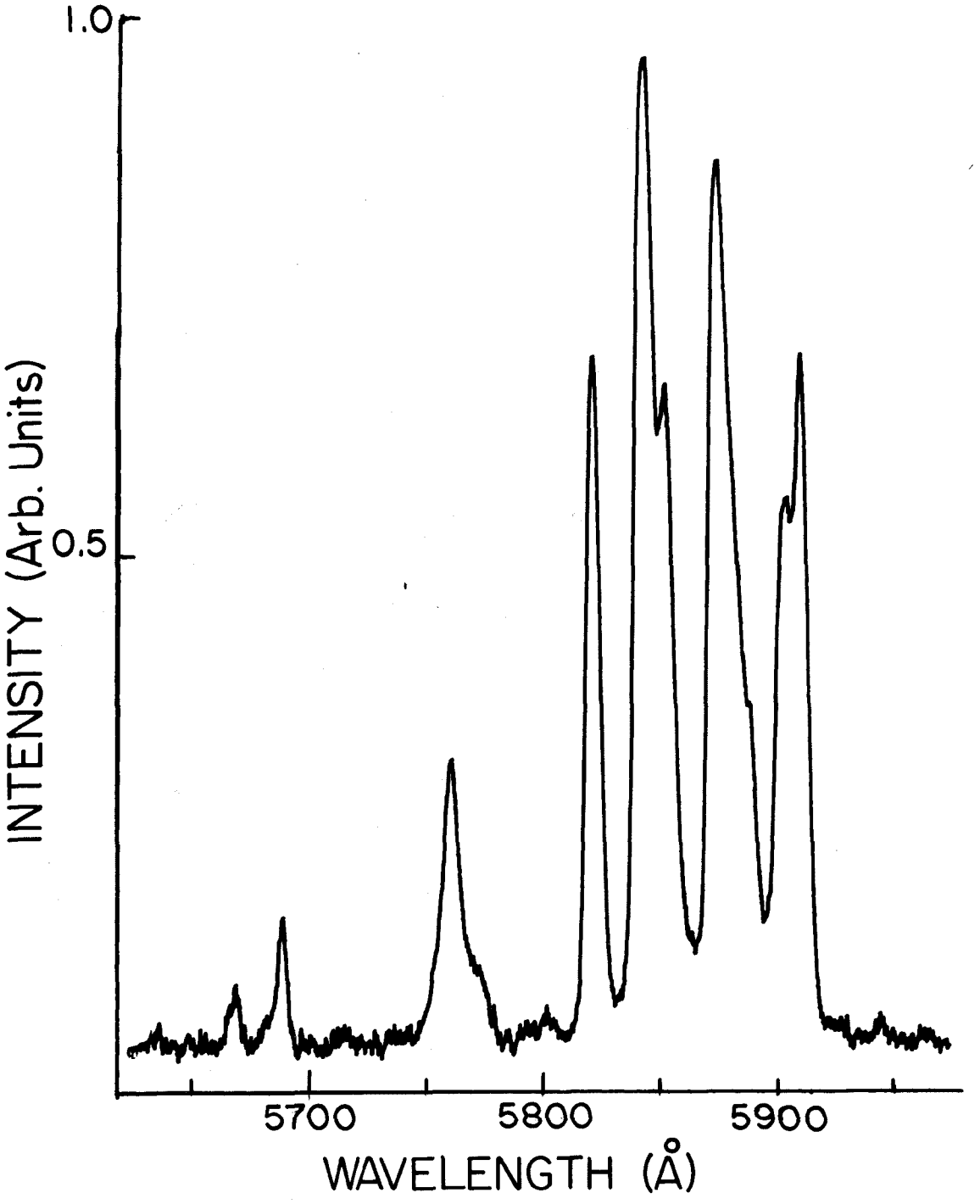

Fig. 5.7 Luminescence spectrum of $CaF_2:Dy^{3+}$ at 77°K after heat treatment.

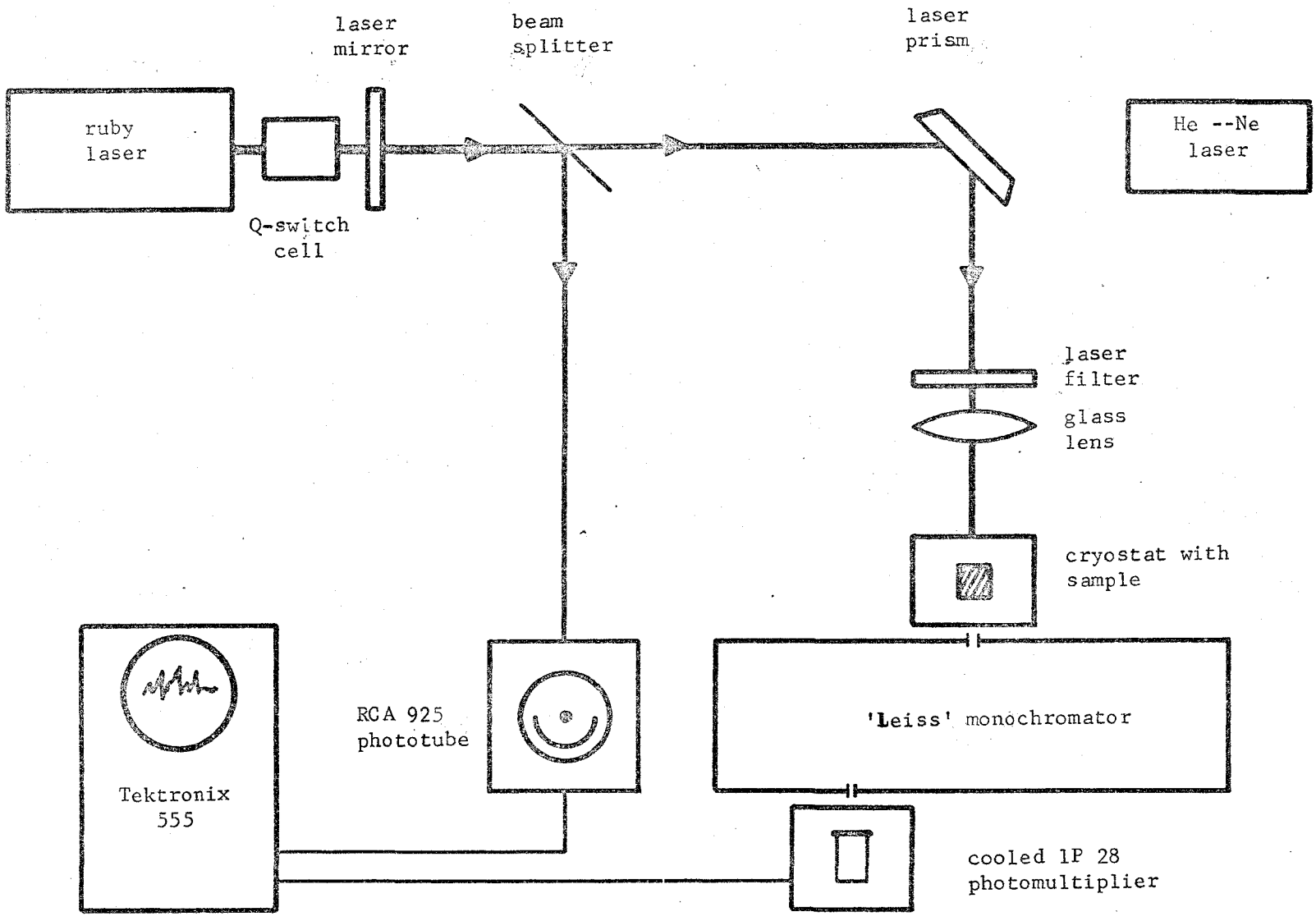

Fig. 5.8 Experimental set up for decay time measurements.

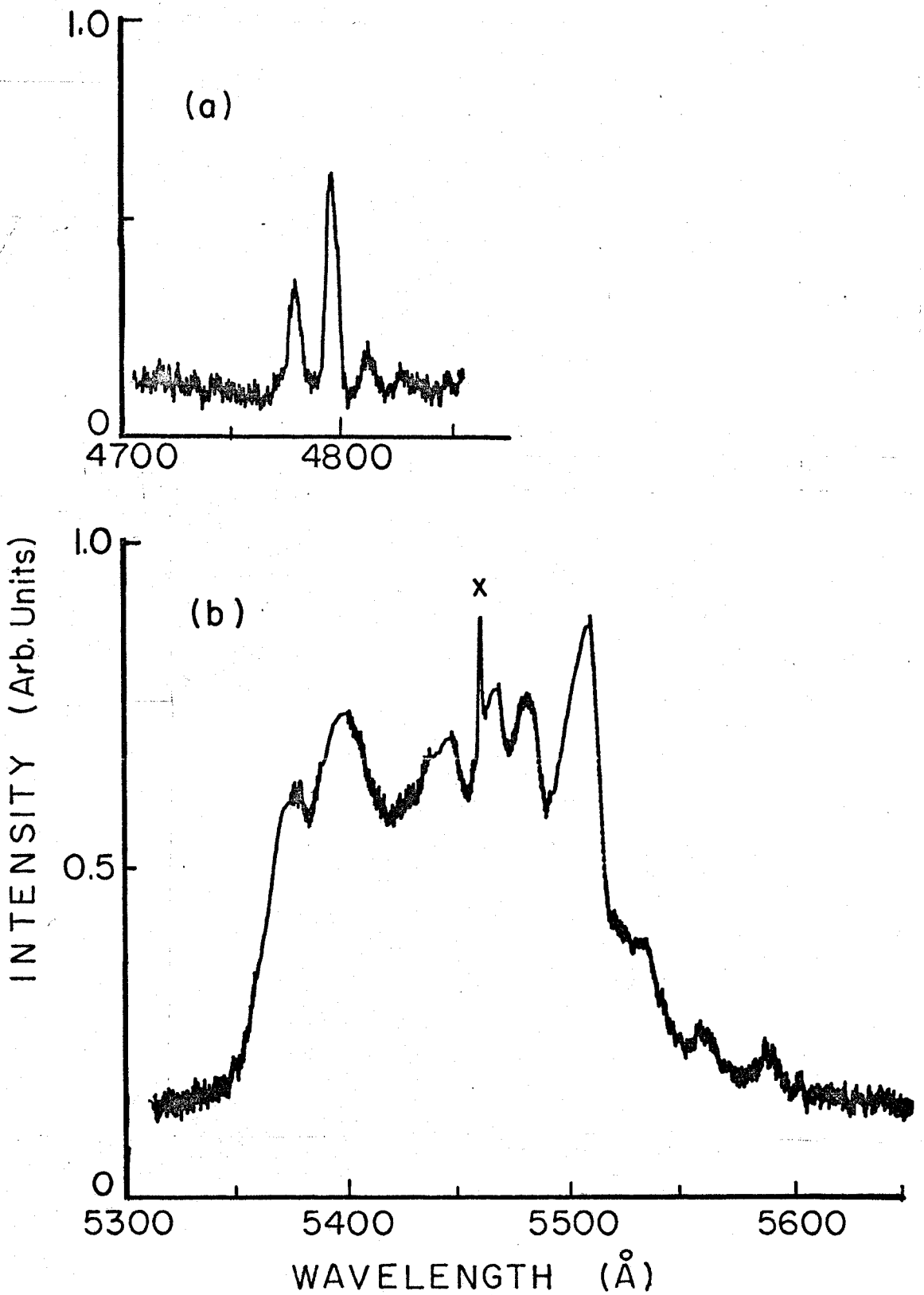

Fig. 5.9. Constant temperature phosphorescence of (a) $CaF_2:Dy^{3+}$ and (b) $CaF_2:Ho^{3+}$. X is the 5460 Å mercury line.

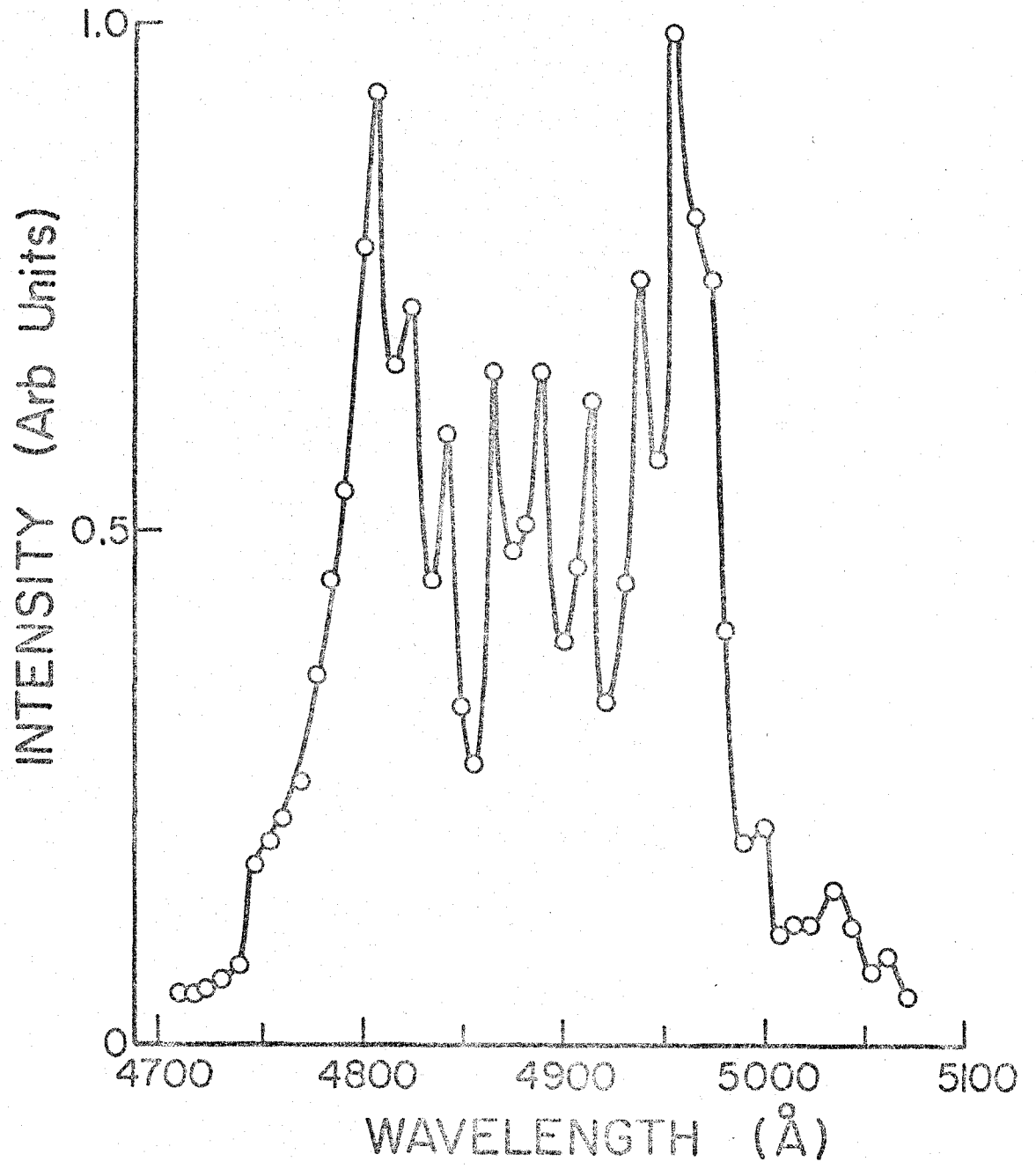

Fig. 5.10. Spectral distribution of enhanced phosphorescence of $CaF_2:Dy^{3+}$ before heat treatment.

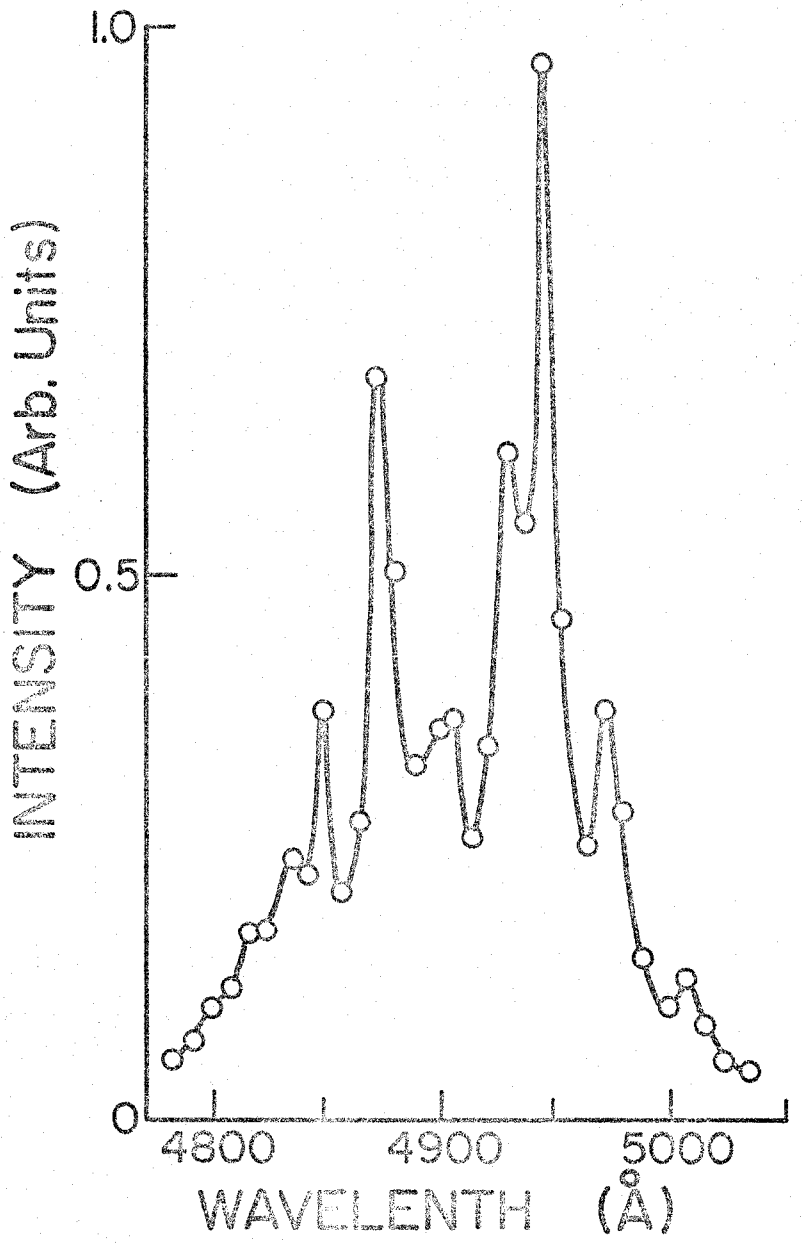

Fig. 5.11. Spectral distribution of enhanced phosphorescence of $CaF_2:Dy^{3+}$ after heat treatment.

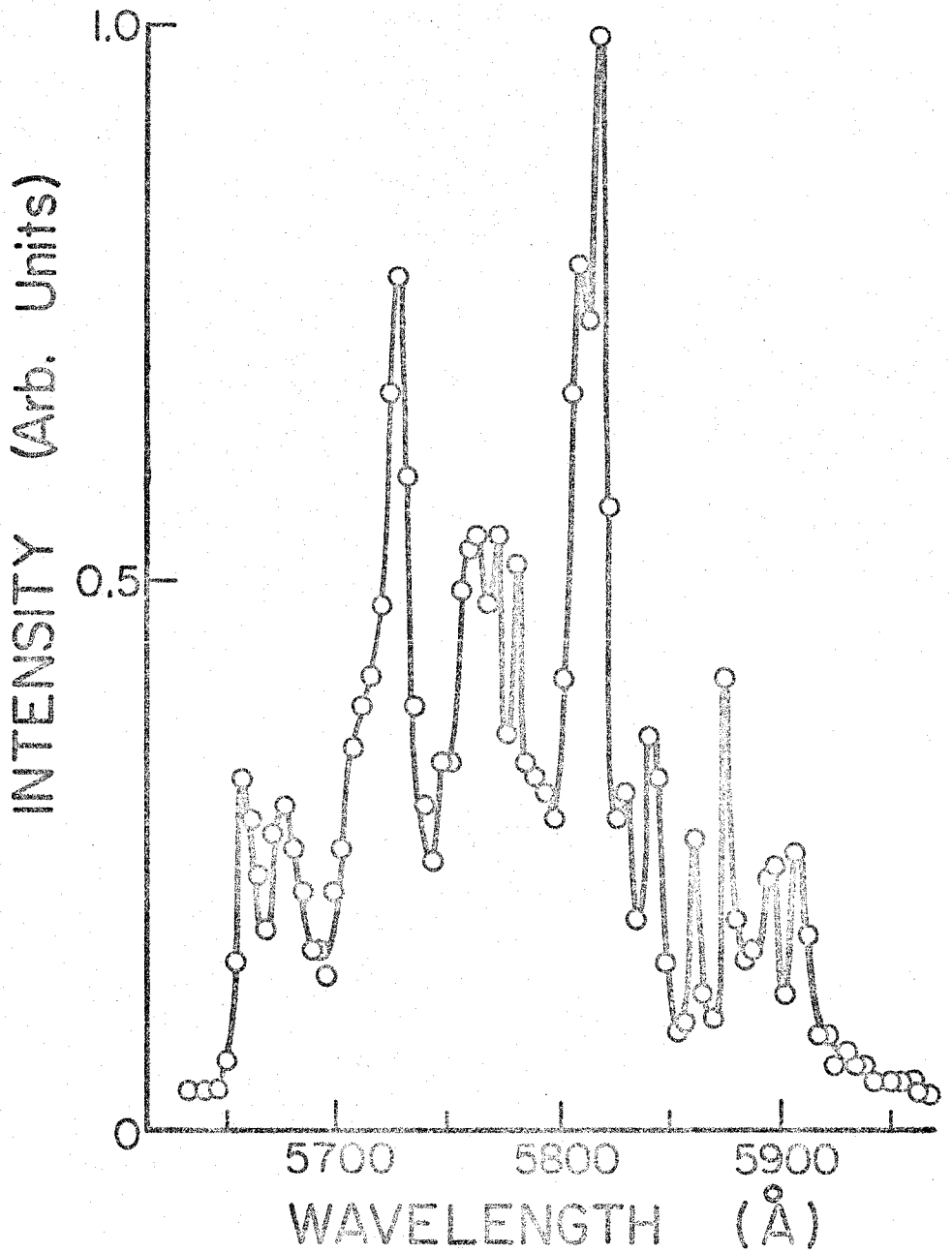

Fig. 5.12. Spectral distribution of enhanced phosphorescence of $CaF_2:Dy^{3+}$ before heat treatment.

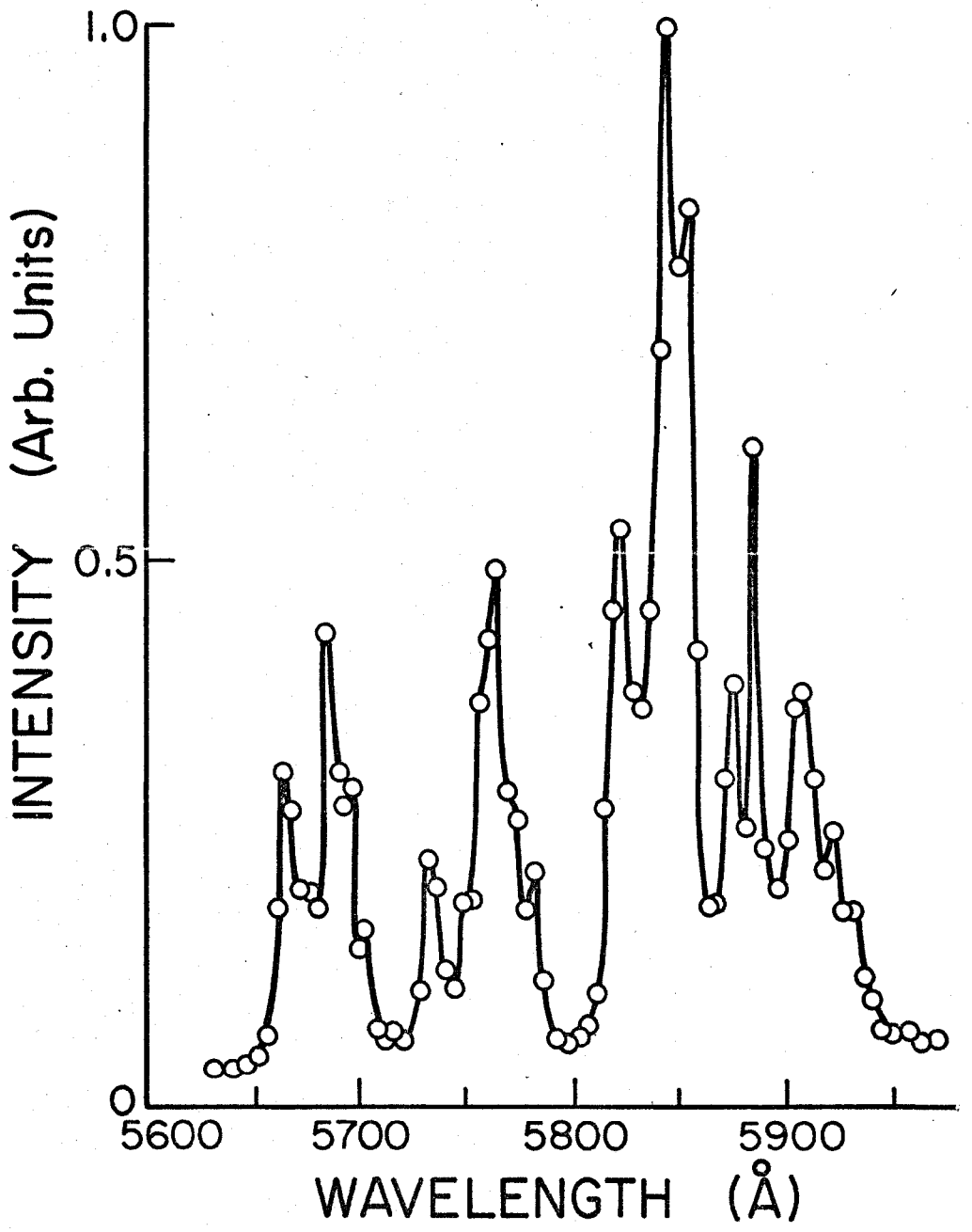

Fig. 5.13. Spectral distribution of enhanced phosphorescence of $CaF_2:Dy^{3+}$ after heat treatment.

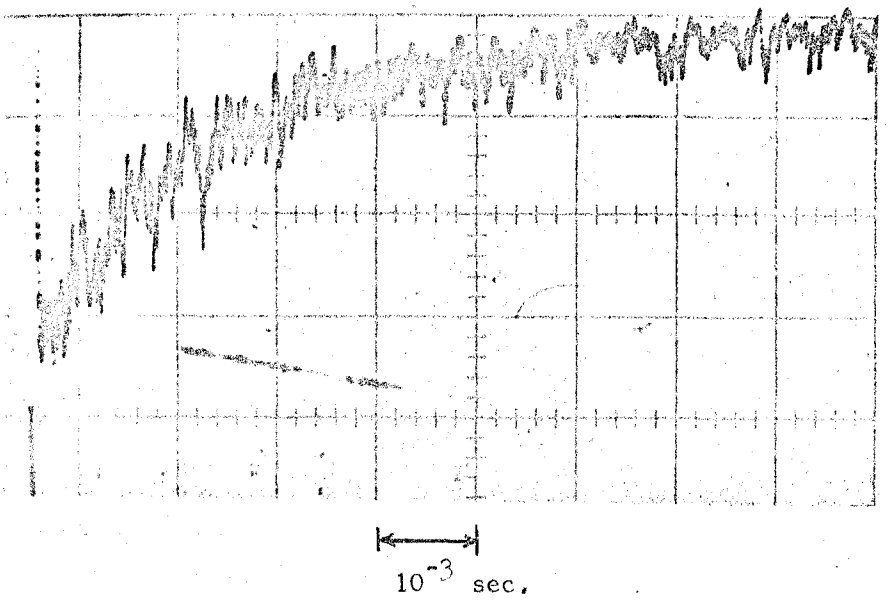

Fig. 5.14 Enhanced phosphorescence decay of $CaF_2:Dy^{3+}$ ($^4F_{9/2}$ to $^6H_{15/2}$) before heat treatment.

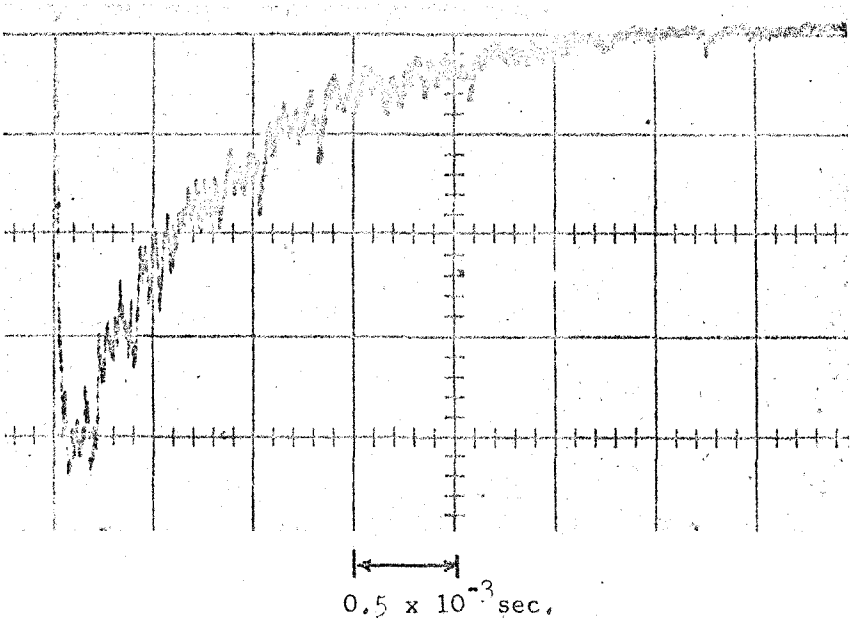

Fig. 5.15 Enhanced phosphorescence decay of $CaF_2:Dy^{3+}$ ($^4F_{9/2}$ to $^6H_{15/2}$) after heat treatment.

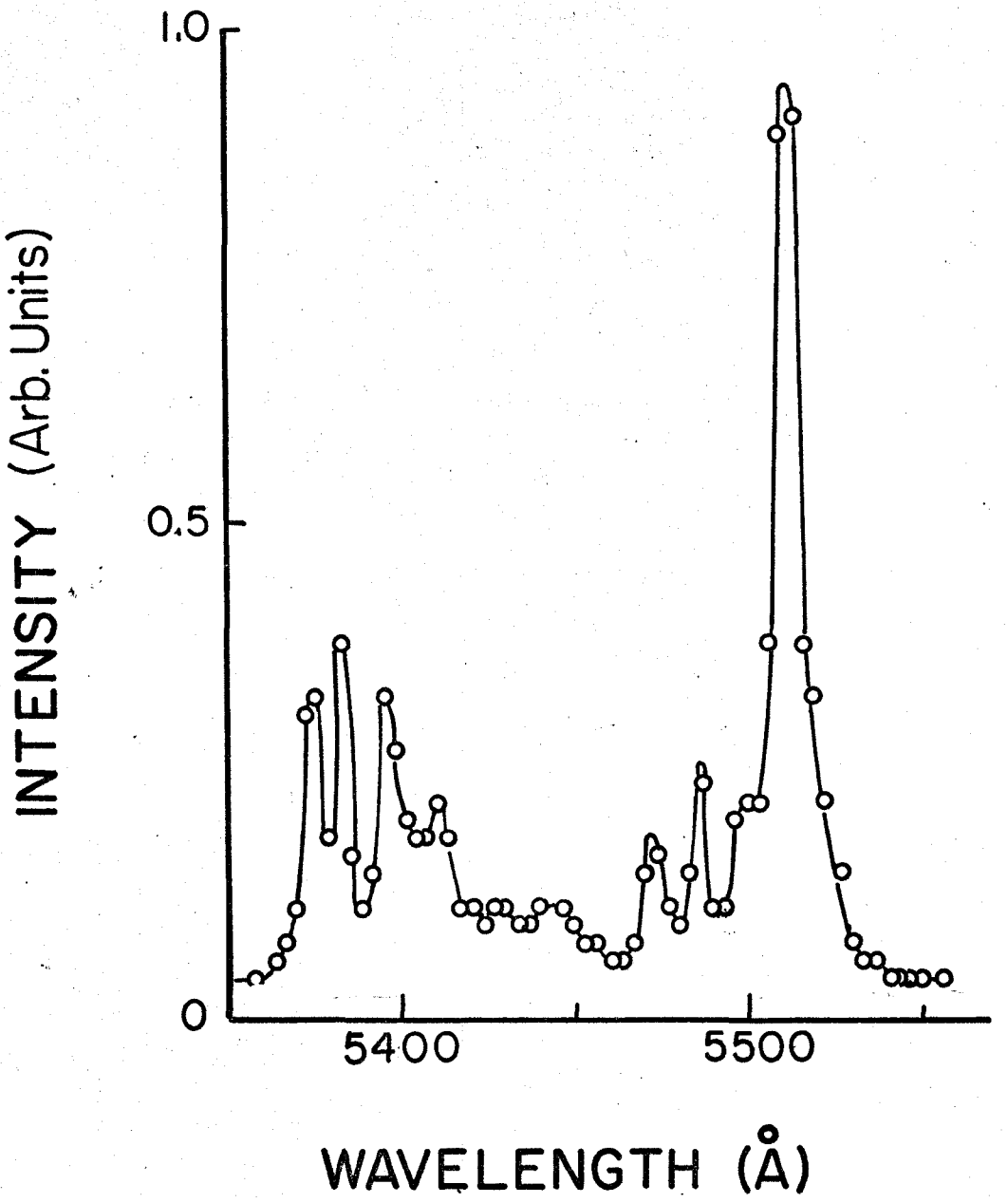

Fig. 5.16 Spectral distribution of amplitudes of enhanced phosphorescence of $CaF_2:Ho^{3+}$ before heat treatment. ($^5F_4$, $^5S_2$ to $^5I_8$)

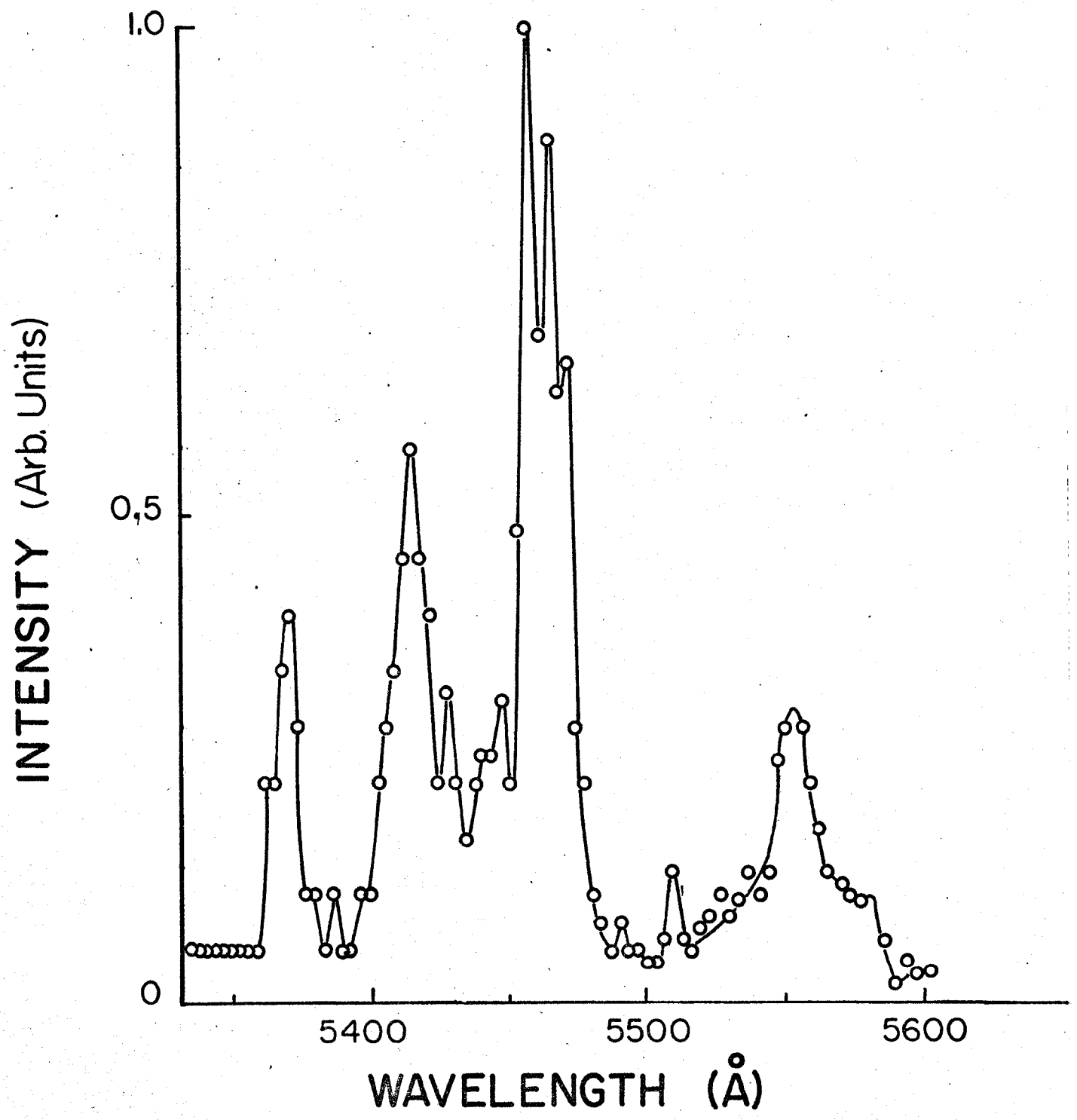

Fig. 5.17 Spectral distribution of amplitudes of enhanced phosphorescence of $CaF_2:Ho^{3+}$ after heat treatment. ($^5F_4$, $^5S_2$ to $^5I_8$)

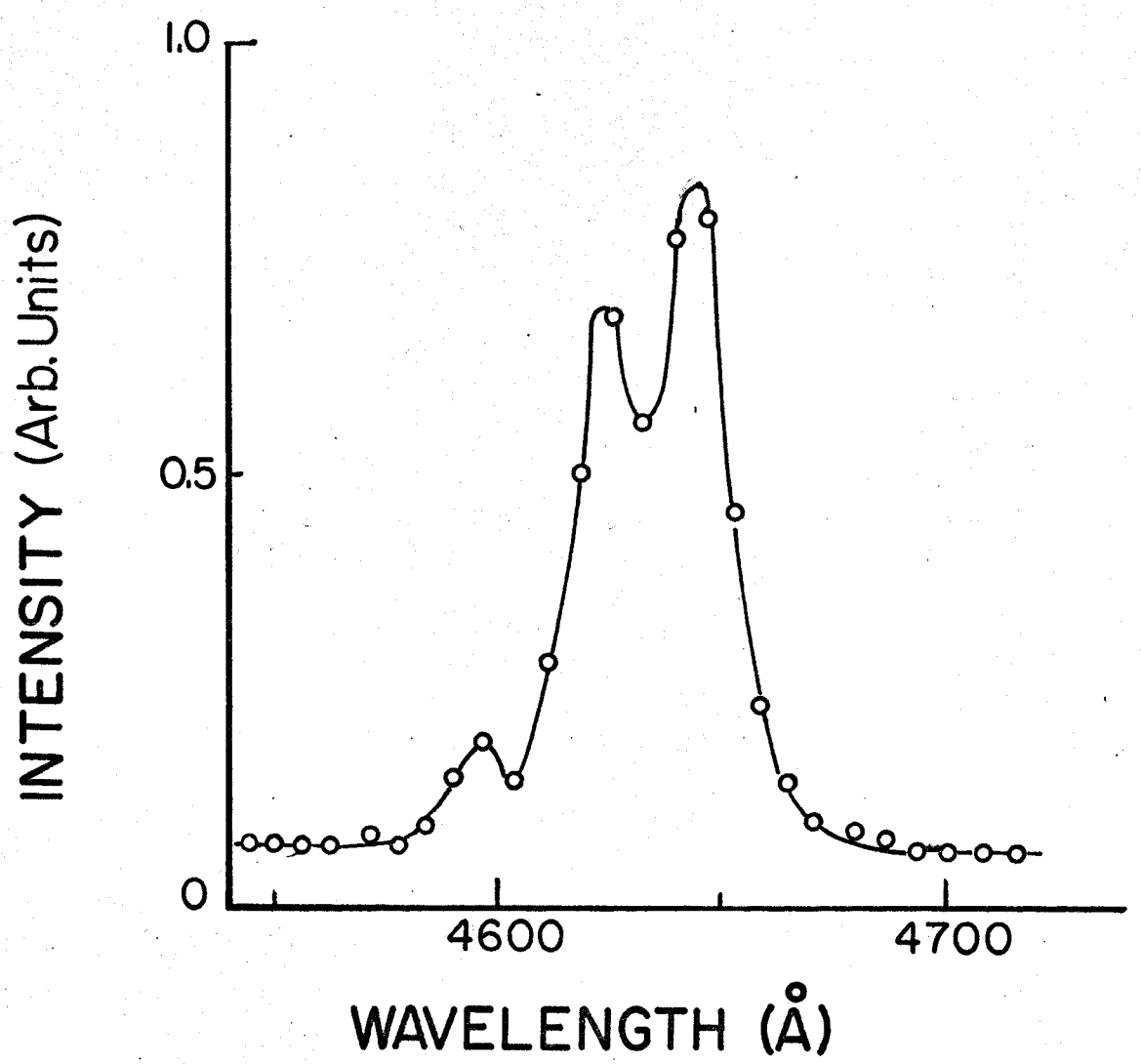

Fig. 5.18 Spectral distribution of amplitudes of enhanced phosphorescence of $CaF_2:Ho^{3+}$ after heat treatment. ($^3K_8$ to $^5I_8$)

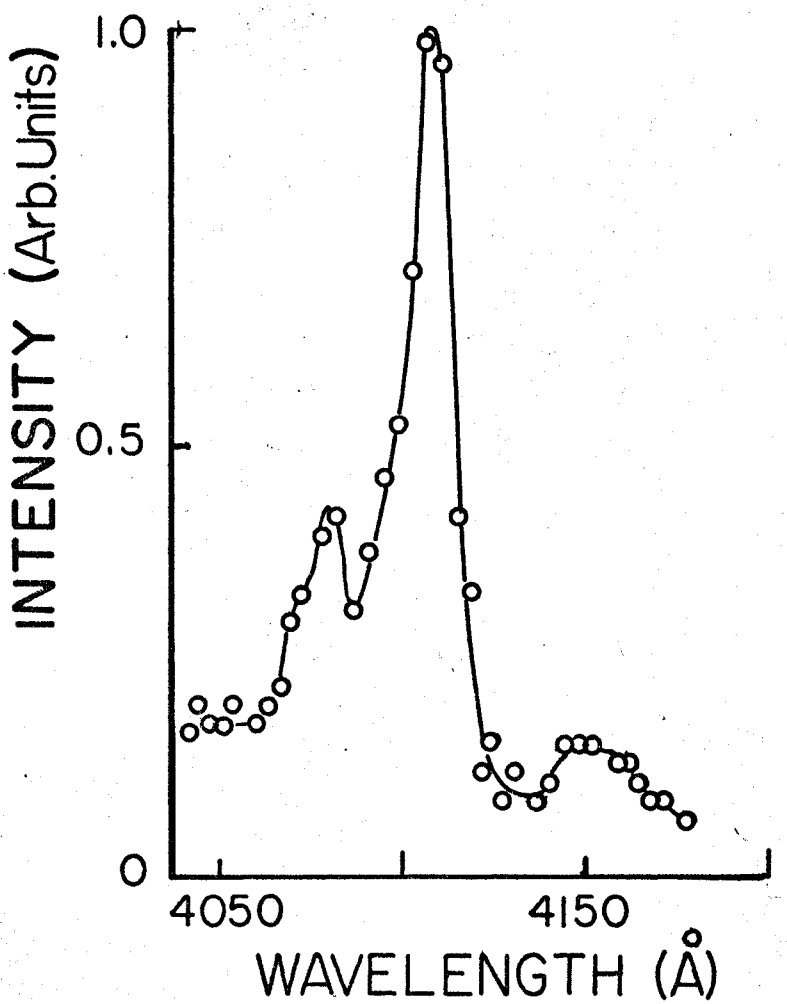

Fig. 5.19 Spectral distribution of amplitudes of enhanced phosphorescence of $CaF_2:Ho^{3+}$ before heat treatment. ($^5G_5$ to $^5I_8$)

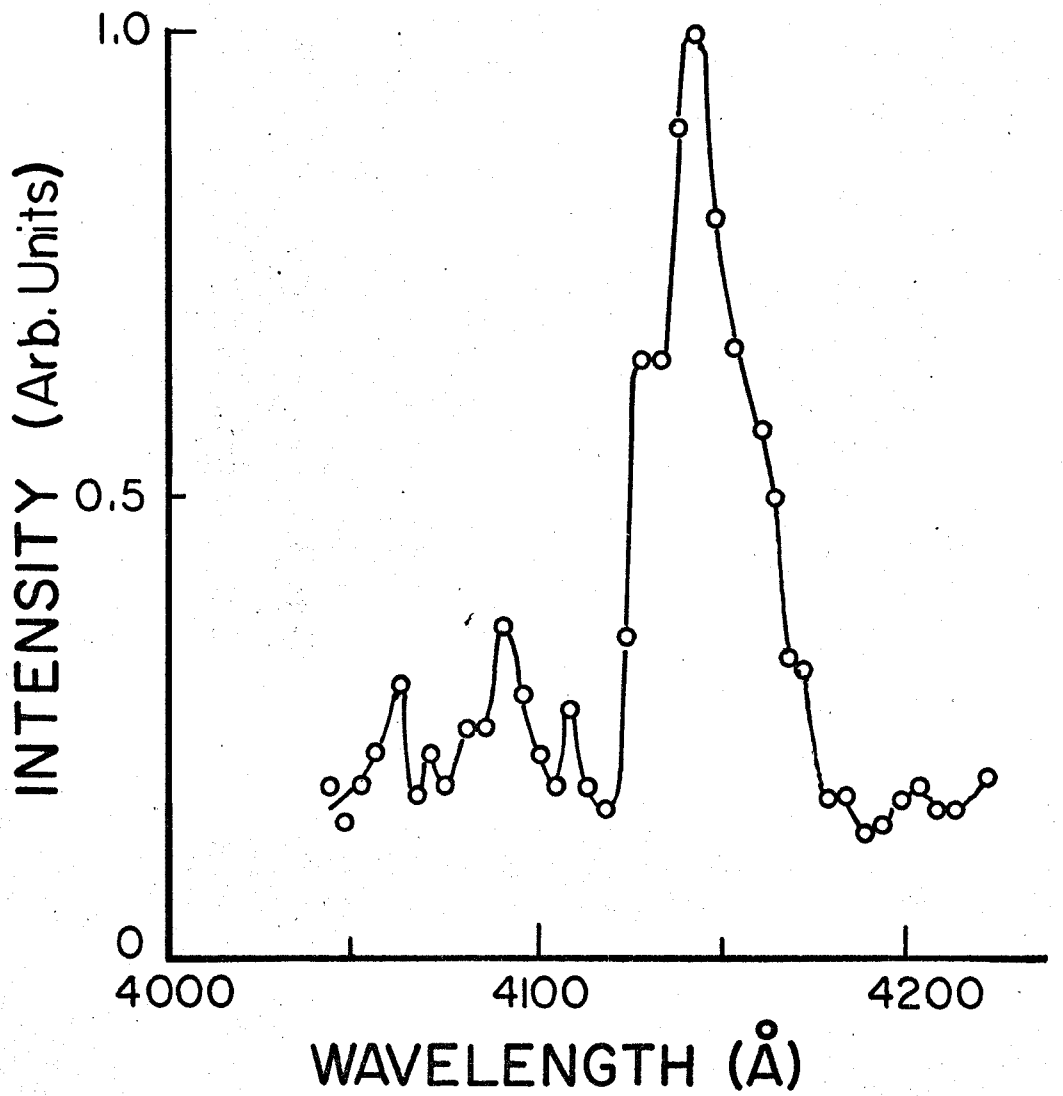

Fig. 5.20 Spectral distribution of amplitudes of enhanced phosphorescence of $CaF_2:Ho^{3+}$ after heat treatment.

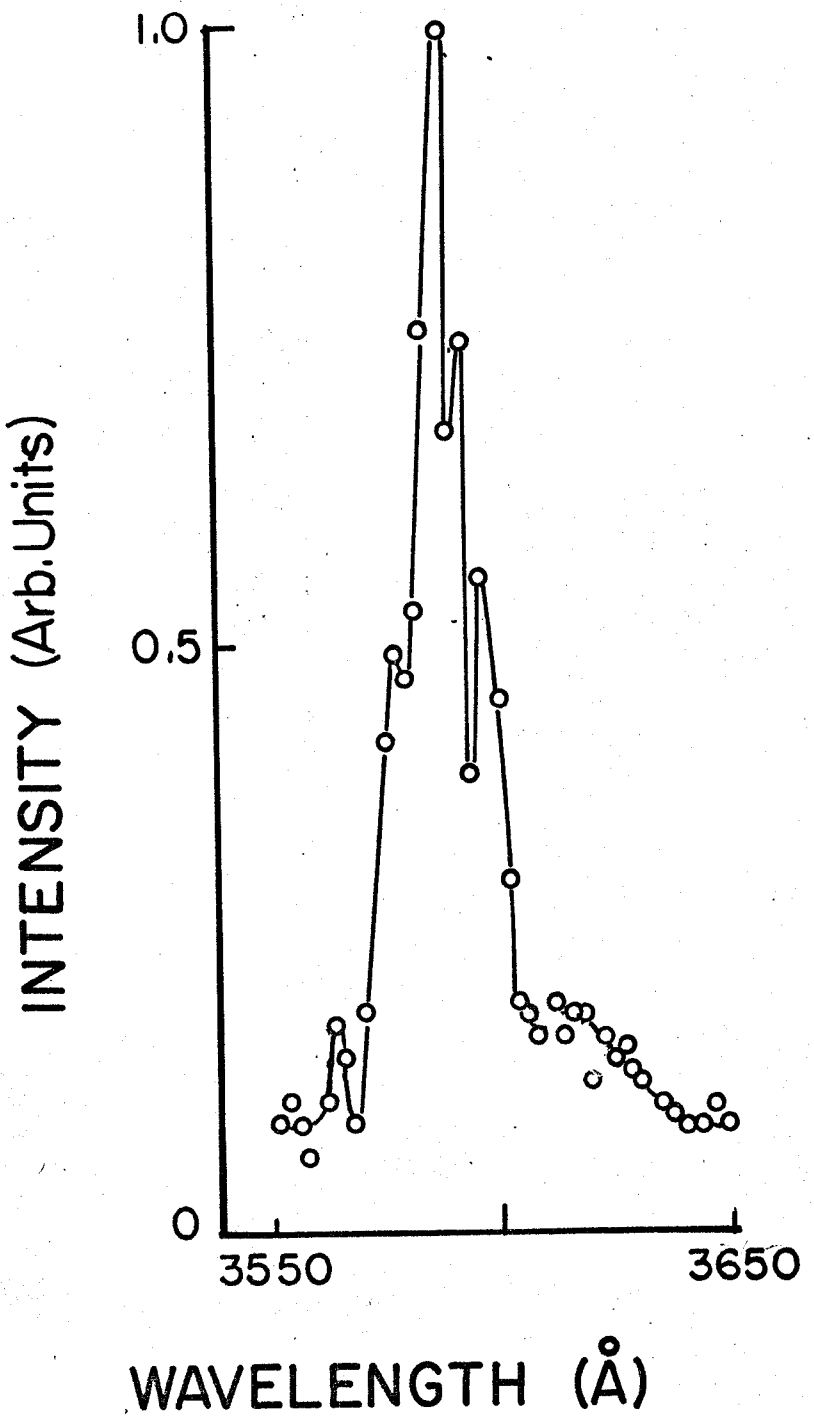

Fig. 5.21 Spectral distribution of amplitudes of enhanced phosphorescence of $CaF_2:Ho^{3+}$ before heat treatment.

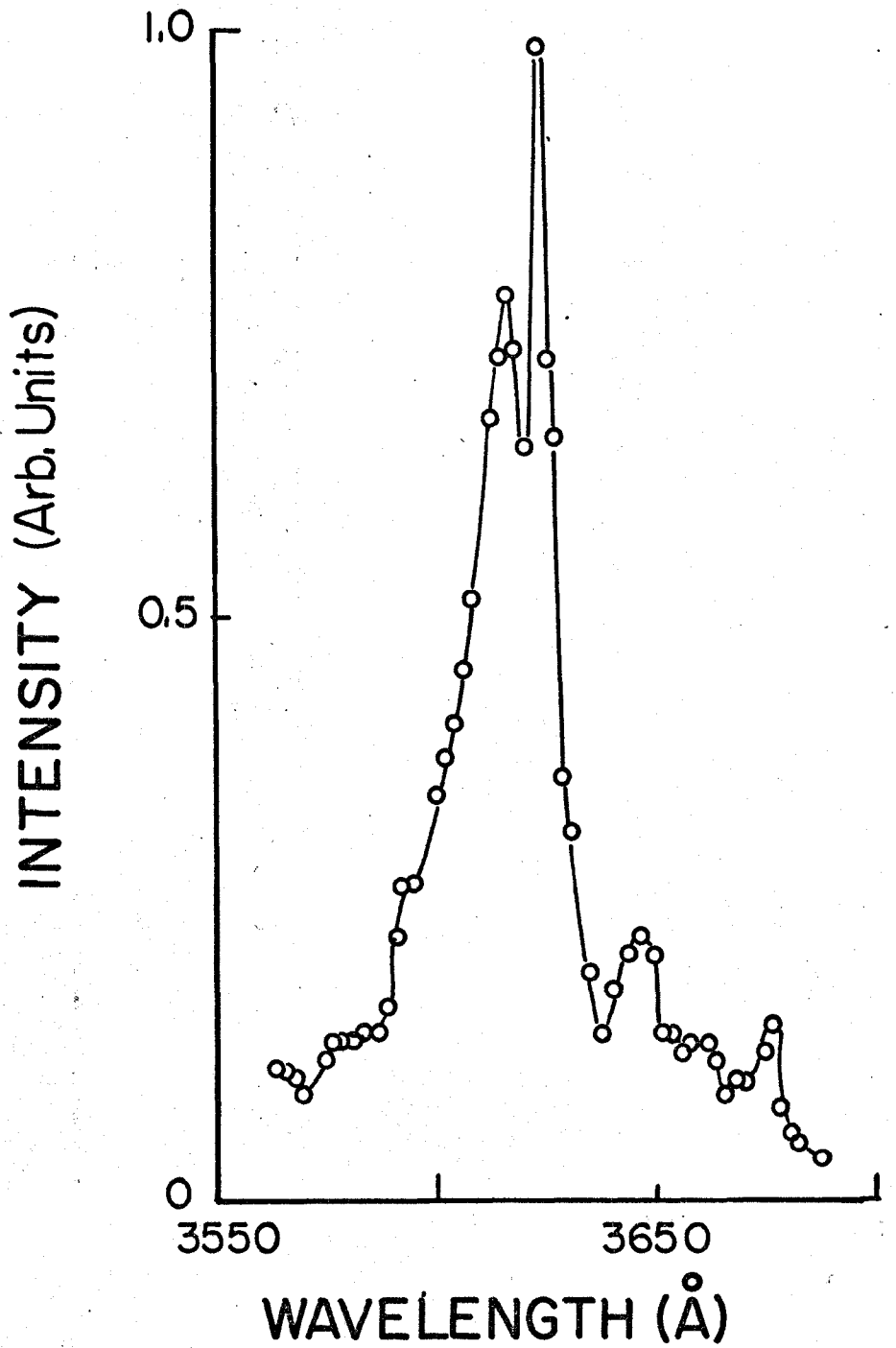

Fig. 5.22 Spectral distribution of amplitudes of enhanced phosphorescence of $CaF_2:Ho^{3+}$ after heat treatment.

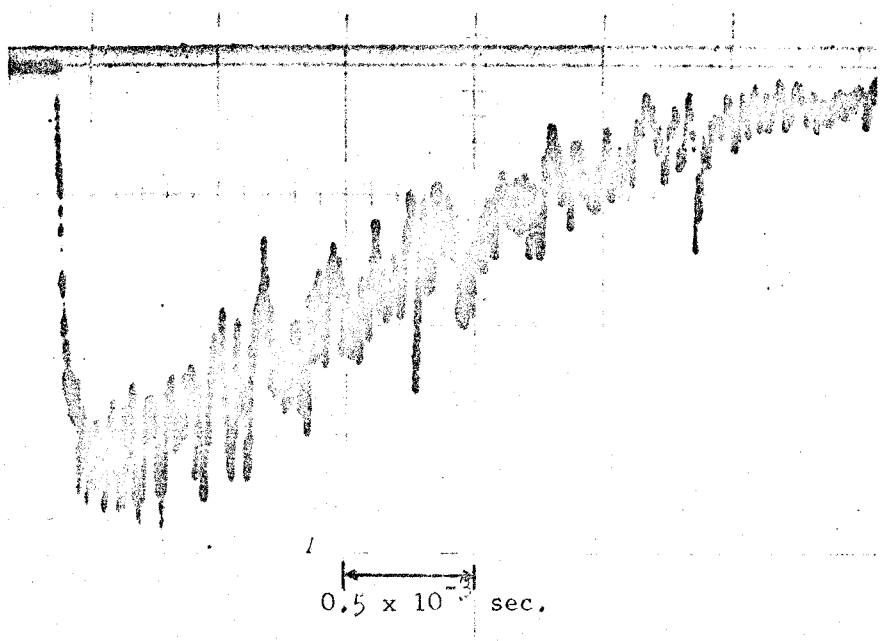

Fig. 5.23 Enhanced phosphorescence decay of $CaF_2:Ho^{3+}$ ($^5F_4$, $^5S_2$ to $^5I_8$) before heat treatment.

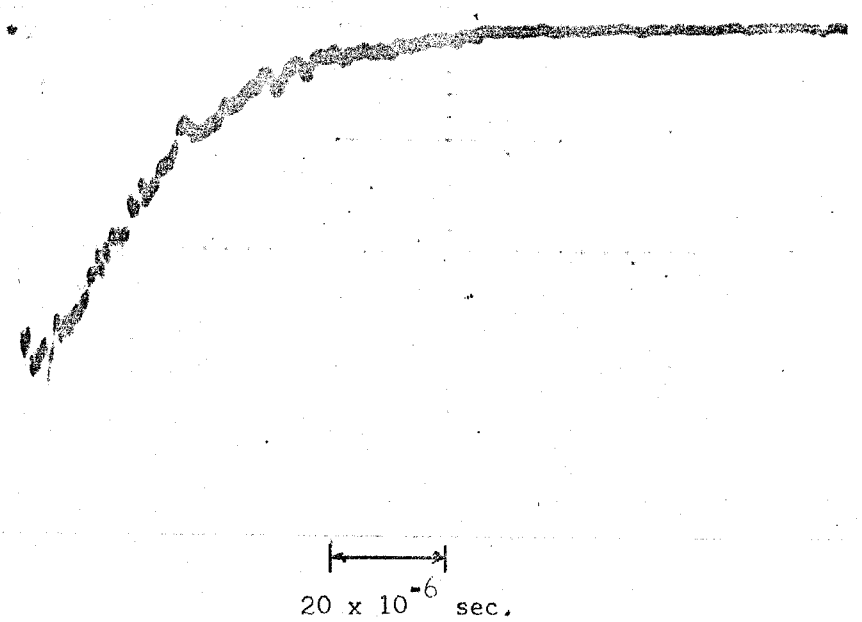

Fig. 5.24 Enhanced phosphorescence decay of $CaF_2:Ho^{3+}$ ($^5F_4$, $^5S_2$ to $^5I_8$) after heat treatment.

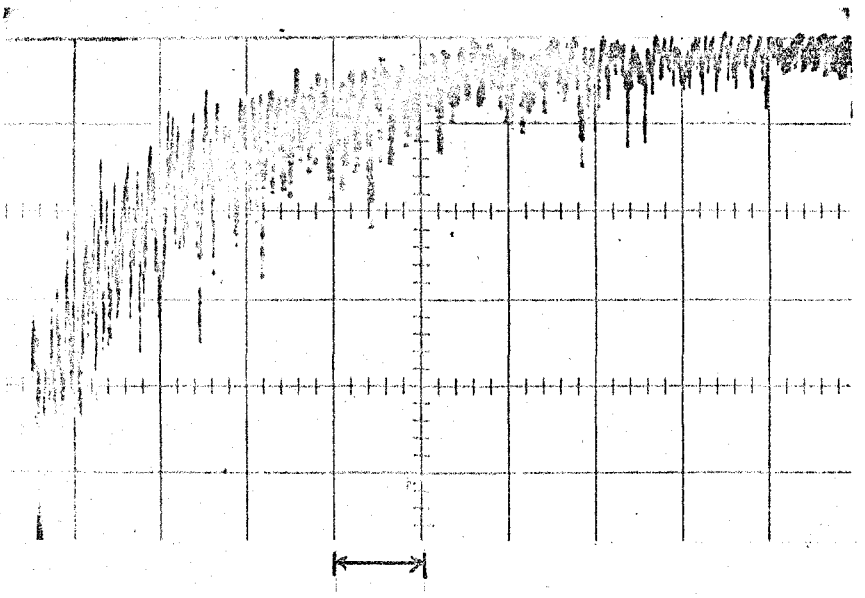

0.2×10^{-3} sec.

Fig. 5.25 Enhanced phosphorescence decay of $CaF_2:Ho^{3+}$ ($^5G_5'$ to $^5I_8$) before heat treatment.

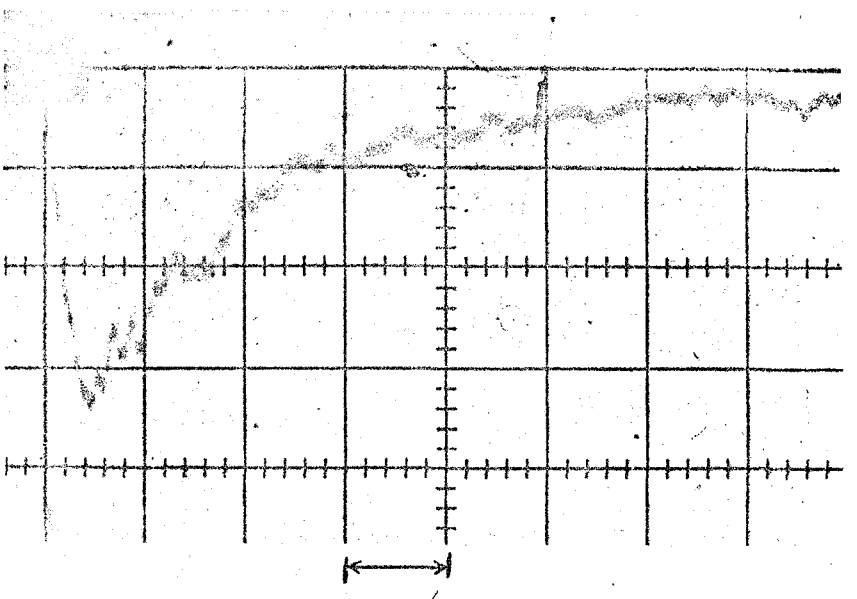

5×10^{-6} sec.

Fig. 5.26 Enhanced phosphorescence decay of $CaF_2:Ho^{3+}$ ($^5G_5'$ to $^5I_8$) after heat treatment.

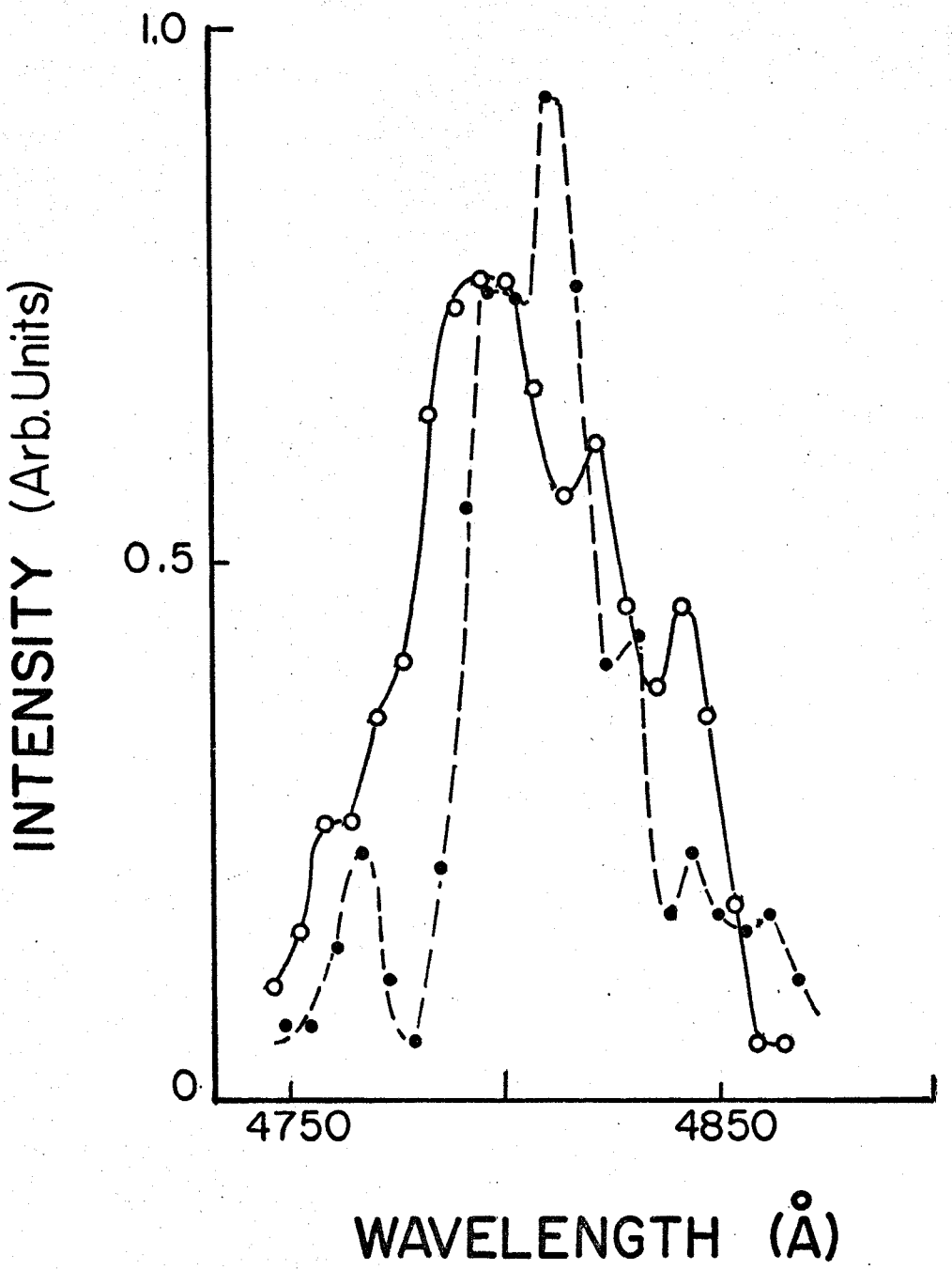

Fig. 5.27 Spectral distribution of laser enhanced phosphorescence of $CaF_2:Dy^{3+}$.

Solid curve: $77^{\circ}K$

Dashed curve: estimated to be about $20^{\circ}K$.

TABLE 5.2. DECAY TIMES OF $CaF_2:Ho^{3+}$ at $77^{o}K$

Upper Level of Transition	$^5F_4, ^5S_2$	$^3K_8$	$^5G_5$	$^5G'_5$
Wavenumber (10^3 cm^{-1})	18.4	21.6	24.3	27.8
Decay Time (10^{-3} sec.)	1.1		0.35	0.31
Decay Time After Heat Treatment (10^{-6}sec.)	26	7.1	23	10

In order to establish the nature of the process involved in the absorption of the laser flux, only the intensity of the incident laser beam was varied (by using filters), and the amplitude of the emission from a fixed peak monitored. The result is presented in Fig. 5.28. A greater uncertainty was involved in the low intensity end because of the much weaker signal.

As a check, the monochromator was replaced by the spectrograph used in part B, and the detector replaced the camera. Using the heated sample of $CaF_2:Dy^{3+}$, a spectrum was obtained by firing the laser forty times; Fig. 5.29.

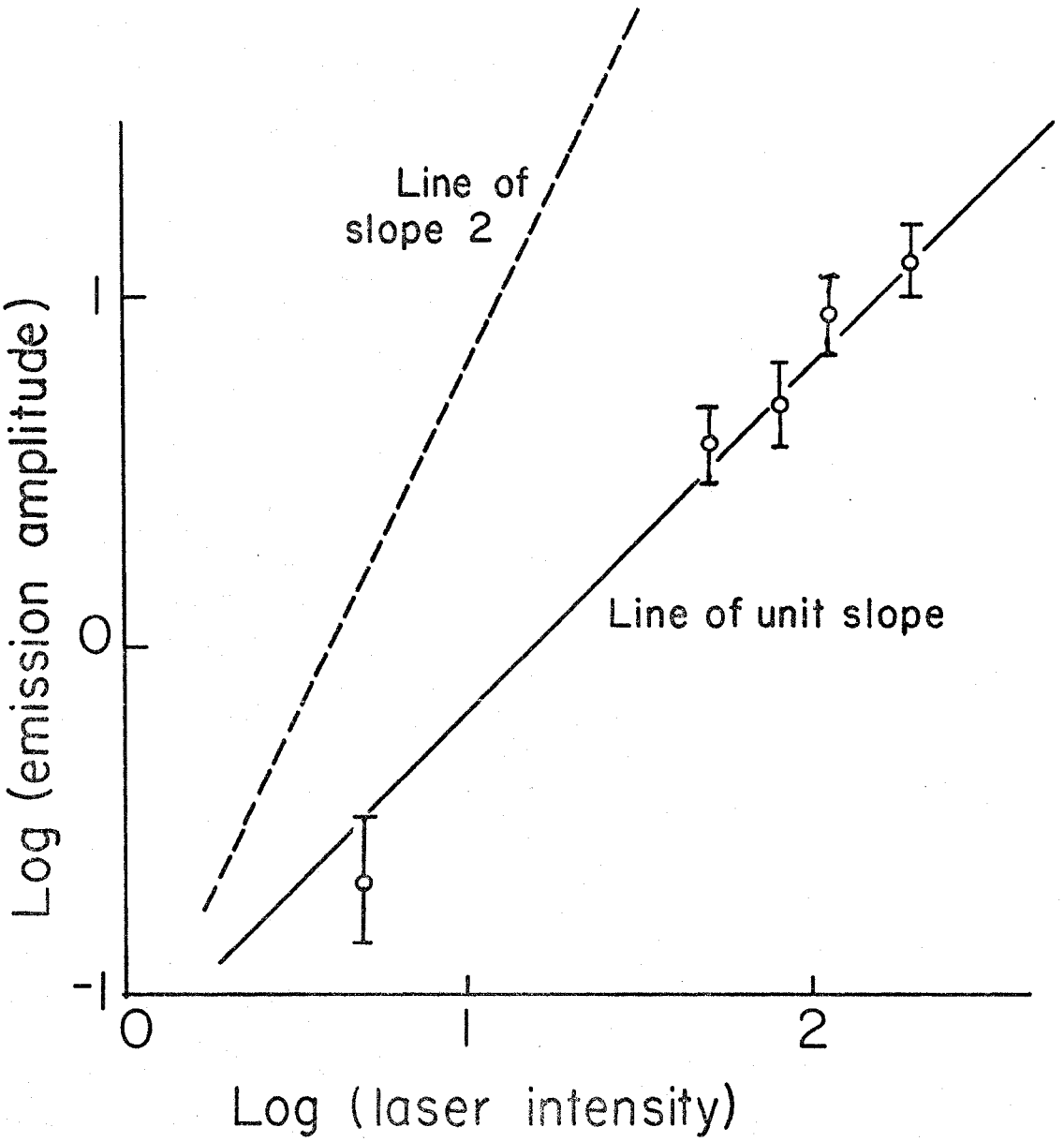

Fig. 5.28 Amplitude of enhanced phosphorescence of unheated $CaF_2:Ho^{3+}$ as a function of laser intensity.

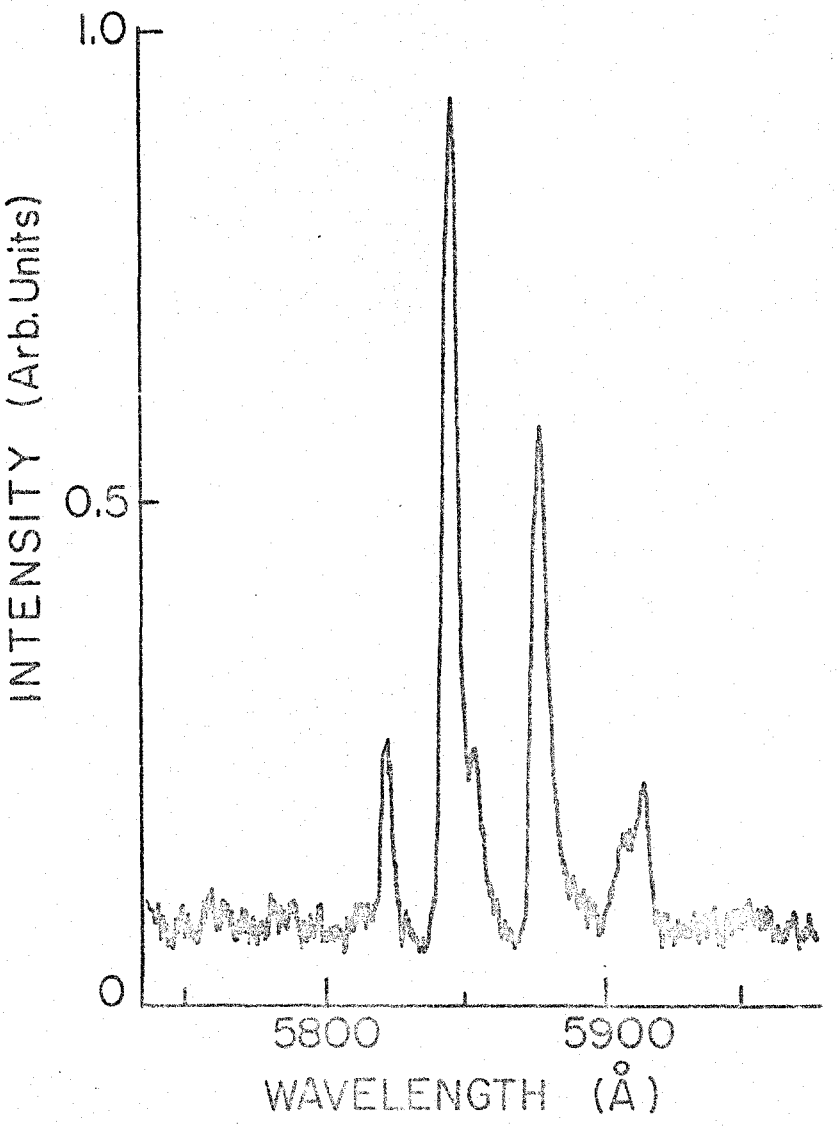

Fig. 5.29. Spectrum of laser enhanced phosphorescence of $CaF_2:Dy^{3+}$ after heat treatment.

D. Thermoluminescence of $CaF_2:Dy^{3+}$

The procedure of taking glow curves and spectra at different glow peaks was similar to that described in ref. 2. Fig. 5.30. shows the glow curves before and after heat treatment. The heating rate was about 11 degress per minute. Fig. 5.31 to 5.34. are the thermoluminescence spectra.

E. Re-excitation experiment on the systems $CaF_2:Gd^{3+}$ and $CaF_2:Ce^{3+}$

The sample was first x-irradiated at room temperature and then cooled down to liquid nitrogen temperature while still being kept in darkness. It was then exposed to ultraviolet (or visible) light from a xenon arc lamp monochromator combination for ten minutes, after which a glow curve was taken. Fig. 5.35 shows a 'regular' thermoluminescence glow curve and two 're-excitation' glow curves using two different re-excitation photon energies. After two or three cycles of x-irradiation, cooling and warming, the sample was heated on a not plate until the colour disappeared before further x-irradiation. Table 5.3 summaries the relative glow peak heights using different photon energies for re-excitation of the system $CaF_2:Gd^{3+}$. Part of this result is presented again in fig. 5.36 (c) together with re-traces of absorption spectra taken with a Cary 14 Spectrophotometer, fig. 5.36 (a,b).

The system $CaF_2:Ce^{3+}$ was treated in a similar manner and the result is presented in fig. 5.37.

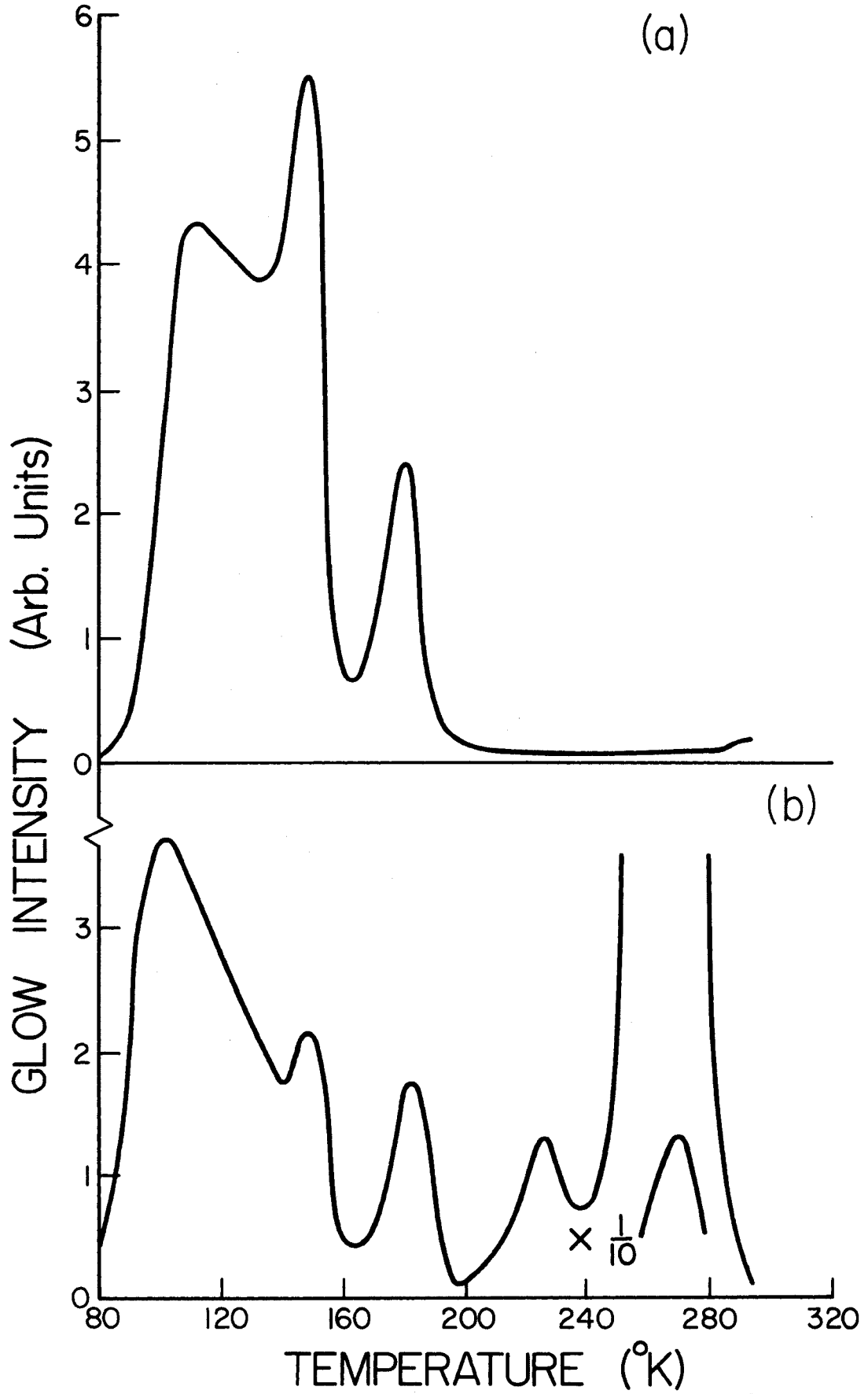

Fig. 5.30 Thermoluminescence glow curves of $CaF_2:Dy^{3+}$, (a) before heat treatment (b) after heat treatment.

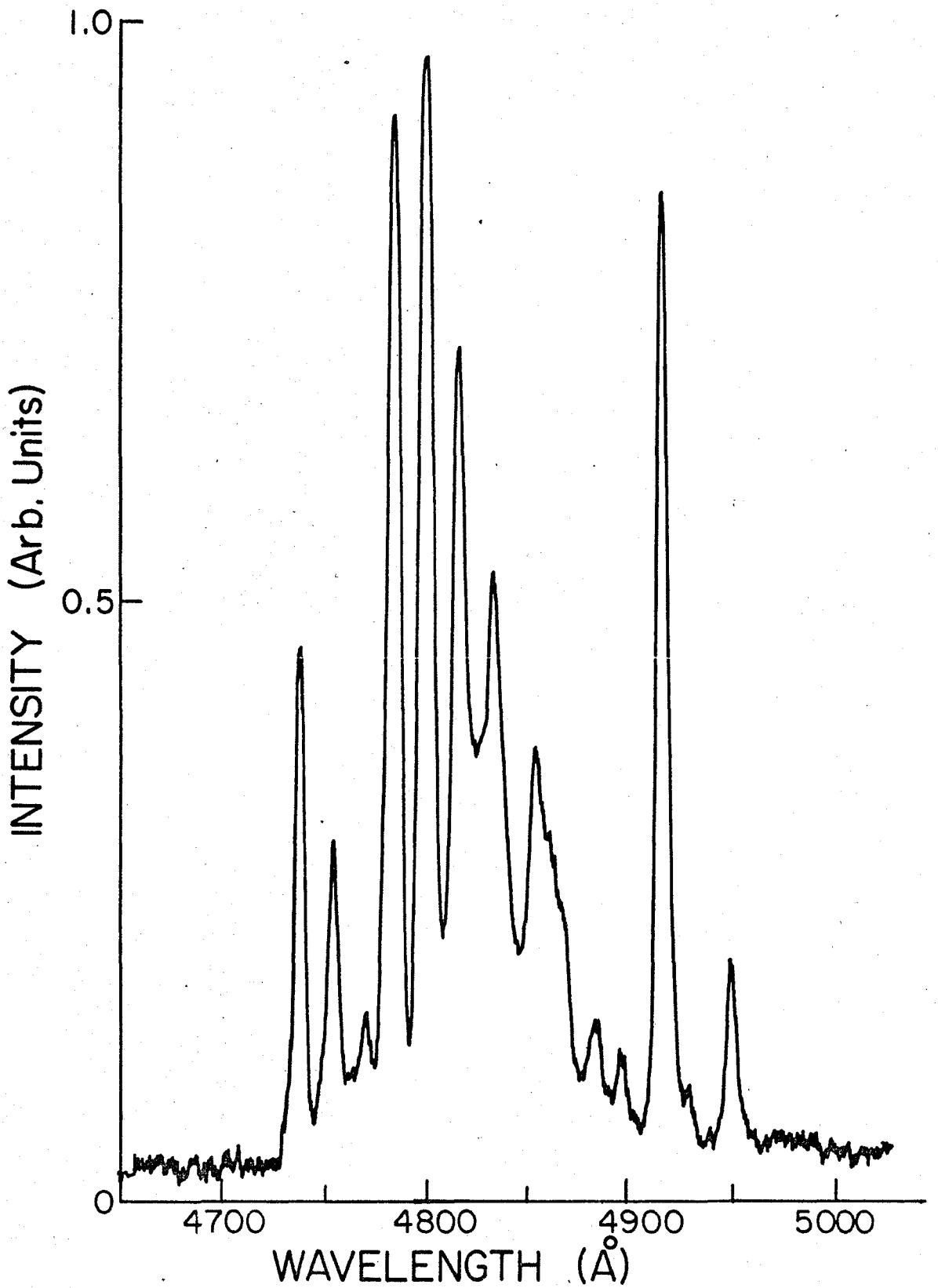

Fig. 5.31. Thermoluminescence spectrum of $CaF_2:Dy^{3+}$ before heat treatment.

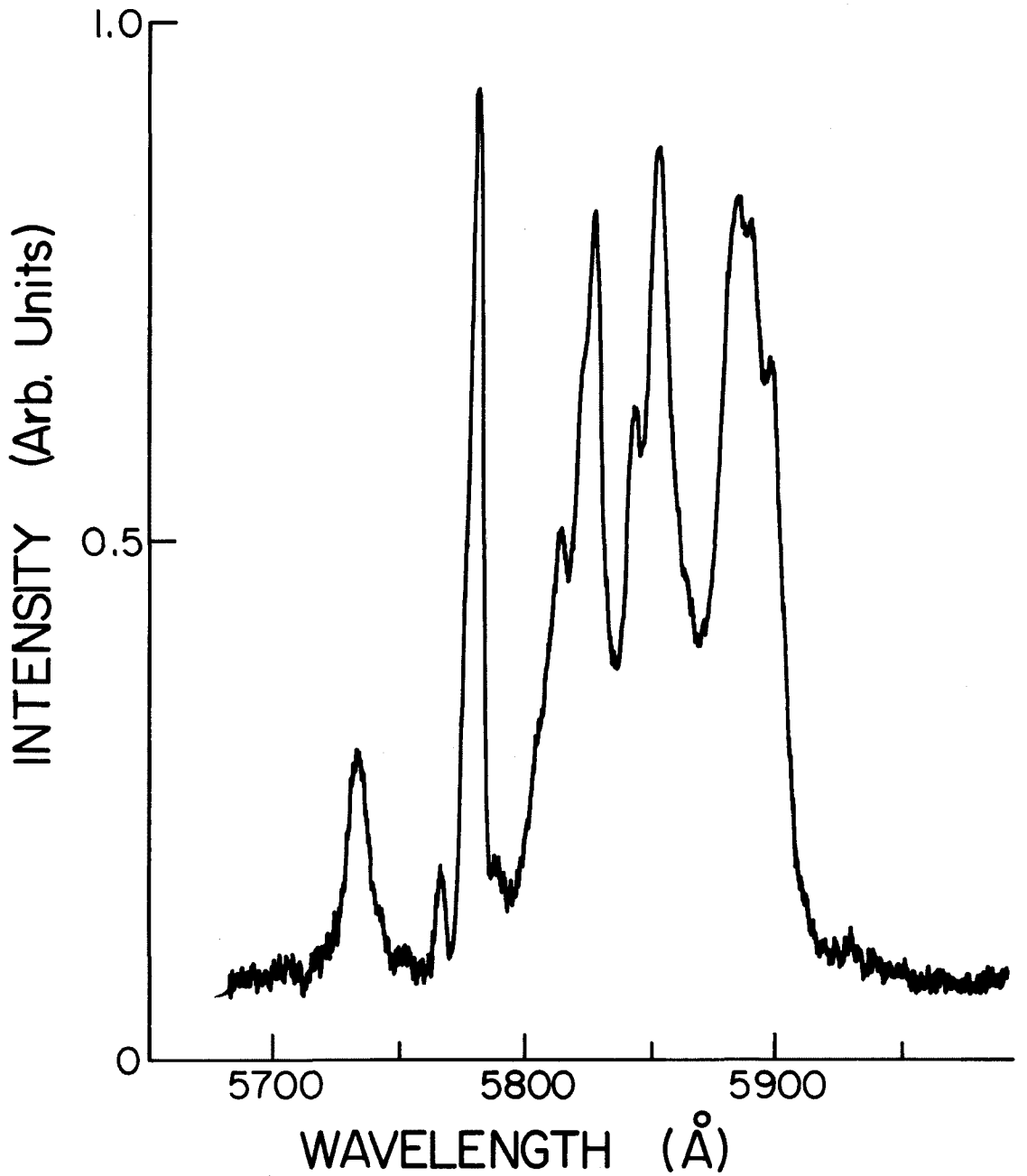

Fig. 5.32 Thermoluminescence spectrum of $CaF_2:Dy^{3+}$ before heat treatment. ($^4F_{9/2}$ to $^6H_{13/2}$)

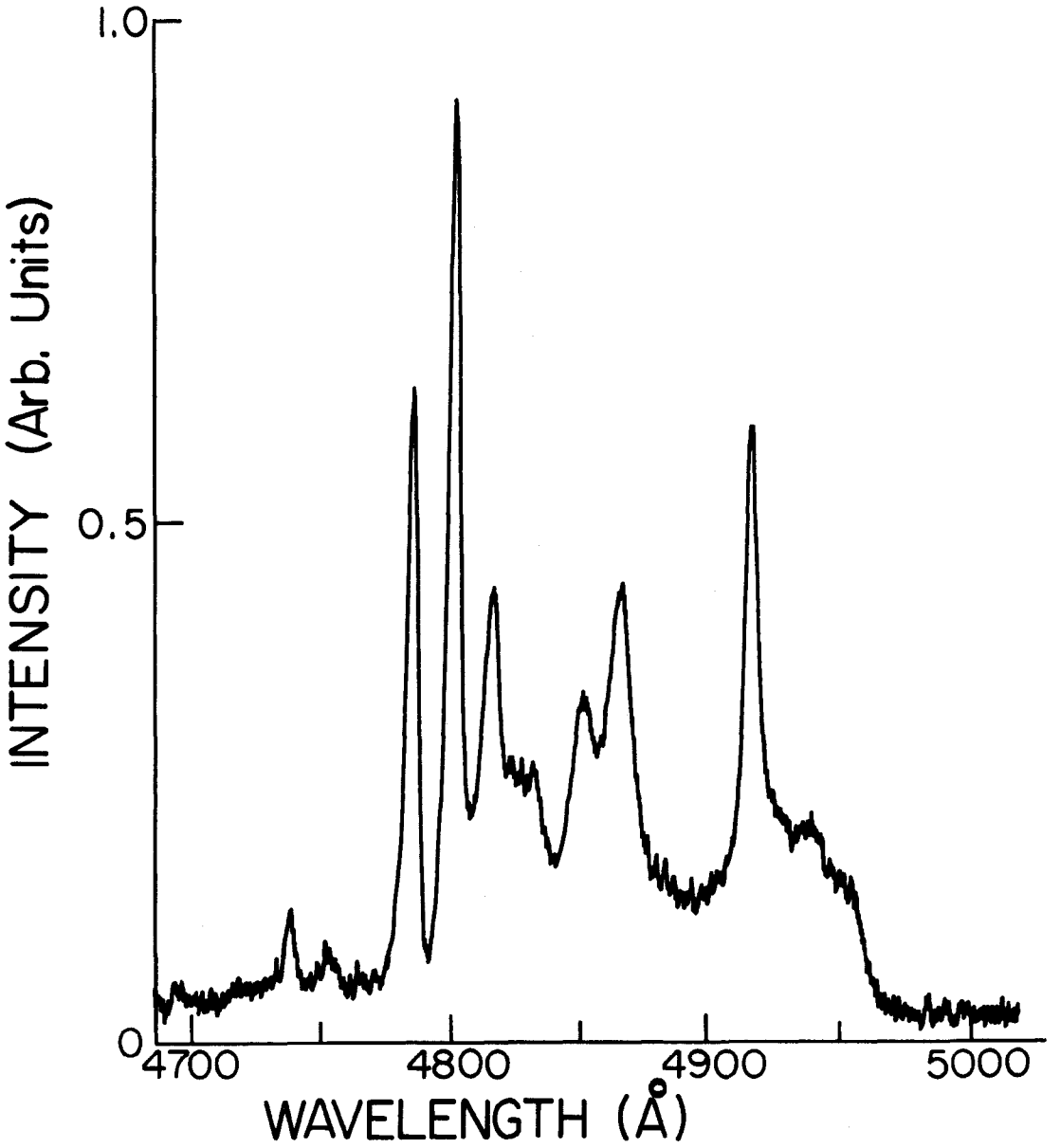

Fig. 5.33 Thermoluminescence spectrum of $CaF_2:Dy^{3+}$ after heat treatment. ($^4F_{9/2}$ to $^6H_{15/2}$)

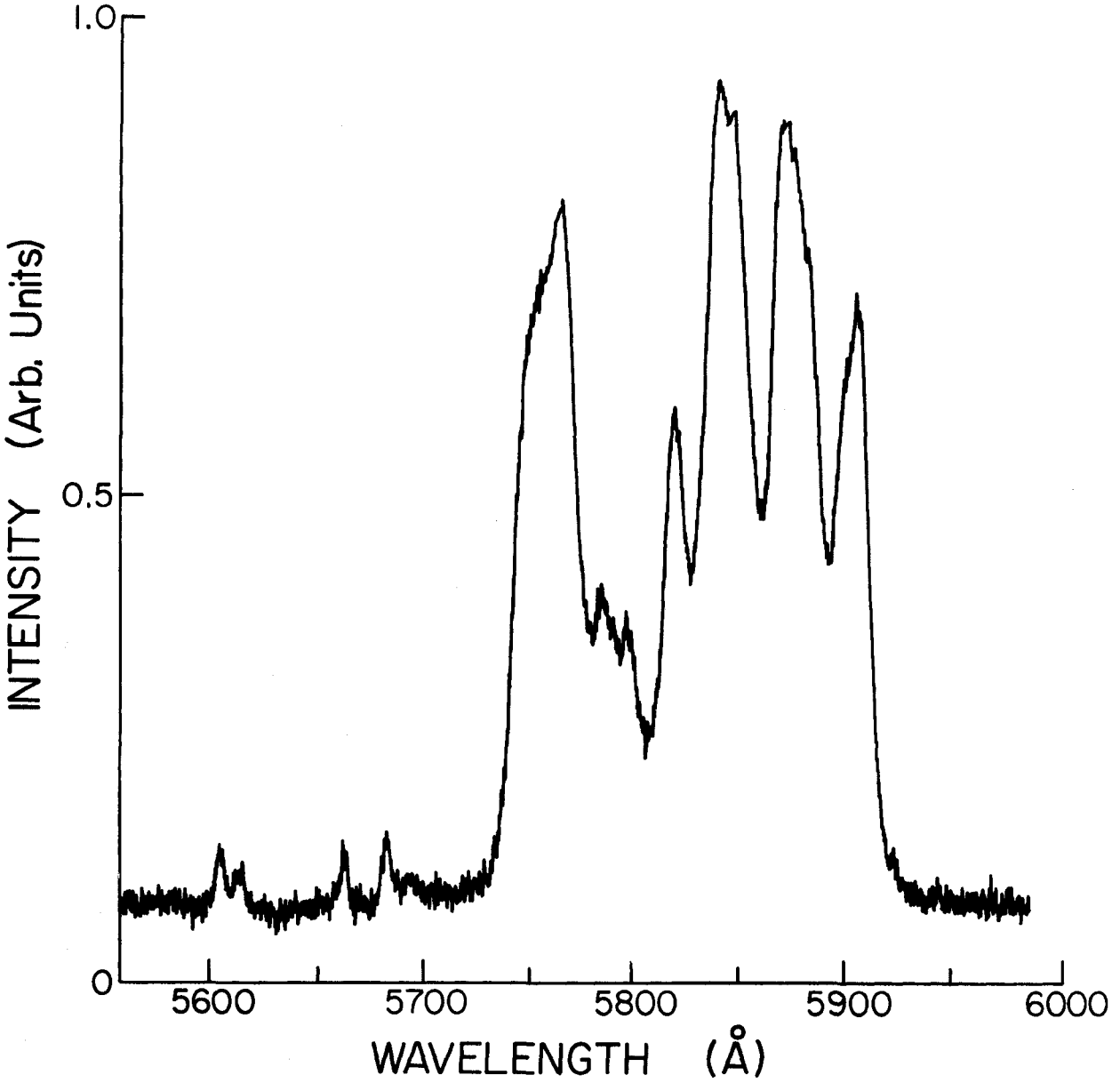

Fig. 5.34 Thermoluminescence spectrum of $CaF_2:Dy^{3+}$ after heat treatment. ($^4F_{9/2}$ to $^6H_{13/2}$)

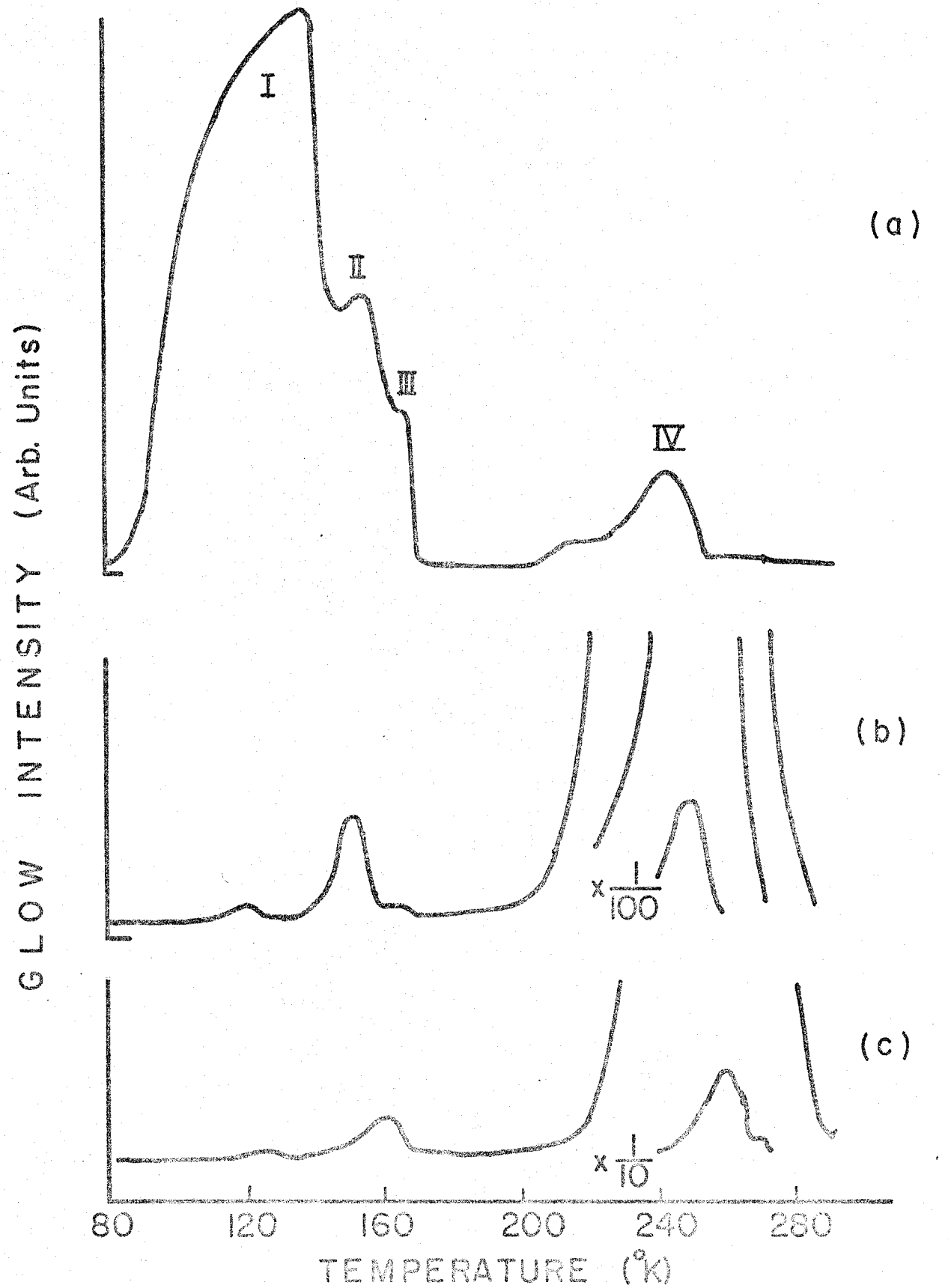

Fig. 5.35. Thermoluminescence of $CaF_2:Cu^{2+}$. (a) regular glow; (b) re-excitation with 3000Å; (c) re-excitation with 2600Å.

Table 5.3 Relative Peak Heights of Re-excitation Glow Curves Using Different Photon Energies.

Wave-length \ Peak number	I	II	III	IV
2800 Å	2	5	2	500
3500	2	3		400
3620		4		1000
3750	3	10	3	1300
3800	3	16	3	1500
4000	2	8	3	800
4500	1	2		350
5000				90
5300				8
5890				4

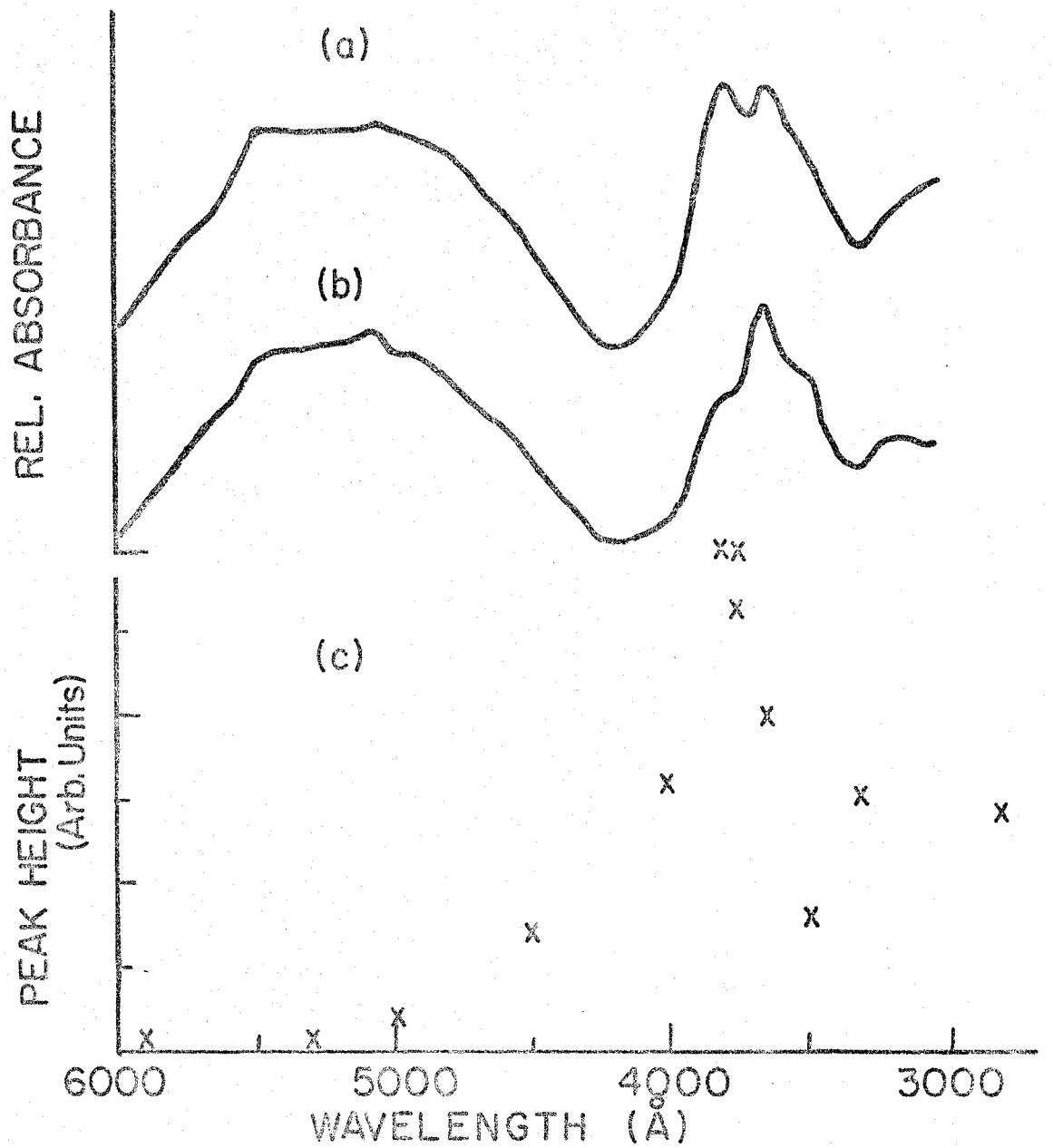

Fig. 5.36. $CaF_2:Sd^{3+}$. (a) relative absorbance after re-excitation with 3600Å, (b) after re-excitation with 3800Å; (c) height of peak IV.

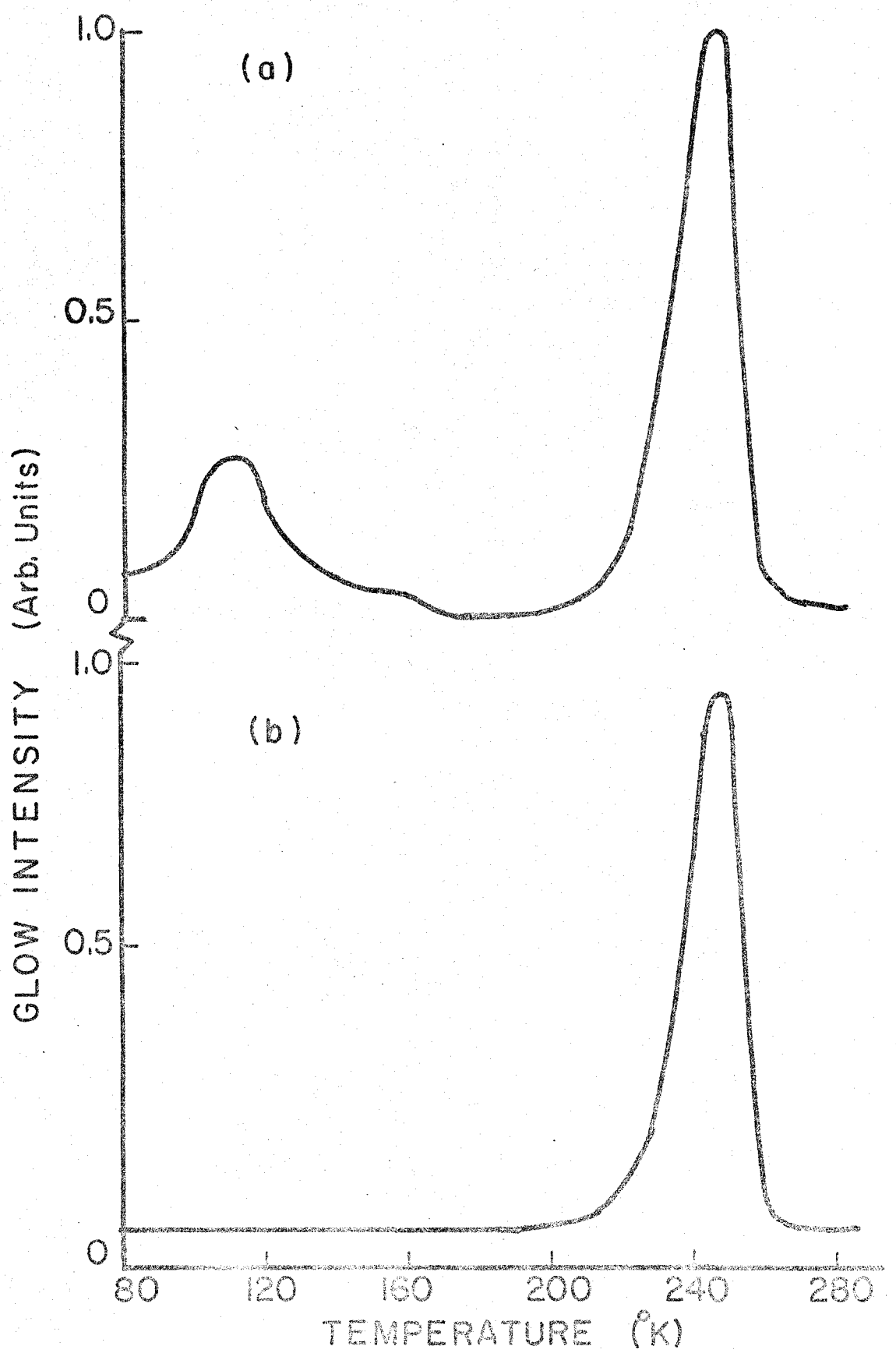

Fig. 5.37. Thermoluminescence glow curves of $CaF_2:Ce^{3+}$ (a) regular glow, (b) re-excitation.

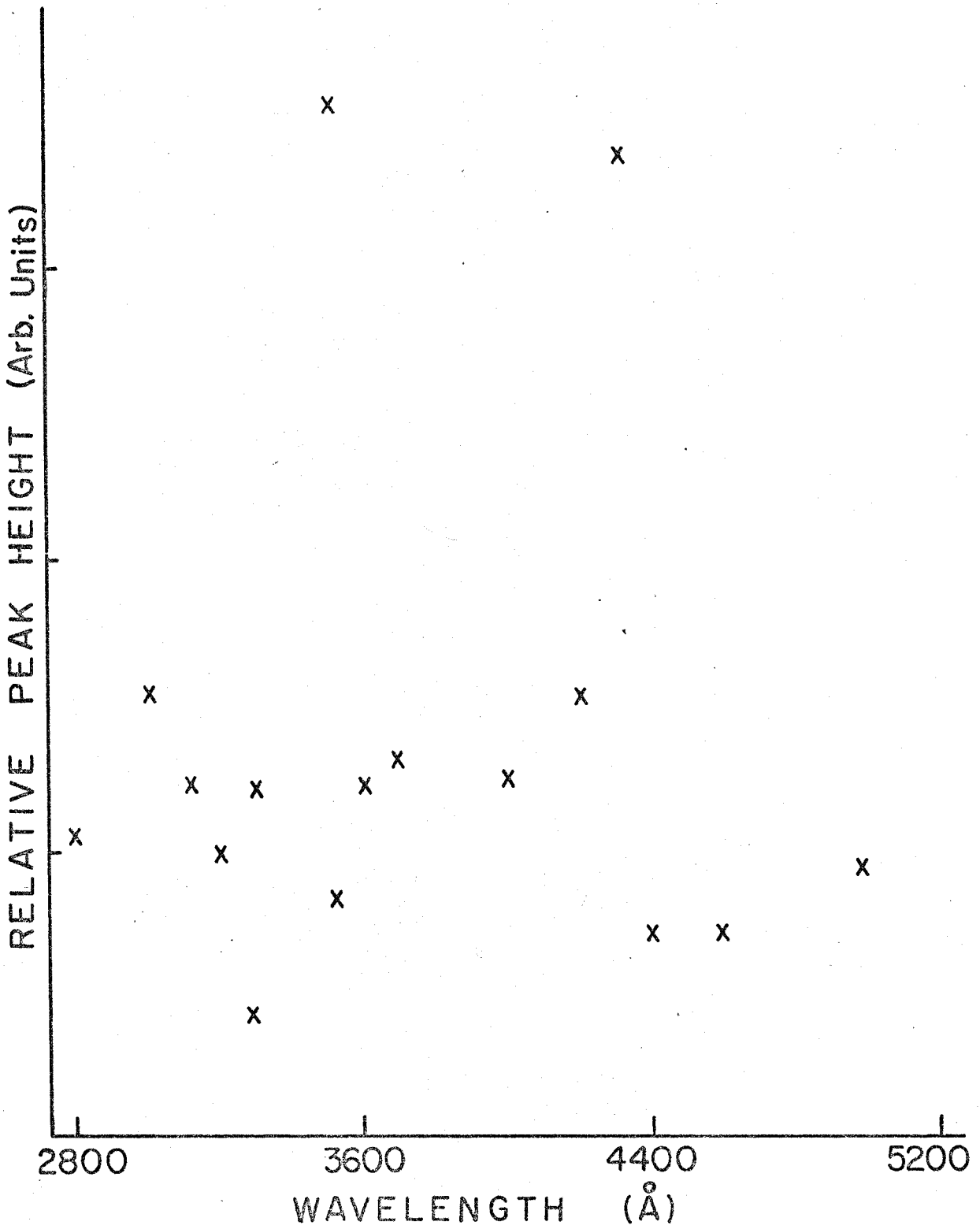

Fig. 5.38 Re-excitation peak heights for $CaF_2:Ce^{3+}$

CHAPTER VI. RESULTS AND DISCUSSION

A. Heat Treatment of Samples

Various aspects of the experimental result indicate that our starting crystal sample contains a mixture of luminescence centres of different symmetries. The heating in open air alters the proportion of these centres in the following way: [1] as mentioned on page 22, the rare-earth ion 'sees' an essentially cubic surrounding when the charge compensator is far away. At the start of the heat treatment, water molecules (in the air) dissociate:

$$H_2O \leftrightarrow H^+ + OH^-$$

The hydroxyl ion diffuses into the surface of the crystal by displacing other fluorine ions, which combine with the hydrogen and escape:

$$H^+ + F^- \rightarrow HF \text{ (escapes)}.$$

Meanwhile the OH^- ion migrates into the interior of the crystal by displacing other fluorine ions in steps. When it occupies a nearest neighbour (to the rare-earth ion) fluorine lattice site, the point symmetry of the rare-earth changes from cubic to trigonal (C_{3v}). If the fluorine ion displaced by the OH^- ion was originally occupying an interstitial site nearest to the rare-earth, then the original tetragonal point symmetry (C_{4v}) becomes tetragonal of a different nature as

the OH^- and the F^- are different ions.

As the heating process goes on, at higher temperature and/or for longer time, or both, the hydroxyl ion decomposes, leaving an oxygen ion at the fluorine lattice in the crystal matrix:

$$OH^- \leftrightarrow O^{--} + H^+.$$

Symbolically, we have

Starting Site Symmetry		First Stage of Heating		Later Stage of Heating
O_h	→	C_{3v}	→	C_{3v}
C_{4v}	→	C_{4v}'	→	C_{3v}'

Within this model, the heat treatment is to produce tetragonal and trigonal sites at the expense of cubic sites. We expect the process of diffusion of the OH^- and O^{--} ions from the surface of the crystal into the interior to be a slow one, so that the concentration of OH^- and O^{--} ions decrease gradually from the surface towards the centre of a sufficiently thick crystal, as illustrated in fig. 6.1.

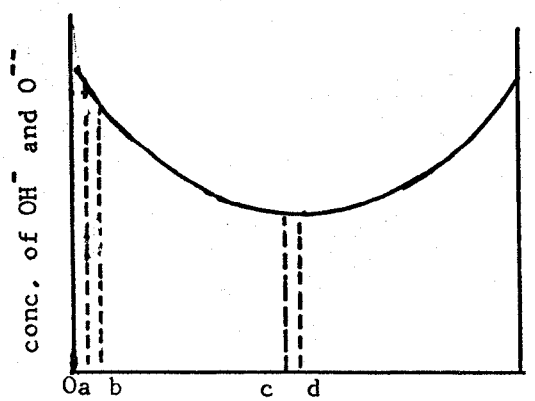

Fig. 6.1 Schemetic diagram of diffusion of ions into crystal.

In the present work with the system $CaF_2:Dy^{3+}$, a crystal sample of 4 mm. thick was heated and then cut into thin slabs parallel to the flat surfaces. There was little difference between the results obtained from the different slabs. This shows a sort of saturation under such heating conditions and sample dimensions. As illustrated in fig. 6.1, the difference in concentration of low symmetry sites is not large for the slabs o-a and a-b.

There is also the alternative of O^{--} ions at the surface diffusing into the crystal, in which case for every O^{--} ion, one lattice F^- is replaced and at the same time a fluorine vacancy is created to preserve electrical neutrality. Now the fluorine vacancy is mobile and may recombine with any interstitial F^- as it moves along. When the recombination takes place at an interstitial site nearest to a rare-earth ion (locally compensated), the cubic environment of the rare-earth is restored[2]. Thus there is this process competing with the aforementioned ones.

B. Excitation Spectra of $CaF_2:Dy^{3+}$

At the time of writing, not many levels above $^4F_{9/2}$ have been identified. The label used in fig. 5.2 is after Dieke[3] for convenience. Above 24000 cm^{-1} there is a high density of observed energy levels. J mixing becomes important as the electronic levels are close enough for significant interaction[4,5]. Besides, there is also the possibility of co-existence of luminescence centres with environment of different point symmetries. Each type of sites splits a J level in a different way. But the centre of gravity of Stark components of a given J-manifold

remains practically fixed. It follows that there will be an overlap between two sets of Stark lines of the same J split from sites of different point symmetries. All these make identification difficult without detailed calculations.

The excitation spectrum is the result of the pump light sending the atoms to some excited states from which they cascade down to one of the fluorescent levels, in this case $^4F_{9/2}$. The terminating level of the fluorescence is the $^6H_{13/2}$ multiplets (to be justified later). The peaks in the spectrum correspond to energy levels higher than $^4F_{9/2}$, provided that the following observation is noted: the error involved is of the order of 50 to 100 cm^{-1} in this spectral range; the ground state ($^6H_{15/2}$ manifold) spreads over a few hundred cm^{-1}, so the present experiment could not tell whether the atoms are pumped from the lowest or higher sub-levels.

The experimental results compare quite satisfactorily with those of Dieke[3,6] and the calculation of Carnall et al.[7], while they do not appear to match those calculated by Wybourne[5]. This might be due to some inadequacy in the wave functions used by the last author, as pointed out before by Schlesinger and Nerenberg[8]. It should be noted, however, that there remains still some controversy in the assignment of some of the higher energy levels[9]. In fig. 6.2, column (A) and (D) are taken from ref. 3 and 7, respectively while columns (B) and (C) are results of the present work before and after heat treating the crystal sample to 900°C. respectively.

The present spectra were taken by monitoring the emission in the 'yellow' (5600 Å to 6000 Å). Basically the same spectra were

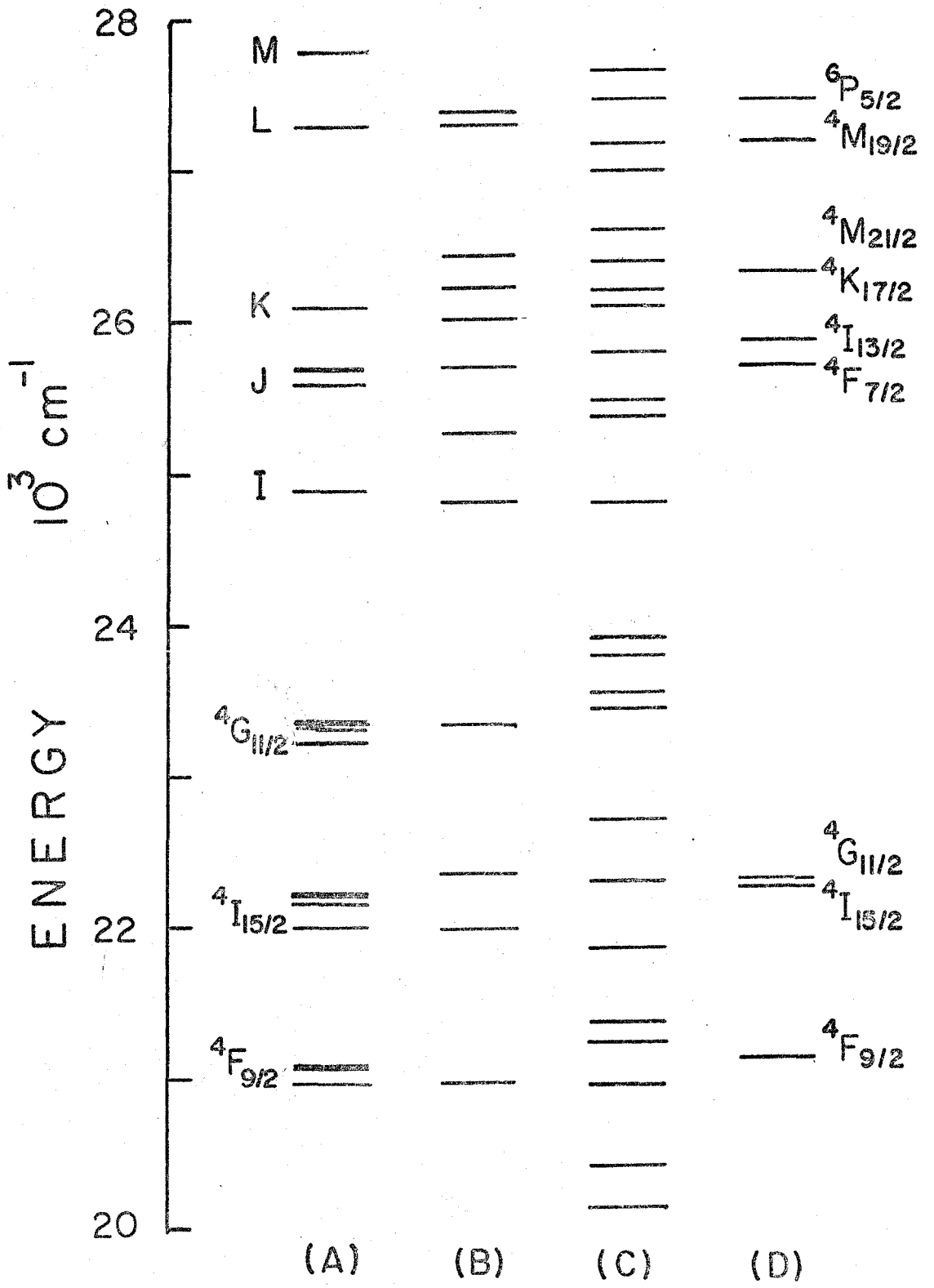

Fig. 6.2 Energy level diagram of $CaF_2:Dy^{3+}$.

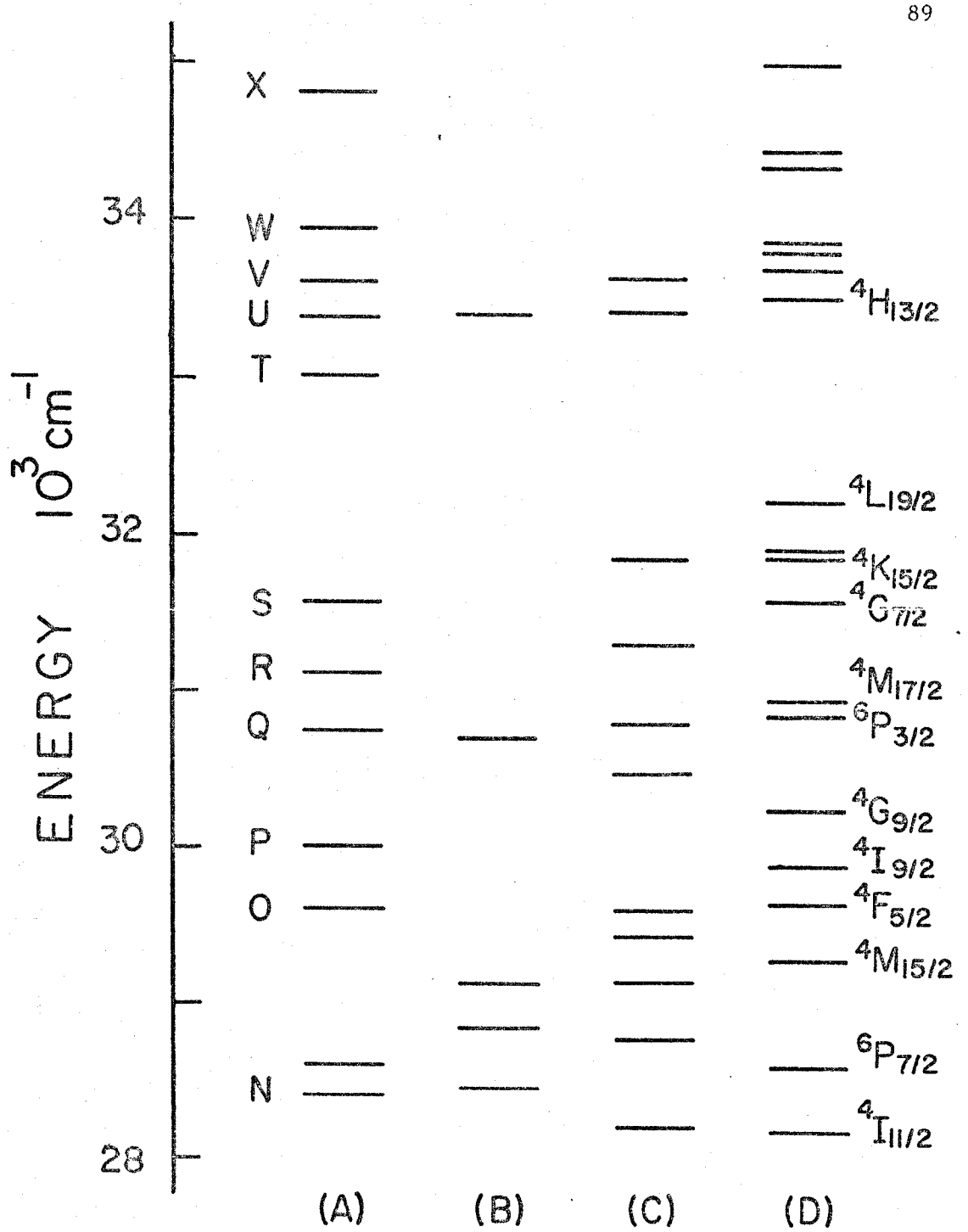

Fig. 6.2 (contd.) Energy level diagram of $CaF_2:Dy^{3+}$.

obtained by monitoring the 'blue-green' emission (4650Å to 5000Å) corresponding to the transition $^4F_{9/2}$ to $^6H_{15/2}$. This indeed justifies the assertion that the 'yellow' emission arises from the same fluorescence level as the 'blue-green', viz., $^4F_{9/2}$, since photons of energy 21000 cm^{-1} are sufficient to cause the 'yellow' emission (fig. 6.3).

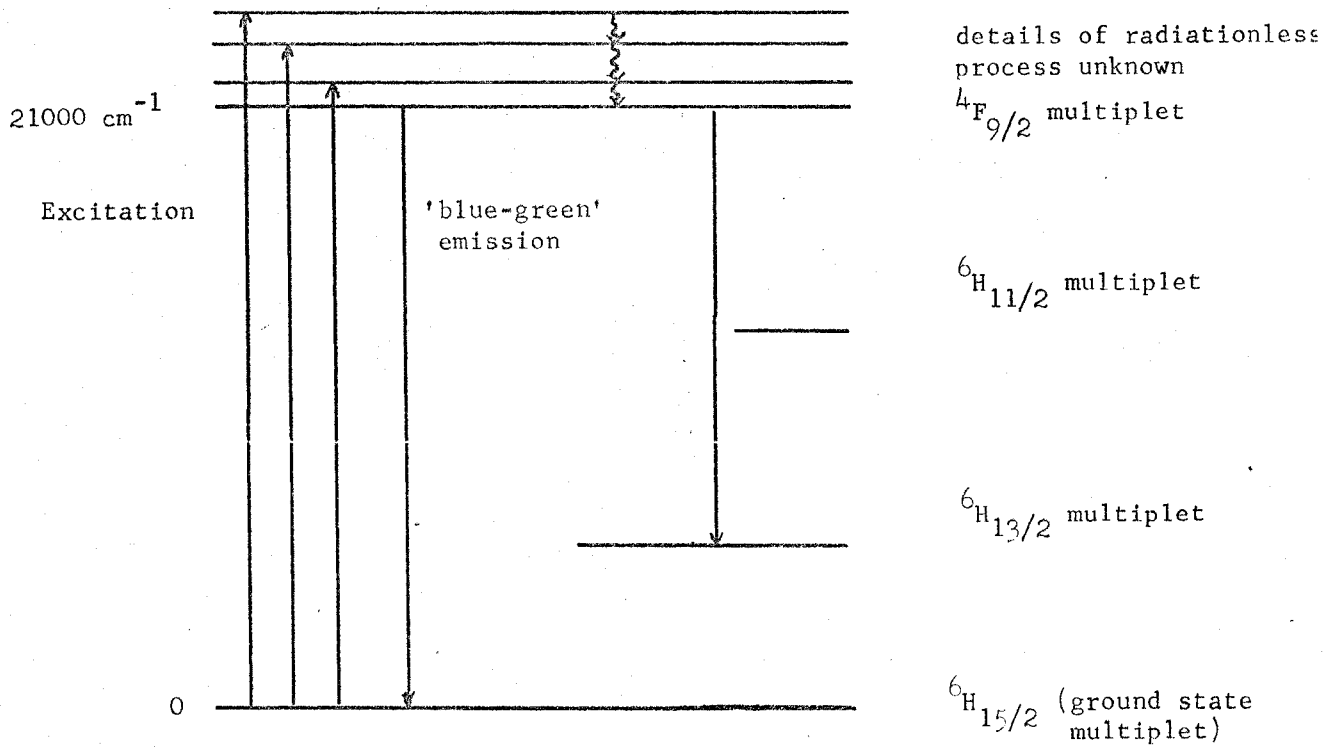

Fig. 6.3 Schemetic diagram of excitation spectrum of $CaF_2:Dy^{3+}$.

C. Fluorescence Spectra of $CaF_2:Dy^{+3}$

Emission spectra in both the 'yellow' and 'blue-green' regions could be obtained by illuminating into any one of the peaks of the excitation spectra. The general features of the spectra obtained using these photons of different energies are essentially the same other

than some minor variations in the relative peak heights. After heat treating the sample, the emission became much stronger and the spectra more complex. While some of the components present before heat treatment subsided, new components appeared as a result of heat treatment. This, however, alone is not sufficient to identify components arisen, say, from cubic sites, as we shall show in decay time measurements.

Emission in the 'red' (6500Å - 6700Å) corresponding to the transition between $^4F_{9/2}$ and $^6H_{11/2}$ has been reported by a number of workers[10-14]. However, this was not observed in the present work presumably due to the very low intensity of the emission and/or different conditions under which the samples have been prepared, as noticed in the work of Schlesinger and Whippey on $CaF_2:Gd^{+3}$[15].

D. Thermoluminescence of $CaF_2:Dy^{+3}$

Before heat treatment the thermoluminescence glow curve exhibits basically three glow peaks at 110°, 149° and 180°K. The glow was strong enough for isolating individual peaks (see ref. 12, Ch. 0). In contrast to the case of $CaF_2:Ho^{+3}$ where the spectrum derived from one glow peak is different from that of another, here the spectra from the three glow peaks are almost identical. In the former case this has been attributed to the relatively high mobility of the charge compensators.

After heat treatment, not only is the shape of the glow curve changed (two more peaks appear at 226° and 270°K.) but also there is a redistribution of the total amount of light emitted amongst the peaks. Here pracitcally all the emission comes from the last (new) glow peak. This undoubtedly points to the direction that the process of heat

treatment has either altered the proportion of luminescence centres at sites of different symmetries or has created new centres, or both. There is no drastic change in the spectra as a result of the heat treatment. Some of the lines become less resolved as some weak lines in between strong ones grow.

Upon comparing fig. 5.32 with the work of Kiss and Staebler[16], one can see that all the peaks in the latter's work are included in the present spectrum, in addition to some other lines. One is led to the conclusion that, at least for the crystal samples used for the present investigation, the X-ray reduction process involved in thermoluminescence is effective for rare-earth ions at sites of cubic as well as other symmetries.

Thermoluminescence spectrum in the 'yellow' ($^4F_{9/2}$-$^6H_{13/2}$) was not reported in literature in connection with the work of Kiss and Staebler or in that of Merz and Pershan[17], despite the fact that the emission is comparable in intensity with that in the 'blue green' region. Once again, as can be seen from fig. 5.33 and 5.34, heat treatment does not change the spectrum to any drastic extent. As before, the whole spectrum appears to be more smeared together as some weak lines climbed up between strong ones.

The following table (6.1) shows the position of the peaks in the TL spectra of $CaF_2:Dy^{+3}$ together with those for the fluorescence spectra before heat treatment. It is apparent that practically all the fluorescence lines are contained in the TL spectra. There is little doubt that these lines come from a mixture of sites of different symmetries. However, it was not possible at this stage to group the

Table 6.1 Emission lines of $CaF_2:Dy^{3+}$ before heat treatment (Å).

Fluorescence	Thermoluminescence	Fluorescence	Thermoluminescence
4740	4739	5732	5733
4750		5743	5740
	4756		5750
4770	4770		5770
4786	4786	5780	5779
4792			5782
4801	4801		5788
	4817	5811	5813
	4834	5818	
	4855		5822
	4865		5827
4876			5844
4885	4883		5852
	4896		5883
	4918		5889
	4928		5899
	4949		5933

spectral lines according to the site symmetries of their luminescence centres. Nevertheless, fig. 6.4 is an empirical energy scheme constructed to fit the experimental data. The fit is within 10 cm^{-1}, which is better than the experimental error.

Incidentally, one might question the possibility of multiple excitation[18] by a single photon in view of the great number of lines in our spectra. Such a possibility has been ruled out by comparison with experimental data of other workers on the one hand, while on the other hand our low dopant concentration in the samples does not favour such energy sharing among the rare-earth ions.

It may appear that the spread of the ground state sublevels is greater than the normal crystal field splitting found in RE ions. This is because of the superposition of spectra coming from sites of different symmetries. Since any attempt to separate them at this stage is no more than speculation, they may as well be left intermingled.

Of course there is always the possibility of phonon assisted transitions. This can be clarified, at least in fluorescence, by running the experiment at helium temperature.

It may also be noted that our glow curve before the heat treatment is almost identical with that obtained by Merz and Pershan. After the heat treatment, the glow curve matches very well with that obtained by Arkhangelskaya[19], who had, undoubtedly, samples with oxygen. This is reassuring that our results are not only self-consistent but also are able to correlate those of other workers.

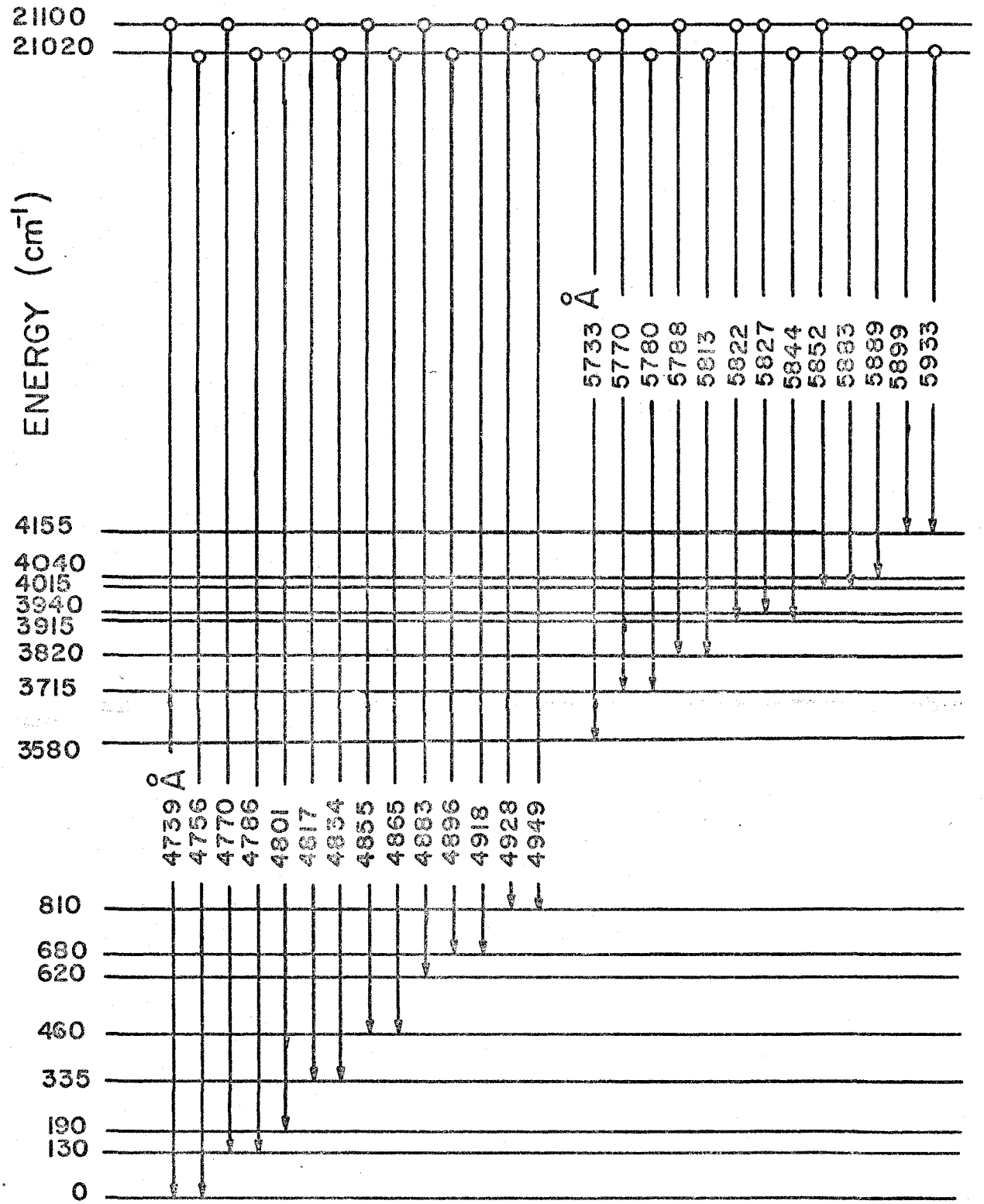

Fig. 6.4 Empirical energy scheme of $CaF_2:Dy^{3+}$.

E. Measurement of Decay Times

The fact that phosphorescence decay can be stimulated by IR has been known for a long time[20]. In ref. 16 it was mentioned that re-oxidation of the RE^{2+} back to RE^{3+} after X-irradiation can be triggered either by heat or by IR (or even visible) radiation. The re-conversion process involves the absorption of a photon by the RE^{2+} ion, which then gives up its extra electron to the conduction band; or by the freeing of captured holes by thermal energy.

With the present experimental set up, the following ions in CaF_2 have been tested and found to exhibit enhanced phosphorescence under laser light, Dy^{3+}, Ho^{3+}, Sm^{3+}, Gd^{3+} and Eu^{2+}. This work has been devoted to studying the first two in greater detail.

The following (fig. 6.5) is a simple model to account for the enhancement of phosphorescence by the laser pulse:

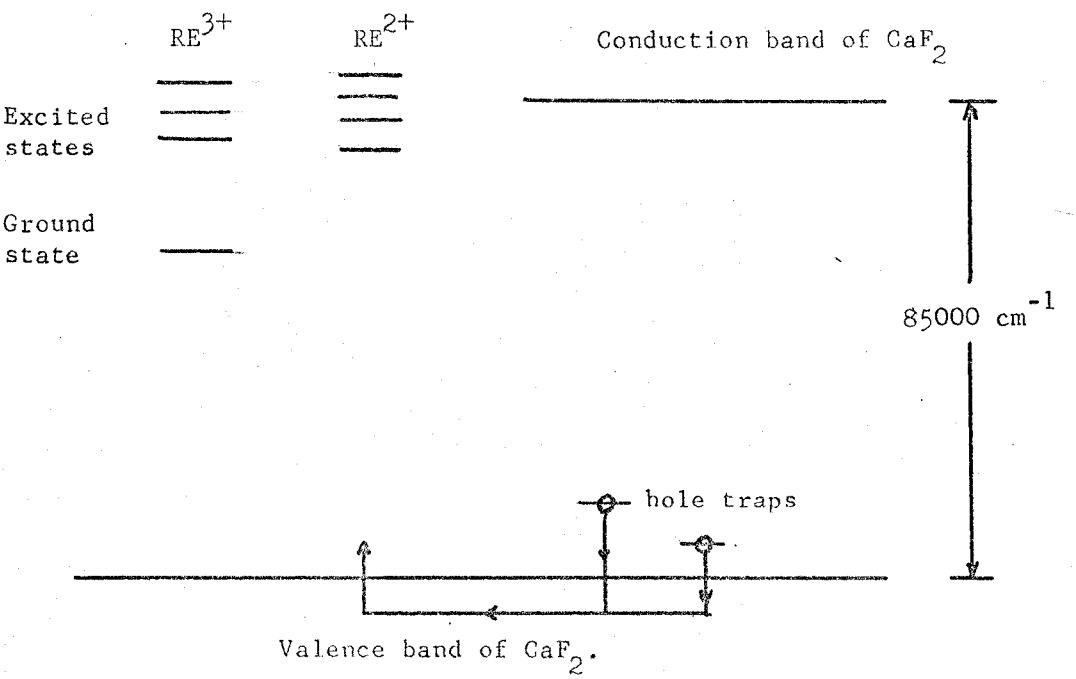

Fig. 6.5 Model of laser enhanced phosphorescence.

Although it is not known exactly how the energy levels of the rare-earth ions fit into the forbidden gap of the CaF_2 matrix, it is quite likely that some of the energy levels lie inside the conduction band of CaF_2. Upon absorption of a laser photon a trapped hole is released and 'wanders' though the crystal matrix. On meeting a RE^{2+} ion the extra electron is returned by the ion and recombination takes place:

$$\text{Hole} + \text{laser photon} \rightarrow \text{released hole}$$

$$\text{released hole} + RE^{2+} \rightarrow RE^{3+}\ (\text{excited}),$$

$$RE^{3+}\ (\text{excited}) \quad \text{relaxation} \rightarrow RE^{3+}\ (\text{ground state}),$$

$$+ \text{ characteristic radiation.}$$

Since the laser pulse has a high photon flux density ($\sim 10^{18}$ photons/pulse) many of the trapped holes are released at each laser pulse, resulting in a 'sudden shower' of RE^{3+} at various excited states. From these excited states the atoms cascade down by some as yet unclear process until they hit some fluorescence levels. Downward transitions from such levels give rise to the observed spectra. Since the supply of atoms to the excited states is pulsed, the subsequent decay is governed by any radiationless process involved. The delay between the laser pulse and the peak of the decay curve is an indication of the rate of recombination[21]. The enhanced phosphorescence was found to be unpolarized although the laser pulse was plane polarized. The phosphorescence was not affected by rotating the plane of polarization of the laser through 90^{o}.

The use of high power laser leaves open the possibility of two photon processes involved in the interaction between the laser and

the atomic system under study. But this has been ruled out by the following experimental facts:

1. observable signals were obtained only after the crystal has been x-irradiated and kept at liquid nitrogen temperature;

2. it is very unlikely that all the rare-earth ions tested have energy difference between the levels of transition satisy the two photon energy requirement at the same time;

3. results shown in fig. 5.28 indicates that the emission depends linearly on the laser intensity; indeed, this alone is sufficient to guarantee a single photon process.

In the system $CaF_2:Dy^{3+}$, the phosphorescence decay is much enhanced at 4800Å and at 4960Å (fig. 5.10). The decay times measured were different at these two peaks (table 5.1). This shows exclusively the co-existence of luminescence centres at sites of at least two different symmetries. The fact that the emission in the 'yellow' has a decay time common to that in the 'blue green' adds much weight to the proposition of its originating from the $^4F_{9/2}$ level.

No emission with energy higher than 21000 cm^{-1} was detected although fluorescence levels are known to exist above this value. One is then inclined to think that the $^4F_{9/2}$ level is in close vicinity of the bottom of the conduction band of the CaF_2 matrix, so that the 'shower' of excited atoms converted from the RE^{2+} following the laser pulse is fed to levels not much higher than $^4F_{9/2}$.

The effect of heat treatment again modified only to a limited extent both the spectral distribution and the decay time.

The situation is quite different for the system $CaF_2:Ho^{3+}$. Enhanced phosphorescence correpsonding to transitions to the $^5I_8$ (ground) state from $^5F_4$ and $^5S_2$, $^3K_8$, $^5G_5$ and $^5G_5'$ was observed. This infers that the conduction band of CaF_2 is at least 27000 cm^{-1} above the ground state of Ho^{3+} (fig. 6.6).

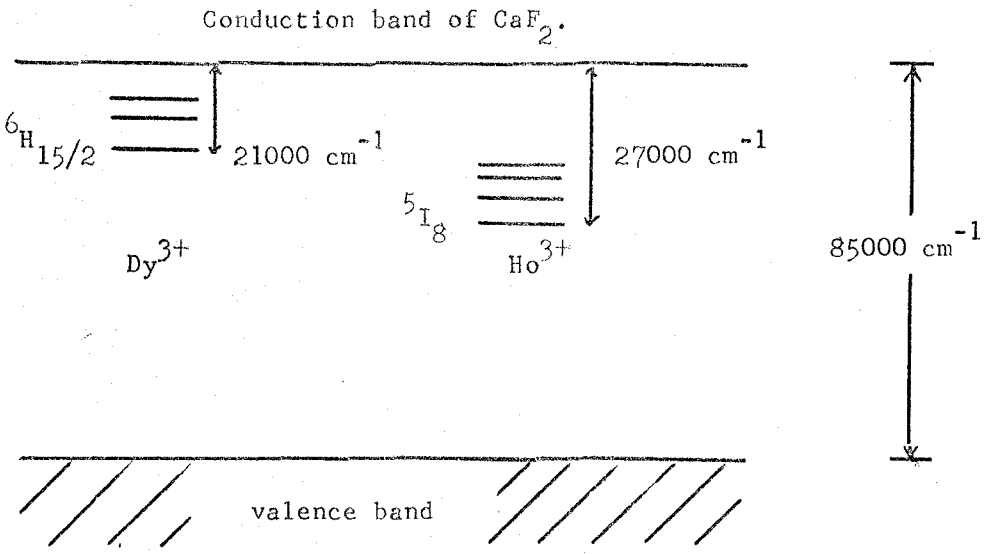

Fig. 6.6 Energy levels of Dy^{3+} and Ho^{3+} in CaF_2.

The effect of heat treatment is more pronounced here than with $CaF_2:Dy^{3+}$. New components appeared much stronger in the spectral distribution so that the original profile was not much preserved. The decay times were systematically reduced about twenty folds, which is quite large compared with the case of $CaF_2:Dy^{3+}$.

Table 6.2 is a comparison of decay times by various workers.

TABLE 6.2 DECAY TIMES OF Dy^{3+} AND Ho^{3+} IN CRYSTALS (IN MICROSECONDS)

	Decay Time	Temp.	Fluor. λ	Remarks	
Dy^{3+} in $LaCl_3$	390	4°K	5720Å	5% conc.	(a)
	540		4660Å		
$DyCl_3 \cdot 6H_2O$					
$Dy(C_2H_5SO_4)_3 \cdot 9H_2O$	10	77°K			(b)
$Dy(BrO_3)_3 \cdot 9H_2O$					(c)
Ho^{3+} in $LaCl_3$	170,460	77°K	5490Å	1%	
	255			2%	(a)
	26		4450A°	1%	
Dy^{3+} in CaF_2	1900	78°K			(c)

(a) Dieke and Hall

(b) Barsch and Dieke

(c) Kiss and Staebler

It is interesting to note that, in the instance of $CaF_2:Ho^{3+}$ at least, the decay times vary with the energy gap between the fluorescence level and the adjacent level below. When the energy levels are close together, transfer of energy between levels in the form of heat becomes more probable; this will shorten the radiative lifetime. Our findings are in harmony with those of other workers[22,23] and are given in the table below:

TABLE 6.3 VARIATION OF DECAY TIMES WITH ENERGY GAP IN $CaF_2:Ho^{3+}$ BEFORE HEAT TREATMENT

Levels	Energy Gap* (cm^{-1})	Decay Time (10^{-3} sec.)
$^5F_4, {}^5S_2 - {}^5F_5$	3000	1.1
$^5G_5 - {}^5F_1$	1800	0.34
$^5G_5' - {}^3K_7$	1500	0.31

*Taken from ref. 3

F. Re-Excitation Experiments

Fig. 5.36 clearly indicates that the trapped holes in the crystal matrix are most easily released by light at 3800Å. It also suggests that only one type of carriers, viz., holes, is responsible for the thermoluminescence system $CaF_2:Gd^{3+}$. In the instance of $CaF_2:Ce^{3+}$ very little correlation can be found between the excitation glow peaks and the wavelength of exciting light.

It should be point out that it is difficult to obtain quantitative results with this kind of experiment, as strictly identical experimental conditions between the runs must be maintained for intensity comparison.

G. Experimental Limitations

In this work an attempt has been made to trigger the re-conversion of RE^{2+} back to RE^{3+} by a 30 mW helium-neon laser chopped mechanically. However, the effort was fruitless. At present this was attributed to the low power of the laser rather than its having photon energy different from the ruby laser (Kiss and Staebler reported that the re-conversion was triggerable using visible light). Perhaps it is worthy of some more investigation using counters and signal averager integrating the signal pulses or employing phase sensitive detection.

In any event, the ruby laser was employed in the present study. The experimental set up leaves much room for improvement. Two main difficulties encountered are:

1. low firing rate of laser--this makes alignment extremely time consuming and difficult,
2. instability of output power of laser.

These cause a large fluctuation in the result and hence a low accuracy. Shot by shot tracing from the screen of the oscilloscope is definitely inferior a technique to, say, sampling[24], in which case the photomultiplier is pulsed and the photocurrent integrated by a recorder with long time constant.

Even for a well recorded oscillogram, any direct measurement made from it gives a precision of hardly more than two significant figures. This hampers a great deal the numerical analysis of the decay curves. For a decay curve such as that shown in fig. 5.24, much effort has been made to represent it by a difference of two exponentials[25,26] since the 'build-up' part of the curve was considerable. However, with the computer programs on hand[27,28] it was not possible to obtain any meaningful result because the data themselves were not accurate enough. The numerical analysis was not persued further because even though a solution could be obtained, it is not necessarily a unique one[29]. Furthermore, the result does not add any more to the understanding of the cascade process. In principle, it was possible to measure the 'build-up' part of the decay curve more accurately on an expanded time scale. But in practice, a more expanded time scale required the use of a low value load resistor across the photomultiplier output. Since the signal was not strong enough, the noise became intolerable when the load resistor was less than 1000 ohms.

H. Possible Improvement and Extension of the Project.

1. Decay time measurement.

As mentioned in the last section, it is more desirable to use a laser with higher repetition rate (say, 100 Hz) so as to improve the signal to noise ratio by sampling or integrating. It is also interesting to see if lasers of different photon energies exhibit this phenomenon of enhanced phosphorescence, and if so, how the efficiency varies with the photon energy. This may shed some light on the nature of the electron-hole recombination process involved.

Once a better accuracy in the data is achieved the spectral lines belonging to the same transition can be grouped together according to their common decay times. This will help sorting out the symmetries of the sites giving rise to the emission. One can test the model proposed in section D by populating the fluorescence levels directly using selective excitation and comparing the decay times. This will give an estimate, at least, of the rate of re-conversion. Also, one can obtain some information about the nature of the cascade process, whether it is level-by-level, or by-passing some of the levels, on reaching the fluorescence level[30].

2. Excitation and Emission Spectra.

Preliminary data have indicated that it is very desirable to work below liquid nitrogen temperature as the lines become much sharper, thus leading to better resolution. Since the emission from $CaF_2:Dy^{3+}$ is rather weak, a more sensitive detector, say, a channeltron, is required to bring out the finer details in the excitation spectra. The McPherson monochromator in this laboratory has shown its capability of giving better resolution and accuracy in a similar set up as compared with the use of the Leiss double monochromator. The former has the advantage of being able to extend into the far ultraviolet region. The excitation spectra are especially valuable in the case of $CaF_2:Dy^{3+}$ since it is very difficult, if not impossible, to get a decent absorption spectrum, particularly in the visible region.

3. Excited State Spectroscopy.

Since the RE^{3+} ions remain in the excited states for a sufficiently long time (10^{-3} sec.), it is quite feasible to perform experiments on this system of excited atoms before they decay. The present experimental set up can easily be modified by adding a light source and an analysing monochromator as shown in fig. 6.5. One of the monochromators, say, number I, can be used in the usual way, while the other can be used either to monitor induced absorption (transmission) in conjunction with a continuous pump light source, or emission and decay when the light source is a flash lamp. The addition of this light source brings the whole experiment to a new dimension, because of its versatility and extension of energy range that can be studied. It is quite conceivable that the population in the excited states is considerable and it is not surprising that harmonic generation might also be obtained on utilizing the anormalous dispersion effect for phase matching similar to what has been done in liquids[31].

4. Identification of Site Symmetries.

The identification of spectral lines originating from sites of different dymmetries is a formidable task. Lifetime measurements can be employed to isolate the lines into different catagories. The nature of each catagory still remains to be determined. But if one has previous knowledge about one of the lines then the whole group is identified, as shown recently by Chilver and Fong[32]. Other simple prodedures that can be followed without serious technical difficulty in this laboratory are variation in dopant concentration[33] and embedding the rare-earth in different host lattices[34]. Using crystals with a

small amount of monovalent cations (e.g., K^+, Na^+) will enhance the intensity of any lines from cubic sites as these cations will remove some of the local charge compensators to the RE^{3+}. Zeeman study is another possibility provided that good single crystals are available. The splitting of spectral lines from sites of lower symmetry than cubic will be anisotropic. Gil'fanov et al.[35] proposed that cubic centres were excited by cathodoluminescence. But since the principle is the same as in thermoluminescence and since the present experimental results point to the fact that cubic centres are not the only ones taking part in the process, one tends to put some reservation on cathodoluminescence as a means to isolating cubic lines.

In passing, it is interesting to note that apparently thermoluminescence in a magnetic field has not been attempted before. This appears to be a very promising technique for Zeeman study since no light source is involved, and hence no serious problem of alignment and stray light.

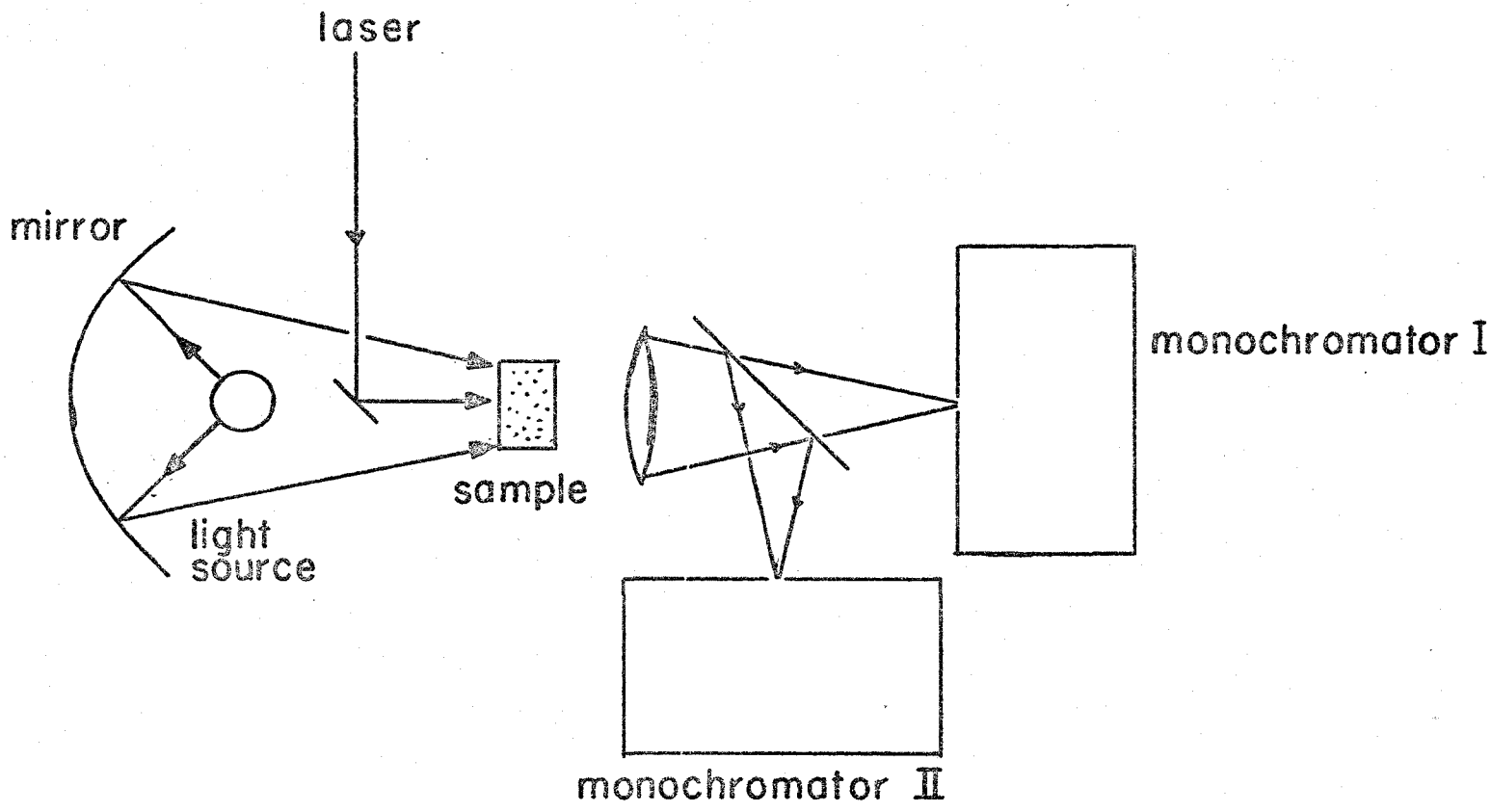

Fig. 6.7 Proposed experimental set up for excited state spectroscopy.

CHAPTER VII. CONCLUSION

In spite of the various limitations in our experimental conditions, the present study was able to yield meaningful results. First, a thermoluminescence spectrum of $CaF_2:Dy^{3+}$ in the 'yellow' was presented. Together with excitation and fluorescence spectra it was confirmed that this emission in the 'yellow' was due to the transition $^4F_{9/2}$ to $^6H_{13/2}$. Then the effect of heat treating the crystal samples on fluorescence, thermoluminescence and the decay time of the excited states was presented. In the case of $CaF_2:Dy^{3+}$ the heat treatment has introduced extra peaks into the excitation and fluorescence spectra as well as the glow curve. These changes were attributed to the formation of new sites for luminescence centres with tetragonal and trigonal symmetry in the crystal which started with, most probably, a mixture of centres with different symmetries already. The total light output from thermoluminescence was more or less evenly divided among the three glow peaks before the heating, but after the heating, practically all the light comes from the (new) last peak. This was not the case with $CaF_2:Ho^{3+}$ whose thermoluminescence glow peaks could be isolated and the spectrum associated with eack peak is different.

The ruby laser was employed to enhance the phosphorescence decay of two rare-earth doped CaF_2 systems. This has been shown to be a single photon process. Spectral distributions of the phosphorescence were obtained using point by point plotting of the amplitudes. These compared favourably with the luminescence and thermoluminescence

spectra. Decay times of some of the excited states were obtained. For $CaF_2:Dy^{3+}$ two decay constants for the same transition were found, indicating the presence of centres at sites of two different summetries. No emission from other levels was observed. Heat treatment shortened the decay times by a factor of two. On the other hand, enhanced phosphorescence from four different upper levels was observed from the system $CaF_2:Ho^{3+}$. Heat treatment shortened the decay times by a factor of twenty. This infers that the changes introduced into the crystal as a result of the heating is felt strongly by the rare-earth. A simple model was rpoposed to account for the enhanced phosphorescence from which one could compare the relative positions of the energy levels of Dy^{3+} and Ho^{3+} in CaF_2. Suggestions were made to improve the experiments and for further investigation.

Quite a lot of work has been done on the first few members of the lanthanide series. Dy^{3+} in CaF_2 is one of the systems less studied because of its great complexity, perhaps. Nonetheless it is challenging because of the many fronts open for attacking the problem. The author feels that what he has accomplished was finding one two pieces of jig-saw puzzles out of the thousands that fit into a small corner of a huge picture painted by the Creator. It seems difficult to complete the whole picture. But as bits and pieces are being knit together, even the incomplete picture begins to make sense.

APPENDIX: SOLUTION OF RATE EQUATIONS (3.4)

For $t < \tau$, (3.4) can be written as

$$\frac{dN_2}{dt} = p_{32} N_3 - p_{21} N_2$$
$$\frac{dN_3}{dt} = -(p_3 + 2\omega)N_3 - \omega N_2 + \omega N_o \tag{A1}$$

where $p_3 = p_{31} + p_{32}$.

Let n_i be the Laplace transform of Ni, i = 2,3, i.e. $n_i(s) = \int_o^\infty e^{-st} N_i dt$.

Taking the Laplace transform of (A1)

$$sn_2 = p_{32} n_3 - p_{21} n_2$$
$$sn_3 = -(p_3 + 2\omega)n_3 - \omega n_2 + \omega N_o \tag{A2}$$

since $N_2(0) = N_3(0) = 0$ and N_o is constant by assumption.

The solutions of the algebraic equations (A2) are

$$n_2 = \frac{\omega N_o}{s} \cdot \frac{p_{32}}{(p_3+2\omega+s)(p_{21}+s) + \omega p_{32}}$$
$$n_3 = \frac{\omega N_o}{s} \cdot \frac{p_{21} + s}{(p_3+2\omega+s)(p_{21}+s) + \omega p_{32}} \tag{A3}$$

Let $s_{1,2}$ be the roots of the equation

$$(p_3 + 2\omega + s)(p_{21} + s) + \omega p_{32} = 0$$

(A3) can be written in partial fractions

$$n_2 = \omega N_o p_{32} \left(\frac{C_o}{s} + \frac{C_1}{s-s_1} + \frac{C_2}{s-s_2} \right)$$

$$n_3 = \omega N_o \left(\frac{d_o}{s} + \frac{d_1}{s-s_1} + \frac{d_2}{s-s_2} \right)$$

with

$$C_o = \frac{1}{s_1 s_2}$$

$$C_1 = \frac{1}{s_1(s_1-s_2)}$$

$$C_2 = \frac{1}{s_2(s_2-s_1)}$$

$$d_o = \frac{p_{21}}{s_1 s_2}$$

$$d_1 = \frac{s_1+p_{21}}{s_1(s_1-s_2)}$$

$$d_2 = \frac{s_2+p_{21}}{s_2(s_2-s_1)}$$

Now e^{ax} and $\frac{1}{s-a}$ constitute a pair of Laplace transforms, therefore

$$N_2 = \omega N_o p_{32} (C_o + C_1 e^{s_1 t} + C_2 e^{s_2 t})$$

$$N_3 = \omega N_o (d_o + d_1 e^{s_1 t} + d_2 e^{s_2 t}) .$$

The solution of rate equations (3.7) follows the same procedure.

REFERENCES

CHAPTER 9.

1. Wybourne, B. G., 'Spectroscopic Properties of Rare Earths', Interscience (1965), Chapter 1.
2. See, for example, Condon, E.U., and Shortley, G. H., 'Theory of Atomic Spectra', Cambridge Press (1935) p. 236.
3. American Inst. of Physics Handbook, p. 6-47.
4. Ibid., p. F-124.
5. McClure, D. S., and Kiss, Z., Journ. Chem. Phys. 39, 3251 (1963).
6. Kiss, Z., and Staebler, D. L., Phys. Rev. Lett. 14, 691 (1965).
7. Hayes, W., and Twidell, J. W., Journ. Chem. Phys. 35, 1621 (1961).
8. Ibid., Proc. Phys. Soc. 81, 371 (1963).
9. Low, W., Journ. Phys. Soc. Japan, 17 suppl. B-1, 440 (1962).
10. Merz, J., and Pershan, P. S., Phys. Rev. 162, 235 (1967).
11. Schlesinger, M., and Whippey, P. W., Phys. Rev. 162, 286 (1967).
12. Ibid., 171, 361 (1968).
13. Ibid., 177, 563 (1969).
14. Stepanov , I. V., and Feofilov, P. P., Soviet Physics Doklady 1, 350 (1956).
15. Dieke, G. H., and Crosswhite, H. M., Applied Optics, 2, 675 (1963).
16. El'yashevich, M. A., 'Spectra of the Rare Earths'. Translated by the U.S. Joint Publications Research Service, New York.
17. Schlesinger, M., and Pai, S. T., Bull. Amer. Phys. Soc. 14, 390 (1969).
18. Weber, M.J., Phys. Rev. 156 231 (1967).

19. Asawa, C.K., Phys. Rev. 155 188 (1967)

20. Varsanyi, F., and Dieke, G. H., Phys. Rev. Lett. 7, 442 (1961).

21. Zverev, G. M. et. al., Soviet Physics JETP, 28, 21 (1969).

22. Steinhaus, , Crosswhite, H. M. and Dieke, G. H., Spectrachemica Acta 5, 436 (1953).

23. Handee, C., and Brown, W., Philips Tech. Rev. 19, 50 (1957).

24. Kaminskii, A. A., et. al., Soviet Physics JETP, 21, 844 (1965).

25. Ewanizky, T. F., Journ. Applied Phys. 39, 5883 (1968).

26. Dieke, G. H. and Hall, L. A., Journ. Chem. Phys. 27, 465 (1957).

27. Barasch, G. E., and Dieke, G. H., Journ. Chem. Phys. 43, 988 (1965).

28. Feofilov, P. P., and Kaplyanskii, A. A., Opt. and Spectr. 12, 272 (1962).

29. Asawa, C. K., Phys. Rev. 141, 251 (1966).

30. Kariss, Ya. E., Opt. and Spectr. 18, 247 (1965).

31. Luks, R. K., et. al., Soviet Physics Solid State, 11, 210 (1969).

32. Gil'fanov, F. Z., et. al., Opt. and Spectr. 24, 302 (1968).

33. Krupke, W. F., and Gruber, Journ. Chem. Phys. 39, 1024 (1963).

34. Low, W., et. al., 'Quantum Electronics, Paris 1963 Conference' ed. by Grivet and Bloembergen, p. 655.

35. Derr, V. E., and Gallagher, J. J., Ibid., p. 817.

36. Kaiser, W., and Garret, C. G. B., Phys. Rev. Lett. 7, 229 (1961).

37. Ershov, B. V., et. al., Soviet Physics Doklady 12, 47 (1967).

38. Ibid., Soviet Physics Solid State, 10, 1300 (1968).

39. Brown, M.R., and Shand, W. A., Phys. Rev. Lett. 11, 366 (1963).

40. Ibid., 12, 367 (1964).

41. Ibid., Phys. Lett. 8, 19 (1964).

42. Ibid., 11, 219 (1964).

43. Esterowitz, L., and Noonan, J., Appl. Phys. Lett. 7, 281 (1965).

44. Ibid., 8, 273 (1966).

45. Hopfield, J. J., et. al., Phys. Rev. Lett. 11, 414 (1963).

46. Hopfield, J. J., and Worlock, J. M., Phys. Rev. 137, A1455 (1965).

47. Swank, R. K., and Brown, F. C., Phys. Rev. Lett. 8, 10 (1962).

48. Ibid., Phys. Rev. 130, 34 (1966).

49. Park, K., Phys. Rev. 140, A1735 (1965).

50. Park, K., et. al., Phys. Rev. Lett. 17, 137 (1966).

51. Frohlich, D., and Mahr, H., Phys. Rev. Lett. 14, 494 (1965).

52. Ibid., Phys. Rev. 141, 692 (1966).

CHAPTER I

1. Shore and Menzel, 'Principle of Atomic Spectra, ' (Wiley), p. 334.

2. Racah, G., Phys. Rev. 62, 438 (1942).

3. See, for example, Slater, J. C., 'Quantum Theory of Atomic Structure' vol. II (McGraw-Hill) Appendix 20.

4. Rotenberg, M., et. al., 'The 3-j and 6-j Symbols', Technology Press, Cambridge, Mass., 1959.

5. Condon, E. U., and Shortley, G. H.: 'Theory of Atomic Spectra', Cambridge University Press, N.Y., p. 177.

6. Racah, G., Phys. Rev. 63, 367 (1943).

7. Ref. 5, Chapter 3.

8. Racah, G., Phys. Rev. 76, 1352 (1949).

CHAPTER II.

1. See for example, Hamermesh, M., 'Group Theory', Addison-Wesley (1962) p. 98.
2. Wyckoff: 'Crystal Structures', Chapter IV, fig. IV 1a.
3. Bleaney, B., Proc. Phys. Soc. B69, 858 (1956).
4. Friedman, E., and Low, W., Journ. Chem. Phys. 33, 1275 (1960).
5. Bethe, von H., Ann. Phys., 3, 133 (1929).
6. See for example, Morse, P.M., and Feshbach, H., 'Methods of Theoretical Physics', vol. II, p. 1264.
7. Judd, B.R., Proc. Phys. Soc. 70 B880 (1957).

CHAPTER III.

1. Weber, M.J., Phys. Rev. 156, 231 (1967).
2. Pollack, S.A., Journ. Chem. Phys. 40, 2751 (1964).
3. Curie, D., 'Luminescence in Crystals'.
4. Di Bartolo, B., 'Optical Interactions in Solids', Wiley, (1968).
5. Stepanov, B.I., and Gribkovskii, V.P., 'Theory of Luminescence', London Life Books Ltd., (1968).

CHAPTER IV.

1. See, for example, Mott, N.F., and Gurney, R.W., 'Electronic Processes in Ionic Crystals', Oxford (1948), Chapter II.
2. Hayes, W., and Twidell, J.W., Proc. Phys. Soc. 79, 1295 (1962).
3. Tzalmona, A., and Pershan, P.S., Phys. Rev. 182, 906 (1969).

4. Schlesinger, M., J. Phys. Chem. Solids, 26, 1761 (1965).

GENERAL READING

1. Curie, C., 'Luminescence in Crystals', Methuen (1960).

2. Leverenz, H.W., 'Luminescence of Solids', Wiley (1950).

3. Garlick, G.F.J., Report of Progress in Physics, 12, 34 (1948).

4. Compton, W.D., and Rabin, H., 'Solid State Physics', 16, 121 (1964).

5. Schulman, J.H., and Compton, W.D., 'Colour Centres in Solids', MacMillan (1962).

CHAPTER VI.

1. Sierro, J., J. Chem. Phys. 34 2183 (1961)

2. Luks, R.K., et al., Sov. Phys. Solid State 11 1810 (1970)

3. Ref. 15, ch.O.

4. Axe, J.D., and Dieke, G.H., J. Chem. Phys. 37 2364 (1962)

5. Wybourne, B.G., J. Chem. Phys. 36 2301 (1962)

6. Dieke, G.H., 'Spectra and Energy Levels of Rare Earth Ions in Crystals' (1968), Interscience, pp. 269 - 278.

7. Carnall, W.T., et al., J. Chem. Phys. 49 4424 (1968)

8. Schlesinger, M., and Nerenberg, M., Phys. Lett. 26 A109 (1968)

9. Fry, J.L., et al., J. Chem. Phys. 48 2342 (1968)

10. Dieke, G.H., and Singh, S., J. Opt. Soc. Am. 46 495 (1956)

11. Rabbinner, N., Phys. Rev. 132 224 (1963)

12. Voron'ko, Yu.K., et al., Sov. Phys. Solid State 7 204 (1965)

13. Luks, R.K., et al., ibid., 11 210 (1969)

14. Al'tshuler, N.S., et al., ibid., 11 2921 (1970)

15. Ref. 11, ch. 0.

16. Ref. 6, ch. 0.

17. Ref. 10, ch. 0.

18. Ref. 20, ch. 0.

19. Arkhangelskaya, V.A., Opt. and Spectr. 16 343 (1964)

20. Leverenz, H.W., 'Luminescence of Solids', Wiley (1950)

21. Weber, M.J., 'Optical Properties of Ions in Crystals', Interscience (1967), ed. Crosswhite and Moos, p.467.

22. Ref. 18, ch. 0.

23. Riseberg, L.A., and Moos, H.W., Phys. Rev. 174 429 (1968)

24. Ref. 23, ch. 0.

25. Ref. 1, ch. 3.

26. Pollack, S.A., J. Chem. Phys. 38 2521 (1963)

27. Rogers, 'FRANTIC, Program for Analysis of Exponential Growth and Decay Curves', MIT Lab. for Nuclear Science, Tech. Rept., no. 76 (1962)

28. Meek, G., 'Least Square Regression Fit to Sum of Two Exponentials' ---- SHARE TY ELS2.

29. Worsley, B.H., and Lax, L.C., Biochem. et Biophy. Acta 59 1 (1962)

30. Weber, M.J., Phys. Rev. 156 231 (1967)

31. Bey, P.P., et al., Phys. Rev. Lett. 19 819 (1967)

32. Chilver, C.R., and Fong, F.K., Chem. Phys. Lett. 7 229 (1970)

33. Osiko, V.V., Sov. Phys. Solid State 7 1047 (1965)

34. Makovski, J., Phys. Lett. 19 647 (1966)

35. Gil'fanov, F.Z., et al., Sov. Phys. Solid State 11 2020 (1970)

VITA AUCTORIS

19th January, 1938.	Born in Hong Kong
June, 1962.	Graduated from the University of Hong Kong with B.Sc. degree.
1962--1966.	Taught in St. Paul's Co-educational College, Hong Kong.
1966--1967.	University of Western Ontario, Make up year.
1967--1968.	University of Western Ontario, Ph.D. preliminary year.
1968--1970.	University of Windsor.